

# **DEVELOPMENT OF AN EFFICIENT ALGORITHM FOR 3D MAGNETOTELLURIC DATA INVERSION**

**Ph. D. THESIS**

*by*

**VISHAL KHATRI**



**DEPARTMENT OF EARTH SCIENCES  
INDIAN INSTITUTE OF TECHNOLOGY ROORKEE  
ROORKEE-247 667 (INDIA)  
JUNE, 2016**

# DEVELOPMENT OF AN EFFICIENT ALGORITHM FOR 3D MAGNETOTELLURIC DATA INVERSION

A THESIS

*Submitted in partial fulfilment of the  
requirements for the award of the degree*

*of*

DOCTOR OF PHILOSOPHY

*in*

EARTH SCIENCES

*by*

VISHAL KHATRI



DEPARTMENT OF EARTH SCIENCES  
INDIAN INSTITUTE OF TECHNOLOGY ROORKEE  
ROORKEE-247 667 (INDIA)  
JUNE, 2016

**©INDIAN INSTITUTE OF TECHNOLOGY ROORKEE, ROORKEE-2016  
ALL RIGHTS RESERVED**



# INDIAN INSTITUTE OF TECHNOLOGY ROORKEE ROORKEE

## CANDIDATE'S DECLARATION

I hereby certify that the work which is being presented in the thesis entitled **“DEVELOPMENT OF AN EFFICIENT ALGORITHM FOR 3D MAGNETOTELLURIC DATA INVERSION”** in partial fulfilment of the requirements for the award of the Degree of Doctor of Philosophy and submitted in the Department of Earth Sciences of the Indian Institute of Technology Roorkee is an authentic record of my own work carried out during a period from December, 2009 to June, 2016 under the supervision of Dr. Pravin K. Gupta, Professor and Dr. Kamal, Associate Professor, Department of Earth Sciences, Indian Institute of Technology Roorkee, Roorkee.

The matter presented in the thesis has not been submitted by me for the award of any other degree of this or any other Institute.

**(VISHAL KHATRI)**

This is to certify that the above statement made by the candidate is correct to the best of our knowledge.

(Pravin K. Gupta)  
Supervisor

(Kamal)  
Supervisor

Dated: June , 2016



# ABSTRACT

---

Magnetotelluric (MT) method is a passive source method used to delineate the subsurface conductivity structure of earth. Natural electromagnetic waves in the frequency range  $10^{-5}$  Hz -  $10^4$  Hz are used as source fields. The horizontal electric and magnetic field components are measured at the earth's surface and analyzed to infer electrical resistivity distribution in the earth's interior. The two orthogonal horizontal electric field components are linearly related to the two horizontal magnetic field components through appropriate transfer function (Cagniard [23], Tikhonov [142]).

The objective of the present study is to understand the mathematical, physical and numerical aspect of 3D MT inversion leading to an efficient 3D inversion software, **3DINV\_FD**, for magnetotelluric data. The estimation of model parameters from the physical fields, measured on earth surface, is termed as an inverse modeling. In magnetitelluric method, the earth is parameterized in terms of electrical resistivity which is of special significance as it carries information about the lithology, pore fluid, temperature and chemical variations. As the EM field is a non-linear function of subsurface resistivity distribution, the inverse problem is also non linear in nature. In the present work, the inverse problem is quasi-linearized and then solved iteratively. The inverse problem is solved using Gauss-Newton with conjugate gradient method. For each inversion iteration, a new forward problem, yielding the response of current resistivity model and several pseudo forward problems, for Jacobian matrix computations, are solved. Therefore, an efficient forward modeling algorithm is a prerequisite for an inversion algorithm.

The mapping of model parameters to measured fields is known as a forward

modeling. For generation of MT response, a boundary value problem is solved analytically or numerically. However, for the problems involving complex geometries one has to seek numerical solutions. Due to its simple mathematics and easy implementation, staggered grid finite difference method (FDM) has been chosen over other numerical techniques for solving the MT boundary value problem. The FDM results in a matrix equation, which is then solved using Bi-Conjugate Gradient Stabilized (BICGSTAB) with DILU preconditioner to compute the MT response.

The quasi-linearization of non-linear problem results in a matrix equation which is solved using Conjugate Gradient (CG) method, a semi-iterative matrix solver that dispenses with the necessity of explicit computation of Jacobian matrix. The initial guess is made on the basis of observed anomaly and other a priori information.

The inversion algorithm **3DINV\_FD** is the culmination of research that started with the development of a primitive algorithm. The algorithm has been written in FORTRAN 90 language and implemented on an Intel Core i7 3.6 Ghz machine with 4 Gbyte of RAM.

**3DINV\_FD** comprises 6887 lines having 44 subroutines and works in double precision arithmetic. The main program has two basic modules - Forward and Inverse. Its special efficiency features which result in cost effectiveness are - (i) Optimal computational parameters for static divergence correction, (ii) BICGSTAB with DILU preconditioner, which results in fast convergence, (iii) Gaussian noise addition to synthetic data, (iv) Computation of multi frequency response in parallel using OpenMP, (v) Use of logarithm of resistivity to ensure positive values of estimated parameters, (vi) In-built computation of regularization parameter and (vii) CG matrix solver for inverse problem. Besides being efficient, **3DINV\_FD** is versatile on account of its

features like (i) Inversion of field/synthetic data, (ii) Error free/erroneous synthetic data and (iii) Inversion of profiling/sounding data.

For establishing the validity of forward modeling algorithm, the published results of various models have been reproduced. The validity of the inversion algorithm **3DINV\_FD** is established by inverting the synthetic data generated from different models. To ensure the stability of the algorithm the inversion is performed after adding the Gaussian noise to the synthetic data. Furthermore, to demonstrate the robustness of the algorithm, the data generated from ModEM algorithm (Kelbert et al. [61]) has been inverted successfully. The synthetic experiments designed to understand the effect of number of sites and their distribution on the inversion, suggest that accurate resolution of the anomalous body data should be acquired along straight profiles whenever possible. And the a priori information about the target body should be taken into account for optimal site selection.

The results of various experiments and inversion of synthetic have established the veracity of the algorithm and also amply displayed the capabilities of the inversion algorithm. Also discussed, is the possible scope of future work in various directions for its upgradation.





# ACKNOWLEDGMENTS

---

First and foremost, I would like to pay my heartiest thanks and regards to my supervisors **Prof. P. K. Gupta** and **Dr. Kamal**, Department of Earth Sciences, Indian Institute of Technology Roorkee. Their able and continual guidance, unfailing patience, motivation and kind advice at every step have helped me in all phases of this work. I learned a lot from them not only in the academic area but in other spheres of life also. I wholeheartedly acknowledge their full cooperation that I received from the very beginning of this work up to the completion in the form of this thesis.

During this research, the department has had three heads; Prof. P. K. Gupta, Prof. A. K. Saraf and Prof. D. C. Srivastava and most fortunately they encouraged me by extending every sort of help as and when sought for.

I am especially thankful to Prof. M. Israil, Department of Earth Sciences for his invaluable help and advice from time to time as when needed. I would like to acknowledge his help by providing me the synthetic data generated from ModEM algorithm.

I would like to make a special note of thank to all faculty members of the Department of Earth Sciences for their co-operation. Thanks are also to Prof. J. P. Narayan, Department of Earthquake Engineering for his constant encouragement during my research work.

I would like to express my sincere thanks to the technical staff of the Department of Earth Sciences, especially to Mr. Nayar, Mr. Rakesh who have helped me in all possible ways during the official work.

The financial support provided by University Grant Commission (UGC), New Delhi

to complete the present work is highly acknowledged.

I express my heartily gratitude to Smt. Mamta Gupta as time spent occasionally during tea, dinner was very pleasant.

I also want to thank to my lovely friends, who helped lighten the burden, especially Dr. Vinay, Ashwani Kumar, Rahul Dehiya, Pramjeet, Amit Kumar, Amit Choudhary, Major Pradeep Sangwan, Sanjay Rauri, Harish Thapliyal, Dr. Krishna Kumar. The help provided by Mr. Rahul Dehiya during write up of the thesis is especially acknowledged.

The ever enthusiastic help of my family members, brother Naveen and bhabhi Bimal who were distant to me but were always by my side whenever the need so arrived and accompany for me to work peacefully during the study period. I am in dearth of proper words to express my abounding feelings and affection for my lovely wife Renu, daughter Dhakshita, niece Samridhi and nephew Dharya.

Finally, I express my heartfelt gratitude to my father, Shri Ranbir Singh and mother, Smt. Indu for their unconditional love, encouragement and blessings. Words can never express my feelings for them. They have been a guiding force all my life gave me necessary energy and happiness to work hard throughout this research work. I also express my feelings of gratitude to all those who helped me in this course but have not been listed here.

At last thanks to the almighty god who has given me the spiritual support and courage to carry out this work.

Roorkee

(Vishal Khatri)

June , 2016

# TABLE OF CONTENTS

---

DECLARATION	i
ABSTRACT	v
ACKNOWLEDGMENTS	viii
TABLE OF CONTENTS	ix
LIST OF FIGURES	xv
LIST OF TABLES	xxi
1 INTRODUCTION	1
1.1 Magnetotellurics . . . . .	1
1.1.1 Source . . . . .	1
1.1.2 Applications . . . . .	2
1.2 Interpretation MT Data . . . . .	5
1.2.1 Forward Modelling . . . . .	7
1.2.1.1 Matrix Solver . . . . .	9
1.2.2 Inversion . . . . .	10
1.3 Thesis Organization . . . . .	13
2 FORMULATION OF MAGNETOTELLURIC FORWARD PROBLEM	17
2.1 Introduction . . . . .	17
2.2 Theory of Electromagnetic . . . . .	18
2.2.1 Constitutive Relations . . . . .	19

2.3	Electromagnetic Properties of Earth . . . . .	20
2.4	Boundary Value Problem of Magnetotellurics . . . . .	22
2.4.1	Governing Equation . . . . .	24
2.4.2	Primary and Secondary Formulation . . . . .	24
2.5	Boundary Conditions . . . . .	26
2.5.1	Interface Boundary Conditions . . . . .	26
2.5.2	Domain Boundary Conditions . . . . .	28
2.6	Response Functions . . . . .	28
2.6.1	MT Response Functions . . . . .	29
2.7	Solution of Boundary Value Problem . . . . .	31
2.7.1	Static Divergence Correction . . . . .	32
2.8	Closure . . . . .	32
<b>3</b>	<b>FORMULATION OF MAGNETOTELLURIC INVERSE PROBLEM</b>	<b>35</b>
3.1	Introduction . . . . .	35
3.2	Mitigation of Ill-posedness . . . . .	37
3.2.1	Inconsistency . . . . .	38
3.2.2	Non-uniqueness . . . . .	38
3.2.3	Instability . . . . .	39
3.3	Types of Inverse Problems . . . . .	40
3.3.1	Least Square Inverse . . . . .	41
3.3.2	Minimum Norm Inverse . . . . .	42
3.3.3	Regularized Inverse . . . . .	42
3.3.4	Weighted Inverse . . . . .	44
3.4	3D MT Inverse Problem Solution . . . . .	46

3.4.1	3DINV_FD Algorithm: Linearized Inversion in Model Space . . .	47
3.4.2	Optimization using Gauss-Newton with Conjugate Gradient Method . . . . .	49
3.4.3	Calculation of Jacobian . . . . .	52
3.5	Closure . . . . .	53
4	<b>NUMERICAL IMPLEMENTATION OF FINITE DIFFERENCE METHOD</b>	<b>55</b>
4.1	Introduction . . . . .	55
4.2	Implementing Finite Difference Method . . . . .	57
4.2.1	Staggered Grid . . . . .	58
4.2.1.1	Grid Specifications . . . . .	59
4.2.2	Weighted Average Conductivity . . . . .	60
4.2.3	Staggered Finite Difference Equation . . . . .	62
4.2.3.1	System Matrix Description . . . . .	63
4.2.4	Divergence Correction . . . . .	64
4.2.5	Forward Matrix Solver . . . . .	67
4.2.6	Transformation and Interpolation . . . . .	68
4.3	Inverse Formulation . . . . .	70
4.3.1	Matrix Solver for Inverse Problem . . . . .	71
4.3.2	Real to Complex Algebra . . . . .	71
4.3.3	Derivative of System Matrix . . . . .	72
4.3.4	Derived Jacobian . . . . .	73
4.3.5	Bypassing Explicit Jacobian Computation . . . . .	75
4.4	Solution of Inverse Problem . . . . .	76

4.5	Closure . . . . .	77
<b>5</b>	<b>DEVELOPMENT AND DETAILS OF 3DINV_FD ALGORITHM</b>	<b>79</b>
5.1	Introduction . . . . .	79
5.2	Sequence of Development . . . . .	79
5.2.1	2D Algorithm Version I . . . . .	80
5.2.2	2D Algorithm Version II . . . . .	81
5.2.3	Version III . . . . .	81
5.2.4	Final Version . . . . .	82
5.3	Saleent Features of <b>3DINV_FD</b> Algorithm . . . . .	83
5.3.1	Source Term . . . . .	83
5.3.2	Optimal Parameters for Static Divergence Correction . . . . .	83
5.3.3	Multi-frequency Response in Parallel . . . . .	84
5.3.4	Field and Synthetic Data . . . . .	84
5.3.5	CG Method . . . . .	84
5.4	Details of Algorithm . . . . .	85
5.5	Structure of Algorithm . . . . .	85
5.5.1	Subroutines in 3DINV_FD . . . . .	88
5.5.1.1	Forward Modeling Subroutines . . . . .	89
5.5.1.2	Inversion Subroutines . . . . .	94
5.6	Closure . . . . .	103
<b>6</b>	<b>FORWARD MODELING ALGORITHM OPTIMIZATION AND VALIDATION</b>	<b>105</b>
6.1	Introduction . . . . .	105
6.2	Validation of 3DINV_FD . . . . .	105

6.2.1	Forward Algorithm Validation . . . . .	106
6.2.1.1	Single Block Model . . . . .	106
6.2.1.2	Two Block Model . . . . .	107
6.2.1.3	Dublin Test Model 1 . . . . .	112
6.3	Algorithm Optimization . . . . .	118
6.3.1	Optimal Computational Parameters for Divergence Correction .	118
6.3.1.1	Experiment Design . . . . .	119
6.3.2	Parallel Programming . . . . .	122
<b>7</b>	<b>3D MT INVERSION RESULTS</b>	<b>125</b>
7.1	Introduction . . . . .	125
7.2	Inversion Results . . . . .	125
7.2.1	Synthetic Data Set 1 . . . . .	126
7.2.2	Synthetic Data Set 2 . . . . .	128
7.2.3	Synthetic Data set 3 . . . . .	130
7.3	Synthetic Experiment . . . . .	131
7.3.1	Experiment 1: Effect of number of sites . . . . .	132
7.3.2	Experiment 2: Effect of distribution of sites . . . . .	136
<b>8</b>	<b>CONCLUSION AND FUTURE SCOPE</b>	<b>143</b>
8.1	Conclusion . . . . .	144
8.2	Scope for Further Research . . . . .	145
<b>A:</b>	<b>ITERATIVE MATRIX SOLVERS AND PRECONDITIONER</b>	<b>147</b>
<b>B:</b>	<b>DOCUMENTATION FOR I/O FILES OF 3DINV_FD</b>	<b>151</b>





# LIST OF FIGURES

---

2.1	Resistivity of rocks.(Geophysics-424 Notes, University of Alberta) . . . . .	21
2.2	Target buried in layered earth . . . . .	25
2.3	Interface boundary condition for tangential component of $\mathbf{E}$ . . . . .	26
2.4	Interface boundary condition for tangential component of $\mathbf{H}$ . . . . .	27
2.5	Interface boundary condition for perpendicular component of $\mathbf{E}$ . . . . .	27
2.6	Interface boundary condition for perpendicular component of $\mathbf{H}$ . . . . .	27
4.1	Staggered grid used for implementing FDM . . . . .	58
4.2	Staggered grid used for implementing FDM . . . . .	59
4.4	Grid cells and associated spacing parameters. The red dotted prism is of average conductivity $\sigma_y(i, j, k)$ . . . . .	61
4.3	Grid cells and associated spacing parameters. The red dotted prism is of average conductivity $\sigma_x(i, j, k)$ . . . . .	61
4.5	Grid cells and associated spacing parameters. The red dotted prism is of average conductivity $\sigma_z(i, j, k)$ . . . . .	62
4.6	Numbering scheme $E_x$ and $E_y$ components in system matrix $\mathbf{A}$ associated with grid $(3 \times 3 \times 4)$ . . . . .	65
4.7	Numbering scheme $E_z$ components in system matrix $\mathbf{A}$ associated with grid $(3 \times 3 \times 4)$ . . . . .	65
4.8	Structure of system matrix $\mathbf{A}$ associated with grid $(4 \times 3 \times 4)$ . . . . .	66
5.1	3D MT inversion algorithm 3DINV_FD in nutshell . . . . .	86
5.2	Flow chart of main program . . . . .	87

5.3	Tree structure of forward subroutines . . . . .	95
5.4	Flow chart of <b>response</b> subroutine . . . . .	96
5.5	Tree structure of inversion subroutines . . . . .	99
5.6	Flow chart of inversion modeling subroutine . . . . .	100
6.1	Single Block Model . . . . .	106
6.2	Comparison of <b>3DINV_FD</b> and published results in COMMEMI paper (Zhdanov et al. [167]) for model 3D-1(B). Abbreviations: FD = finite difference method, IE = integral equation method, D = direct solution, S = stationary field approximation, I = iterative solution. . . . .	108
6.3	(a)Cross-section view of the synthetic model and (b)Profiles where data are generated. . . . .	109
6.4	Comparison of apparent resistivities in $Z_{xy}$ and $Z_{yx}$ modes between results from <b>3DINV_FD</b> algorithm and Siripunvaraporn et al. [129] along profile A. . . . .	109
6.5	Comparison of apparent resistivities in $Z_{xy}$ and $Z_{yx}$ modes between results from <b>3DINV_FD</b> algorithm and Siripunvaraporn et al. [129] along profile B. . . . .	110
6.6	Comparison of apparent resistivities in $Z_{xy}$ and $Z_{yx}$ modes between results from <b>3DINV_FD</b> algorithm and Siripunvaraporn et al. [129] along profile C. . . . .	110
6.7	Comparison of phase in $Z_{xy}$ and $Z_{yx}$ modes between results from <b>3DINV_FD</b> algorithm and Siripunvaraporn et al. [129] along profile A. . . . .	111

6.8	Comparison of phase in $Z_{xy}$ and $Z_{yx}$ modes between results from <b>3DINV_FD</b> algorithm and Siripunvaraporn et al. [129] along profile B. . . . .	111
6.9	Comparison of phase in $Z_{xy}$ and $Z_{yx}$ modes between results from <b>3DINV_FD</b> algorithm and Siripunvaraporn et al. [129] along profile C. . . . .	112
6.10	Plan and cross-section view of Dublin test model ( $\rho_1 = 10 \Omega \text{ m}, \rho_2 = 1 \Omega \text{ m}, \rho_3 = 10000 \Omega \text{ m}$ ). . . . .	113
6.11	Comparison of Apparent resistivities in $Z_{xy}$ and $Z_{yx}$ modes for time period 100 sec along profile A. . . . .	114
6.12	Comparison of Apparent resistivities in $Z_{xy}$ and $Z_{yx}$ modes for time period 100 sec along profile B. . . . .	114
6.13	Comparison of Apparent resistivities in $Z_{xy}$ and $Z_{yx}$ modes for time period 100 sec along profile C. . . . .	115
6.14	Comparison of Apparent resistivities in $Z_{xy}$ and $Z_{yx}$ modes for time period 100 sec along profile D. . . . .	115
6.15	Comparison of Apparent resistivities in $Z_{xy}$ and $Z_{yx}$ modes for time period 1 sec along profile B. . . . .	116
6.16	Comparison of Apparent resistivities in $Z_{xy}$ and $Z_{yx}$ modes for time period 10 sec along profile B. . . . .	116
6.17	Comparison of Apparent resistivities in $Z_{xy}$ and $Z_{yx}$ modes for time period 100 sec along profile B. . . . .	117
6.18	Comparison of Apparent resistivities in $Z_{xy}$ and $Z_{yx}$ modes for time period 1000 sec along profile B. . . . .	117

6.19	Plan and cross-section view of the model. . . . .	120
6.20	Computation time comparison . . . . .	121
6.21	Computation time comparison . . . . .	123
7.1	Cross-section and plan view of the simple synthetic model used for testing inversion algorithm. . . . .	126
7.2	Distribution of sites for data generation. . . . .	127
7.3	Inversion result of fitting the synthetic data generated from single block model (Figure 7.1). . . . .	128
7.4	Distribution of sites for data generation. . . . .	129
7.5	Inversion result of fitting the synthetic data generated from two block model. . . . .	130
7.6	Cross-section view across the conductive block at $X = 0$ m of inversion results of fitting synthetic data generated from (a): algorithm developed in present work, (b): ModEM algorithm (Kelbert et al. [61]). . . . .	131
7.7	Location of observation sites where data is recorded. . . . .	133
7.8	Left column:Plan view at different depths of the inverted model for 5 profile case. Right column: Relative misfit in resolved parameters with respect to the FDI results. . . . .	133
7.9	Location of observation sites where data is recorded. . . . .	134
7.10	Left column:Plan view at different depths of the inverted model for 3 profile case. Right column: Relative misfit in resolved parameters with respect to the FDI results. . . . .	134
7.11	Location of observation sites where data is recorded. . . . .	135

7.12	Left column:Plan view at different depths of the inverted model for single profile case. Right column: Relative misfit in resolved parameters with respect to the FDI results. . . . .	135
7.13	Location of observation sites where data is recorded. . . . .	138
7.14	Left column:Plan view at different depths of the inverted model for 9 perturbed profile case. Right column: Relative misfit in resolved parameters with respect to the FDI results. . . . .	138
7.15	Location of observation sites where data is recorded. . . . .	139
7.16	Left column:Plan view at different depths of the inverted model for 5 perturbed profile case. Relative misfit in resolved parameters with respect to the PFDI results (middle column) and FDI results (right column). . . . .	139
7.17	Location of observation sites where data is recorded. . . . .	140
7.18	Left column:Plan view at different depths of the inverted model for 3 perturbed profile case. Relative misfit in resolved parameters with respect to the PFDI results (middle column) and FDI results (right column). . . . .	140
7.19	Location of observation sites where data is recorded. . . . .	141
7.20	Left column:Plan view at different depths of the inverted model for one perturbed profile case. Relative misfit in resolved parameters with respect to the PFDI results (middle column) and FDI results (right column). . . . .	141



## LIST OF TABLES

---

5.1	Control parameters description . . . . .	88
5.2	Grid parameters and other run-time control parameters . . . . .	88
5.3	Description of various forward subroutines. . . . .	91
5.4	Description of various inversion subroutines. . . . .	101
6.1	Dimensions and resistivities of the anomalous bodies in 3D-2 model. . .	107
6.2	Dimensions and resistivities of the anomalous bodies in DTM1. . . . .	112
6.3	Comparison between computation time of serial and parallel code . . .	124





## INTRODUCTION

### 1.1 Magnetotellurics

Magnetotellurics(MT) as a method of electromagnetic imaging of the Earth was first introduced in 1950's (Tikhonov [142], Cagniard [23]). The MT method is a natural(passive) source method and uses the natural variation of the electric(telluric) and magnetic fields over a wide range of periods as source. These fields are generated in ionosphere and magnetosphere due to the interaction of solar winds and near-earth plasma with the Earth's magnetic field. More details about the MT sources are discussed next.

#### 1.1.1 Source

The electromagnetic fields used as source in MT method is generated mainly by two major processes(Simpson and Bahr [123]):

1. The electromagnetic waves above 1 Hz are generated by thunderstorm activity.

The waveguide formed between the ionosphere and earth's surface, partially trap the electromagnetic waves generated by individual lightning strokes. These

trapped waves can travel long distances and the lightning somewhere in the world is enough to provide a continuous source at any location of the earth's surface. The measured field at the earth's surface is a superposition of waves generated from individual lightnings and as long as the measurements are far away from the individual thunderstorms this superposition can be considered as a plane wave.

2. Solar wind consists of ionized particles flowing radially outward from the sun. These ionized particles are deflected by the earth's magnetic field at the outer region of the magnetosphere and are guided around the earth to the far tail, along the magnetic field lines. When moving around the earth they distort the earth's magnetic field and generate their own field. The variations of these external magnetic fields can be measured at the earth's surface. The typical frequencies of these variations are from about  $10^{-5}$  to 1 Hz.

Both of the above source mechanisms create small, but measurable, time-varying electromagnetic signals. The problem is that the amplitudes of these signals vary considerably, which means that data have to be acquired for hours or even days at one MT site to ensure sufficient signal strength at all frequencies of interest.

### **1.1.2 Applications**

As MT method uses fields over a wide frequency range from  $10^{-5}$  to  $10^4$  Hz, the depth of investigation ranges from 10 m to up to 200 km. Due to large depth of investigation MT is used for a variety of applications, such as

1. *Deep crustal/mantle and geoelectric investigation*

Magnetotellurics is widely used to study the deep crustal structure and its electric properties in different regions of the world. Bhattacharya and Shalivahan [15] and Shalivahan and Bhattacharya [122] resolved the crust–mantle Moho boundary over the Eastern Indian (3.3 Gyr) and Slav (4.03 Gyr) cratons and observed that upper mantle beneath these two cratons cannot be of pure olivine. Manglik et al. [76], applying 1-D joint inversion to seismic and MT data from a segment of the Kuppam- Palani geo-transect in the Southern Granulite Terrain (SGT) suggested a velocity of 5.45 km/s for low velocity and electrically conducting mid-crustal layer. The study also showed the presence of a 60 km thick sub-crustal layer below which the resistivity decreases to about 100  $\Omega$ -m. Patro et al. [103] observed that the basalt cover, below the flood basalts in the Deccan Volcanic Province, have an average thickness of 400 m with the exception of central parts of the profile where it reaches up to 700 m. The crust is in general highly resistive, but several subvertical zones of enhanced conductivity were delineated in the middle-to-lower crust. Patro and Egbert [104] delineated the extensive areas of high conductivity in the lower crust beneath all of southeastern Oregon, and beneath the Cascade Mountains, contrasting with very resistive crust in Siletzia and the Columbia Embayment. Significant variations in upper mantle conductivity were also observed, with the most conductive mantle beneath the Washington backarc, and the most resistive corresponding to subducting oceanic mantle. Patro and Harinarayana [105] reported that the MFT and MBT zones are expressed by a conductive feature of about 10–40  $\Omega$ -m indicating, the presence of Siwalik molasse sediments of Gangetic foreland basin. An anomalously high

conductive ( $2\text{--}5\ \Omega\text{-m}$ ) region in the crust in the depth range of  $3\text{--}15\ \text{km}$  was also reported to the north of MBT. Arora et al. [3] observed that the Indus Tsangpo Suture, as a sub-vertical conductive structure, dips northeast and merges with a mid-crustal conductor. A north dipping zone of low resistivity was also reported at the top of the underthrust Indian Plate.

In literature there are many other references available where MT method has been used for studying the crustal structure of earth, e.g., Kumar and Manglik [63], Rawat et al. [109], Tezkan [139], Brasse and Soyer [18], Brasse et al. [17], Lezaeta et al. [68], Habibian et al. [47], Manglik and Verma [77], Berdichevsky et al. [14], Bubnov et al. [22, 21], Gurk et al. [44], Lahti et al. [65], Hill et al. [53], and Miglani et al. [84].

## 2. *Geothermal studies*

In Bakreshwar region of West Bengal geothermal study was done by Sinharay et al. [124]. they reported two conductive zones of about  $100\ \text{ohm-m}$  and  $15\ \text{ohm-m}$  at a depth of about  $8\ \text{km}$  and  $12\ \text{km}$  respectively and thicknesses of these two conductive zones are  $2.3\ \text{km}$  and  $3.4\ \text{km}$  respectively. Various other researchers e.g., Cumming and Mackie [30], Heise et al. [51, 50], Jones et al. [57] and Newman et al. [94] have also used MT for geothermal studies.

## 3. *Environmental studies*

Tezkan et al. [140] used the radio magnetotellurics and transient electromagnetics to study the waste deposit site in Cologne (Germany) and observed that due to the highly conducting waste deposit only the top of the waste site ( $\sim 5\ \text{m}$ ) and the lateral boundary of it could be resolved. By interpreting transient electromagnetic data on the same profile, they reported the lower boundary of

the waste deposit at a depth of 20 m. The industrial and domestic waste sites in Hermsdorf and Mellendorf were investigated by Tezkan et al. [141] using radiomagnetotelluric method and they showed that the radiomagnetotelluric technique is a powerful tool for waste site exploration.

#### 4. *Mineral exploration*

3D MT inversion have been used in the field of oil and mineral exploration by Farquharson and Craven [34], Tuncer et al. [145] and Türkoğlu et al. [146].

## **1.2 Interpretation MT Data**

The process of deducing the right message from the observed data is termed as data interpretation, a word which aptly implies its indeterminate nature. With reference to geophysics, the data interpretation is a two step procedure. The first step involves quantitative interpretation where physical earth parameters are estimated from observed data. This is followed by the second step, wherein, the obtained geophysical model is translated in terms of meaningful geology and the success in the endeavor depends upon a proper appreciation and balancing of all the physical and geological factors.. Thus, the whole process of retrieving a reasonable geological structure from observations is called geophysical data interpretation. For quantitative interpretation, it is assumed that there is a specific physico-mathematical theory that relates the model parameters (numerical values/statistics of the specific properties) to the data. The mapping from model to measured fields based on relevant physical laws, a model and a set of specific conditions relevant to the problem, is termed as 'direct' or 'forward problem'. In contrast, the mapping from measured data to the model parameters using general principles is termed as 'inverse problem'. Thus, quantitative interpretation of

data is an inverse problem and its solution is obtained through inverse theory.

Geophysical inverse problems are usually ill-posed and as such their solutions are inherently non-unique (Backus and Gilbert [9], Tikhonov and Arsenin [143]). The ill-posedness is caused by inadequate and insufficient data or sometimes by invalid assumptions used in defining the solution space of possible models. The non-uniqueness arises due to the existence of an infinite number of models which may explain the data within the limits set by the accuracy of measurements. In addition, ill-conditioned system having erroneous data lead to instability that is prone to get amplified during inversion. The problem is further compounded by non-linearity that is inherent in the mathematical relations describing the physical experiment. These problems are regularized by replacing the ill-posed problem by an equivalent well-posed problem. This replacement yields a stable, albeit approximate solution possessing essential features of the exact solution.

The present study deals only with the first step of data interpretation, i.e. quantitative interpretation. The literature of electromagnetic modeling can be classified into two categories: (i) developments in forward modeling algorithm and (ii) developments in inversion algorithm. The progress in the development of three-dimensional(3D) MT forward modeling and inversion has significantly increased in the last few decades. This progress is driven by the fact that there is ambiguity in two-dimensional interpretation (Siripunvaraporn et al. [131], Ledo [66], Simpson and Bahr [123] and Newman et al. [96]) and increasing number of 3D MT data acquisition. A brief review of literature for these two classes is presented here.

### 1.2.1 Forward Modelling

In forward modeling the physical properties of the model (conductivity distribution, frequency, etc) is taken into consideration to compute the variations of the electromagnetic fields on and in the earth model. There are three basic numerical techniques which are commonly used for 3D MT forward modeling namely

1. *Integral Equation Method (IEM)*

In this method Maxwell's equations are first reduced to second-kind Fredholm's integral equation. The main advantage of this method is that only anomalous part is discretized. This method has been used for three-dimension modeling by different developers (Hohmann [54], Wannamaker [152], Xiong and Tripp [160], Avdeev et al. [7], Zhdanov et al. [169], Gribenko and Zhdanov [42] and Gribenko et al. [41]). This reduces the size of matrix A but the matrix is dense and full. It is a tedious task to solve this full matrix rather than sparse ones. Due to non-availability of efficient algorithms for computation of Green's functions in other cases, the use of IEM is limited to confined targets buried in layered earth.

2. *Finite Element Method (FEM)*

It is believed that it can give accurate geometry because in the method EM fields are decomposed into some basic functional (edge, nodal). Due to this fact the structure of the matrix is complex and we have to make extra efforts to solve it. This method had been implemented by different developers (Hohmann [54], Rodi [111], Reddy et al. [110], Badea et al. [10], Mitsuhashi and Uchida [86], Nam et al. [90], Farquharson and Miensopust [35] and others). This method results in a large complex and sparse system matrix.



### 3. *Finite Difference Method (FDM)*

This method is commonly used for solving Maxwell's equations. In this method a rectangular grid is used, although we can use fixed or staggered grid. Complete fixed grid solution for modeling was given by Weaver [157], who used triangular grids using finite difference, but this makes the system matrix more complicated. In fixed grid,  $\mathbf{E}$  and  $\mathbf{H}$  field values are defined at the same point. The staggered grid proposed by Yee [162] is widely used for EM forward modeling, in which electric field is calculated at the centre of the edge of the block and magnetic field is calculated at the centre of the block or vice-versa. In case of staggered grid the electric field components and the magnetic field components are continuous on the edges and the faces of the homogeneous prisms respectively or vice-versa. For 3D case, staggered grids yields more accurate results than obtained using fixed grid. Various developers e.g. Mackie et al. [73, 74], Mackie and Madden [72], Smith [133, 134], Wang and Fang [151], Newman and Alumbaugh [92], Sasaki [118], Siripunvaraporn et al. [129], Fomenko and Mogi [37], Streich [135] and Yan et al. [161] have implemented FDM using staggered grid for calculating three-dimensional response. Mackie et al. [74] calculated  $\mathbf{H}$  field values from model and  $\mathbf{E}$  field values was calculated using curl of  $\mathbf{H}$ . FDM results in a large complex, sparse and symmetric and non-hermitian system matrix. The main advantage of FDM over FEM is its simplicity to implement and iterative solvers for FDM are more efficient compared to those used for FEM.

For a more comprehensive study of three-dimension modeling from theory to application reader is advised to refer Avdeev [4], Börner [16].

### 1.2.1.1 Matrix Solver

Every numerical method transforms the forward problem to a linear system of equations which are solved with the help of a matrix solver. For differential equation methods (FEM and FDM), the iterative solvers are preferred over direct solver because these solvers need less memory and computation time. Direct solvers may be efficient if solutions for multiple righthand side vectors are needed for same system matrix like in case of controlled-source electromagnetic (Streich [135]). However, in case of MT, system matrix is different for each frequency. The iterative solvers based on Krylov subspace method are widely used in MT forward modeling. These methods require matrix-vector multiplication which is easy to compute particularly because differential equation methods produce a very sparse system matrix. Since the system matrix is complex and non-hermitian, for solving such a linear system, some of the popular iterative solver are the generalised minimal residual (GMRES) (Saad and Schultz [115]), quasiminimal residual (QMR) (Freund and Nachtigal [39]) and biconjugate gradient stabilised (BICGSTAB) (Van der Vorst [149]).

These methods differ in both memory requirements, number of computations in each iteration and robustness. GMRES is a well-known Arnoldi-based method proposed by Saad and Schultz [115]. This method leads to a non-increasing sequence of residual norms and, therefore, it always guarantees smooth and monotonically decreasing convergence, which may not necessarily be fast enough. This method requires one matrix-vector multiplication per iteration. The main disadvantage of GMRES is its large storage requirement because the solver stores all previously-generated Arnoldi vectors. To overcome this issue some modification has been proposed as restarted-GMRES and hybrid GMRES. QMR (Freund and Nachtigal [39]) and

BICGSTAB (Van der Vorst [149]) are two Lanczos-based methods. These methods require relatively less memory which does not vary during iterations. The number of iterations needed to converge for all three solvers may be approximately of the same order, however, the amount of work per iteration differs. Whereas GMRES needs one matrix-vector multiplication per iteration, QMR and BICGSTAB need two. The QMR and BICGSTAB methods produce oscillatory behavior as far as residuals norm is concerned. For more details about the method reader is advised to refer the book of Saad [114]. Another important issue regarding the iterative solver is the condition number of the system matrix which could be of the order of  $10^9$  to  $10^{12}$  (Avdeev [4]) for case of EM modeling. In case of FD and FE the most popular preconditioners are Jacobi, SSOR, incomplete LU decomposition (ILU) and multigrid. The right choice of preconditioner is very essential for efficient computation. In fact the choice of preconditioner is more critical than the iterative solver. The literature survey suggests that the ILU preconditioner is most preferred in EM modeling and widely used by developers.

### 1.2.2 Inversion

The 3D EM inverse problem is much more difficult to solve than the corresponding forward problem because the inverse problem is ill-posed and non-linear in nature. And due to the noisy and limited data, the inversion is a non-unique problem meaning that multiple models can fit the observed data equally well. Furthermore, the solution of inverse problem is very computation intensive as thousand of model parameters need to be recovered. It would require many iterations to converge if at all it converges. The inverse problem is regularized to make it stable. The inversion process is a

set of mathematical formulations for obtaining the meaningful information about the sub-surface structure from data. This is achieved by minimizing the misfit between the data (synthetic or real) and the computed response. So, forward modeling is the main part of inversion process and both these processes are interfaced by an iterative process to obtain a conductivity model which, within specified error limits justifies the data.

A pertinent question is why we need a 3D inversion code for MT data interpretation because data can be acquired along the profile and can be interpreted using 2D inversion algorithm. Considerable efforts have been made in the direction of interpreting the MT profile data using 2D inversion codes. This approach requires that the dimensionality analysis be carried out before performing the 2D inversion. A good review of 2D MT inversion including modeling, dimensional analysis and interpretation is summarized in Ogawa [97]. The dangers of interpreting the MT data which is recorded over a 3D structure using 2D inversion algorithm is that if the data is influenced by 3D structures, 2D inversion can lead to misleading interpretation. However, Ledo [66] proposed that it is still possible to carry out 2D inversion on some modes (either TM or TE). Though it is significantly influenced by the position of the 3D structure with respect to the regional 2D strike direction. Becken et al. [12] suggested separation of data into TM and TE modes using the vertical magnetic transfer function for 2D inversion with synthetic data. However, in practice, these methods, such as Ledo's analysis and mode separation are not straight forward to justify, unless the 3D structures are already known, which is indeed the objective of these exercises. Another reason to move on to 3D inversion is that due to logistic reason, acquiring the MT data along the straight profile is not always possible. Therefore, in case the data is scattered through a corridor

along a profile, the data need to be projected on the profile to be interpreted using 2D inversion. The availability of efficient 3D inversion code allows the scattered data to be interpreted without adding any bias or position error to the observed data.

For the 3D inverse problem, the main algorithms used by various researchers are Occam's inversion (e.g., Constable et al. [29], Degroot-Hedlin and Constable [31], Siripunvaraporn and Egbert [126, 128], Siripunvaraporn et al. [132, 130]), Gauss-Newton (GN) method (e.g., Haber et al. [46], Sasaki [119, 120] and Gunther et al. [43]), quasi-Newton (QN) method (e.g., Haber [45], Avdeev and Avdeeva [5]). These methods require computation of the Jacobian (sensitivity) and the Hessian or its approximation at each inversion iteration. This leads to a need of solving a large and dense linear system of equations. The construction and storage of Jacobian matrix is very difficult to handle in case of 3D inversion. The alternative approach is to bypass the formation of Jacobian, using the Gauss-Newton with conjugate gradient (GN-CG) method (e.g., Mackie and Madden [72], Newman and Alumbaugh [91], Gunther et al. [43], Siripunvaraporn and Egbert [127]). In this approach the Jacobian matrix is employed only in the product with an arbitrary vector. This is equivalent to solving two forward problems at each CG iteration. The method was used by Mackie and Madden [72] to solve the 3D MT inverse problem. Newman and Alumbaugh [91] used this approach to solve the cross-well EM data and Ellis et al. [33] used this technique to invert airborne TEM synthetic data. Another approach called nonlinear conjugate gradient (NLCG) was introduced at the start of this century to solve the 3D EM inverse problem (Newman and Alumbaugh [92], Rodi and Mackie [112], Mackie and Watts [75] and Zhanxiang and Hu [163]). This method requires computation of gradient rather than Jacobian. The motivation to use NLCG comes

from the fact that it needs to solve one forward and one adjoint problem at each NLCG iteration. Since then NLCG has been applied in many EM inversion codes. The computation needed in an inversion iteration is less in case of NLCG in comparison to Newton type algorithm, but it is offset by the fact that the convergence rate in case of NLCG is close to linear whereas it is of the order of quadratic in case of Newton type schemes. Rodi and Mackie [112] through the 2D MT data inversion reported that the NLCG takes more time than Gauss-Newton method and preconditioned NLCG is equivalent to Gauss-Newton as far as computation time is concerned. It is not yet clear which approach is better for 3D EM inversion. With all these advancement the solution of 3D EM problem is still very challenging task due to non-uniqueness and unsuitability as reported by Newman et al. [96].

The regularization of the objective functional of EM inverse problem is another important subject. The common practice is to seek smooth model parameters. In many algorithms it is achieved by using the model covariance matrix as the finite difference approximation to the Laplacian ( $\nabla^2$ ) operator (e.g., Constable et al. [29], Rodi and Mackie [112], Newman and Alumbaugh [92] and others). The prior information such as faults or oceans can be easily included in the regularization functional (Siripunvaraporn and Egbert [126]). A detailed review of methods used for 3D EM inversion is available in Avdeev [4] and Siripunvaraporn [125].

### **1.3 Thesis Organization**

When the present study was launched in 2010, availability of few algorithms for interpretation of 3D MT data led to the the conclusion that there is scope for further development of 3D MT inversion algorithm. The objective of study is fulfilled with

the development of an efficient software **3DINV\_FD** which is capable of inverting synthetic or real MT data. The thesis write up has been organized into eight chapters briefly summarized below.

In the present chapter 1, literature review is presented.

In chapter 2, the mathematical formulation of forward problem is presented, which covers a brief description of EM theory and ranges of electrical properties within the earth. It also formulates a boundary value problem comprising the governing partial differential equations and requisite boundary conditions. The basic theory of magnetotellurics along with the computations of MT response functions is discussed. The need for applying static divergence correction is also described.

In chapter 3, the characteristics of ill-posed EM inverse problem and some techniques for its alleviation are presented. Besides the different methodologies for solving inverse problem the quasi-linearized scheme for solution of inverse problem, adopted in the present work, is also described.

In chapter 4, In order to successfully implement the FDM for solving forward and inverse problems, the discrete governing equations, implementation of staggered grid, structure of coefficient matrix, transformation matrices derived for response functions and the computation required for bypassing the explicit construction and storage of Jacobian matrix are discussed.

In chapter 5, the sequence of development with a critical review of various primitive versions of the algorithm is discussed. Description of salient efficiency and versatility features, structure, control and grid parameters, important subprograms of the algorithm and flow chart of the algorithm are presented

In chapter 6, validation of the algorithm **3DINV\_FD** is described by comparing its

results with some published results. Steps taken to improve the efficiency are discussed.

In chapter 7, the inversion results of data sets derived from synthetic models are presented. Details and results of synthetic experiment conducted to understand the effect of number of observation points on the quality of inversion are discussed.

In chapter 8, we discuss further improvement steps that need be taken to make the algorithm more accurate, efficient and versatile.

Finally, the Appendix A presents CSR storage scheme to store the system matrix. The basic steps of matrix solvers (BICGSTAB and CG) used in the algorithm along with the steps of DILU preconditioner are given in Appendix A. In Appendix B, sample input and output files are presented.





# FORMULATION OF MAGNETOTELLURIC FORWARD PROBLEM

## 2.1 Introduction

The geoelectromagnetic methods deal with the observation and analysis of electromagnetic (EM) fields with a view to derive pertinent information about the geoelectric structure of subsurface. The observed field can be viewed as a superposition of the primary and secondary fields. Primary fields, generated by an external source, induce secondary currents in the earth which, in turn, give rise to the secondary fields and the inhomogeneities present in the real earth invariably disturb the pattern of secondary currents and fields, leading to perturbation of the total EM fields. These perturbed fields, measured on the earth's surface, provide an insight into the resistivity distribution within the earth. This helps in deciphering the electrical structure of the earth and also in understanding the ongoing physical processes.

The mechanism of perturbed fields can be understood only when the capability of generating responses of arbitrary resistivity distributions is fully developed. The computation of EM response of a given earth model, with prescribed resistivities, is known as the forward problem of EM induction.

An exhaustive knowledge of EM theory, based on the fundamental Maxwell's equations, is essential for solving the forward problem. In literature there exists a vast number of texts on EM theory differing in their emphasis on mathematical background, computational aspects and applications. For completeness, a brief account of electromagnetic theory is presented here.

## 2.2 Theory of Electromagnetic

The propagation and attenuation of EM fields is governed by Gauss's law of electric fields due to charges, Faraday's law of induction, the law of non-existence of magnetic monopole and Ampere's law for magnetic induction due to current. Maxwell's equations are the concise mathematical statements of these laws that, assuming linear, isotropic medium and an  $e^{i\omega t}$  time-dependence, can be written as the following first order partial differential equations

$$\nabla \cdot \mathbf{D} = q_{free}, \quad (2.2.1)$$

$$\nabla \times \mathbf{E} = -i\omega\mathbf{B}, \quad (2.2.2)$$

$$\nabla \cdot \mathbf{B} = 0, \quad (2.2.3)$$

$$\nabla \times \mathbf{B} = \mu\mathbf{J} + i\omega\mu\mathbf{D}. \quad (2.2.4)$$

Here,  $\mathbf{D}$ ,  $\mathbf{E}$ ,  $\mathbf{B}$  and  $\mathbf{J}$  are the vectors representing the electric displacement in Coulombs/ $m^2$ , the electric field in Volts/metre(m), the magnetic induction in Tesla

and electric current density in Amperes/ $m^2$  respectively. Similarly,  $q_{free}$ ,  $\omega$  and  $\mu$  are the scalars representing free electric charge density in Coulombs/ $m^3$ , the spectral angular frequency in Hertz and the magnetic permeability in Henry/m. It can be easily established that, for  $\mathbf{E}$  and  $\mathbf{H}$  having continuous first and second derivatives, equation (2.2.3) can be derived from equation (2.2.2), while equation (2.2.1) can be derived from equation (2.2.4). The displacement current term was added into the Ampere's law by Maxwell to guarantee the charge conservation. The conservation of electric charge law (equation of continuity) in differential form can be written as

$$\nabla \cdot \mathbf{J} = -i\omega q_{free}. \quad (2.2.5)$$

### 2.2.1 Constitutive Relations

As there are four vectors involved in the two vector Equations (2.2.2) and (2.2.4), we require constitutive relations to express these equations in terms of two independent EM vectors. These relations state the dependence of various vectors on the material properties, the electrical conductivity ( $\sigma$ ) and the dielectric permittivity ( $\varepsilon$ ) as

$$\mathbf{J} = \sigma \mathbf{E} \quad (2.2.6)$$

and

$$\mathbf{D} = \varepsilon \mathbf{E}. \quad (2.2.7)$$

Here,  $\sigma$  in Siemens/m and  $\varepsilon$  in Farad/m are the second order tensors which may be functions of position vector  $\mathbf{r}$  and spectral angular frequency  $\omega$ . A third constitutive relation between magnetic flux density  $\mathbf{B}$  and the magnetic field intensity  $\mathbf{H}$  is

$$\mathbf{B} = \mu \mathbf{H}, \quad (2.2.8)$$

where  $\mathbf{H}$  is in Amperes/m. Using equations 2.2.6, 2.2.7 and 2.2.8, Maxwell's equations in other form can be written as

$$\nabla \cdot \mathbf{E} = \frac{q_{free}}{\varepsilon}, \quad (2.2.9)$$

$$\nabla \times \mathbf{E} = -i\omega\mu\mathbf{H}, \quad (2.2.10)$$

$$\nabla \cdot \mathbf{H} = 0, \quad (2.2.11)$$

$$\nabla \times \mathbf{H} = \sigma\mathbf{E} + i\omega\varepsilon\mathbf{E}. \quad (2.2.12)$$

The constitutive relations are not always linear or single-valued. For example,  $\sigma$  and  $\varepsilon$  may be functions of  $\mathbf{E}$ . In order to ascertain which of these functional dependencies are of relevance in the context of the various EM methods, a discussion of geoelectromagnetic properties follows.

## 2.3 Electromagnetic Properties of Earth

For an isotropic earth, the parameter tensors  $\sigma$ ,  $\varepsilon$  and  $\mu$  reduce to scalars and are, in general, functions of position only. The only other functional dependence of importance is with respect to frequency. In some studies, the dependence of resistivity on temperature has been used to gather information about the thermal gradient in earth. Several texts have discussed the electrical properties of rocks and minerals, notable amongst these being Grant and West [40], Keller and Frischknecht [62] and Ward and Fraser [156]. Here, a brief account of the ranges of  $\sigma$ ,  $\varepsilon$  and  $\mu$  widely encountered in the earth, is presented.

The parameter electrical conductivity,  $\sigma$ , or its inverse, the electrical resistivity,  $\rho$ , which is more popular in geophysical literature, has the widest range of all physical parameters of earth (Figure 2.6.1). The resistivity varies in the range  $10^{-8}$  -  $10^{13}\Omega\text{m}$

for different rocks and minerals. This wide range results from the diverse physical phenomena that contribute to the resistivity of rocks. In the upper crust, the ionic conduction of electrolytes in the pores of rocks is the primary contributor to resistivity of rocks, while in the lower crust and upper mantle the electronic mode of conduction is the primary contributor. In the former case, if it is desired to account for electrode and membrane polarization through a change in resistivity, it becomes frequency dependent and complex in nature. For surface rocks, water present in pore spaces is the most important factor controlling the resistivity. It has been shown that the anomaly caused by a target, buried in a conducting host medium, gets enhanced as the contrast in the resistivity values of the target and host medium increases. However, it asymptotically reaches a maximum value, rendering the cases, where the resistivity contrast is greater than 1000, indiscernible from each other. Hence, such cases can be modeled as if the target is suspended in free space.

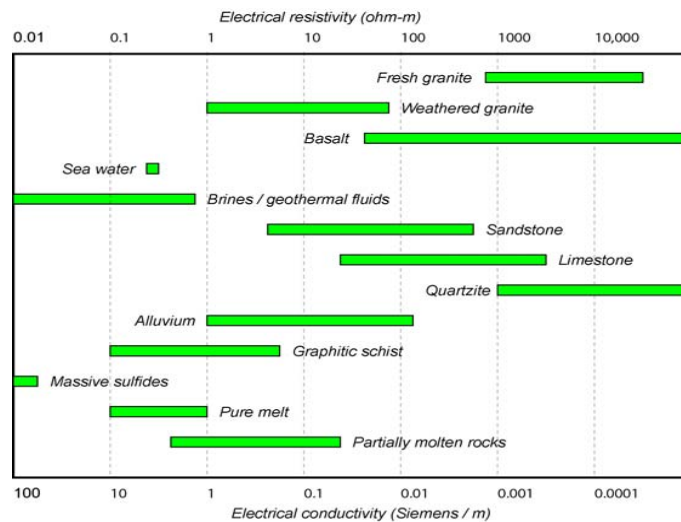


Figure 2.1: Resistivity of rocks.(Geophysics-424 Notes, University of Alberta)

The free space value of electric permittivity is  $\epsilon_0 = 10^{-9}/36\pi$  Farad/m. With the exception of water ( $\epsilon/\epsilon_0 \ll 80$ ), electric permittivity rarely varies by more than an

order of magnitude. For most rocks and earth materials the typical value is  $\varepsilon \approx 9\varepsilon_0$ . The primary contributions to  $\varepsilon$  are only due to the microscopic phenomena like the lengthening of bonds between the atoms and the preferred orientation of molecules along the direction of the field. However, if the macroscopic phenomena, like electrode and membrane polarization, are accounted through permittivity,  $\varepsilon$  attains large values and becomes frequency dependent.

The magnetic permeability  $\mu$  in most geophysical situations equals its free space value  $\mu = 4\pi \times 10^{-7}$  Henry/m. Only for the ferromagnetic minerals it goes upto  $6\mu_0$ . In the case of remanent magnetization studies,  $\mu$  becomes non-linear and multivalued due to the phenomenon of hysteresis.

## 2.4 Boundary Value Problem of Magnetotellurics

In MT the field variations can be studied by solving the Maxwell's equations (2.2.10) and (2.2.12). The solution can be achieved for  $\mathbf{E}$  or  $\mathbf{H}$  by transforming these equations into a well posed MT Boundary Value Problem (BVP). For this purpose a right-handed Cartesian coordinate system, with  $z$  direction being positive downward and air-earth interface at  $z = 0$ , is considered. Furthermore, to obtain the induction equation in the earth following assumptions are also made about the physical nature of earth:

1. A plane wave is propagating vertically downwards along the  $z$ -axis.
2. Earth is a linear and isotropic medium so that the change in output is proportional to the change in input field and the physical variables  $\sigma$ ,  $\varepsilon$  and  $\mu$  are scalars. In particular  $\mu$  is assumed to be equal to  $\mu_0$ , its free space value, throughout.

3. Earth is a source free and passive medium.
4. The flat earth model is appropriate as only the EM fields with periods less than 1 day are to be studied.
5. Since the frequencies used are less than  $10^5$  Hz and the resistivities commonly encountered in earth are less than  $10^4$   $\Omega$ -m, the free charge decays instantaneously.
6. For frequencies less than  $10^5$  Hz, the displacement current term in Ampere's law is negligibly smaller than the conduction current term and is neglected.

In view of the all these assumption conservation of charge law equation 2.2.5 and Maxwell's equations (2.2.10, 2.2.12) respectively get simplified as

$$\nabla \cdot \mathbf{J} = 0, \quad (2.4.1)$$

$$\nabla \times \mathbf{E} = -i\omega\mu\mathbf{H}, \quad (2.4.2)$$

$$\nabla \times \mathbf{H} = \sigma\mathbf{E}. \quad (2.4.3)$$

The fields governed by these equations are termed quasi-static because inspite of the field being time dependent, its variation is very slow and at any given instant of time it behaves like a static field. Thus, for the quasi-static case, the two equations (2.4.2) and (2.4.3) are sufficient to describe the complete behavior of EM fields.

The two steps for defining a BVP comprise development of the governing partial differential equation and of the requisite boundary conditions for each of the field vectors  $\mathbf{E}$  and  $\mathbf{H}$ .



### 2.4.1 Governing Equation

To eliminate  $\mathbf{H}$ , from equations (2.4.2) and (2.4.3), take curl of the equation (2.4.2) and then use equation (2.4.3) to form the second order differential equation for  $\mathbf{E}$  as

$$\nabla \times \nabla \times \mathbf{E} + i\omega\mu_0\sigma\mathbf{E} = 0. \quad (2.4.4)$$

Similarly,  $\mathbf{E}$  can be eliminated from equations (2.4.2) and (2.4.3) by switching the roles of equations (2.4.2) and (2.4.3), to get the equation satisfied by  $\mathbf{H}$  as

$$\nabla \times \left( \frac{1}{\sigma} (\nabla \times \mathbf{H}) \right) + i\omega\mu_0\sigma\mathbf{H} = 0. \quad (2.4.5)$$

So, either of the two, equation (2.4.4) or equation (2.4.5) can be used as the governing equation for the MT boundary value problem. In the present work equation (2.4.4) is used for computing electric fields and then magnetic fields are computed using equation (2.4.2).

### 2.4.2 Primary and Secondary Formulation

To solve the governing differential equation (2.4.4) primary and secondary field formulation is used. Hence, total electric field  $\mathbf{E}$  is viewed as a superposition of the primary and secondary fields as

$$\mathbf{E} = \mathbf{E}_p + \mathbf{E}_s. \quad (2.4.6)$$

Here, subscripts 'p' and 's' denote normal (primary) and anomalous (secondary) fields respectively. The normal field is the response of a simplified model whose response can be computed easily while the anomalous field is the response of the anomalous bodies or inhomogeneities present in the simplified model. For example, as shown in Fig. 2.2,

the 2-D model consisting of a buried body in a layered earth can be viewed as if a body of anomalous conductivity is superimposed over the normal layered earth model.

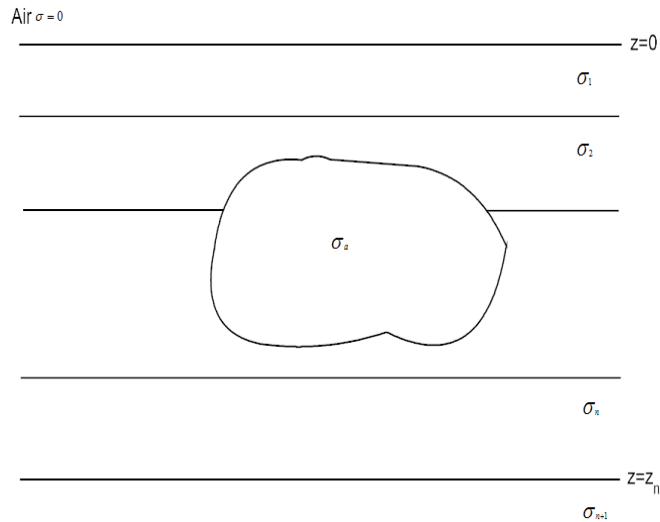


Figure 2.2: Target buried in layered earth

The conductivity at a point,  $\sigma$ , is the sum of the layer conductivity,  $\sigma_p$ , and the anomalous conductivity,  $\sigma_s$ , which is non-zero only in the body. Thus

$$\sigma = \sigma_p + \sigma_s . \quad (2.4.7)$$

On substituting these superposition relations (2.4.6 and 2.4.7) in equation (2.4.4), the equation can be partitioned into two equations for the primary and secondary electric fields as

$$\nabla \times \nabla \times \mathbf{E}_p + i\omega\mu_0\sigma_p\mathbf{E}_p = 0, \quad (2.4.8)$$

$$\nabla \times \nabla \times \mathbf{E}_s + i\omega\mu_0\sigma\mathbf{E}_s = -i\omega\mu_0\sigma_s\mathbf{E}_p. \quad (2.4.9)$$

The primary source fields have their origin in the electric currents blowing in and beyond the ionosphere which, in turn, arise from the complex interactions of solar radiations and plasma flux with the earth's magnetosphere and ionosphere. The primary field, the external inducing field due to source, is horizontal and laterally

uniform. As the source is treated as a plane wave incident normally on the earth, the domain of study can be treated as source free and the effect of source is accounted through the boundary conditions.

Finally, equations (2.4.8) and (2.4.9) are the governing differential equations of the MT BVP. In order to complete the statement of a well posed MT BVP, the necessary and sufficient boundary conditions for the equations (2.4.8) and (2.4.9) must be specified.

## 2.5 Boundary Conditions

There are two types of boundary conditions first one is called ‘Interface Boundary Condition’, and is defined at the interface where discontinuity in electrical properties occurs within the domain of study and the second one is known as ‘Domain Boundary Condition’, and is defined at the domain boundary. The former are either explicitly applied or circumvented by defining appropriate smooth resistivity function at a point on the interface of different regions. The domain boundary conditions explain the asymptotic behaviour of field or its integrated effect on a boundary.

### 2.5.1 Interface Boundary Conditions

1. The tangential components of  $\mathbf{E}$  are continuous, i.e.

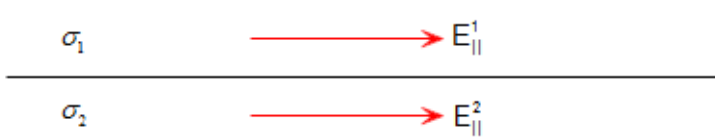
$$\hat{\mathbf{n}} \times (\mathbf{E}^1 - \mathbf{E}^2) = 0. \quad (2.5.1)$$


Figure 2.3: Interface boundary condition for tangential component of  $\mathbf{E}$

2. The tangential components of  $\mathbf{H}$  are discontinuous, the discontinuity being equal

to the surface current density  $\mathbf{J}_s$ , i.e

$$\hat{\mathbf{n}} \times (\mathbf{H}^1 - \mathbf{H}^2) = \mathbf{J}_s. \quad (2.5.2)$$

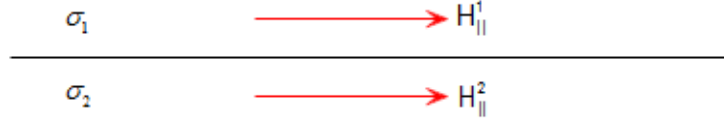


Figure 2.4: Interface boundary condition for tangential component of  $\mathbf{H}$

3. The normal components of  $\mathbf{E}$  are discontinuous, the discontinuity being equal to the surface charge density  $q_s/\epsilon$  i.e

$$\hat{\mathbf{n}} \cdot (\mathbf{E}^1 - \mathbf{E}^2) = q_s/\epsilon. \quad (2.5.3)$$

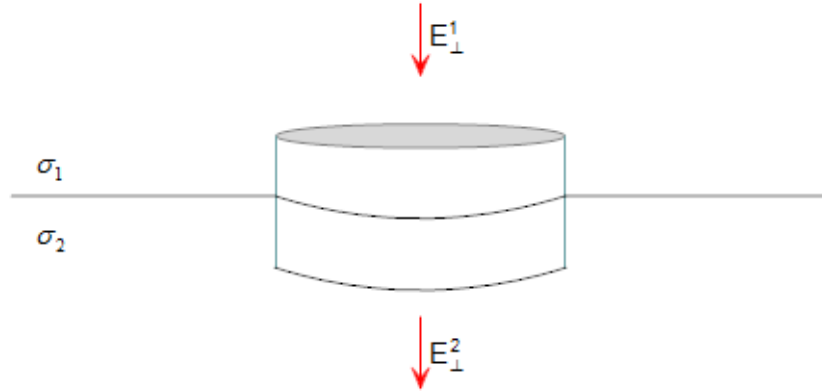


Figure 2.5: Interface boundary condition for perpendicular component of  $\mathbf{E}$

4. The normal components of  $\mathbf{H}$  are continuous, i.e.

$$\hat{\mathbf{n}} \cdot (\mathbf{H}^1 - \mathbf{H}^2) = 0. \quad (2.5.4)$$

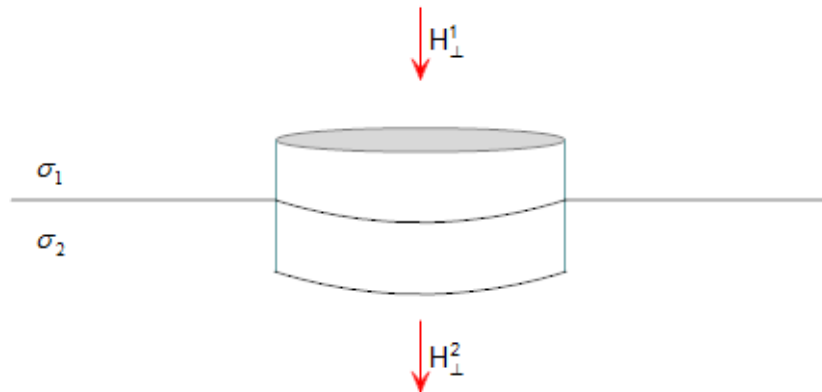


Figure 2.6: Interface boundary condition for perpendicular component of  $\mathbf{H}$

In the presented work, the interface boundary conditions are circumvented by defining the volume weighted average of conductivity at the grid points, where field values are computed.

## 2.5.2 Domain Boundary Conditions

These boundary conditions are applied on the bounding surfaces of the domain. One can apply either Dirichlet or Neumann or mixed boundary conditions (BCs). Dirichlet BC means that the EM field variable values are known at the boundary, while Neumann BC means that the normal derivative of fields is known at the boundary. The mixed BC means that a linear superposition of the field variable and its normal derivative is known.

We would apply Dirichlet boundary conditions at the four vertical side surfaces of the solution domain. The bottom boundary surface is assumed to be underlain by a perfectly conducting halfspace.

## 2.6 Response Functions

The solution of the BVP provides the electric field values. The obtained electric field values can be transformed into magnetic field components by using appropriate Maxwell's equations. These field values recorded at the surface of the earth are the observations/data for the inverse problem. Since observations do not directly reflect the effect of changes in the physical property, i.e. electrical resistivity in a perceptible manner, derived observables (response functions) are obtained from these. Although these response functions do not give a direct functional relationship with the subsurface resistivity, yet these do reflect the bulk information about the resistivity structure. The explicit relations between several response functions and the field component values are available in literature (Cagniard [23], Schmucker [121]).

The choice of response function is governed by the aim of study, whether the interest

lies in lateral or vertical variation of resistivity. The spatial variation of resistivity can be studied in two modes. First is profiling, where, for a given frequency, the observations are taken at points along a profile. Second is sounding, where, for different frequencies the observations are taken at a single point. Profiling gives information about lateral variations while sounding gives the information about vertical variations of resistivity. To discover lateral variations at different depth levels, soundings must be performed at several points along a profile or alternatively profiling must be carried out at different frequencies.

The details about these methods and their applications are available in standard references like Kaufman and Keller [58], Berdichevskii et al. [13], Nabighian [88, 89] and Vozoff [150].

The geoelectromagnetic methods use the natural earth's magnetic field with time periods ranging from fraction of a second to several years or the frequency ranging from  $10^{-5}$  Hz to  $10^4$  Hz. The variations in the period ranging from 10 min to 24 hour are particularly suited for mapping electrical inhomogeneities in earth's crust and upper mantle. The MT method employs the ratio of different field components as response functions. These functions are independent of strength of the primary signal and are dependent only on the electrical properties of the earth. In MT, the response function, impedance, is the ratio of horizontal and mutually perpendicular electric and magnetic field components.

### **2.6.1 MT Response Functions**

The magnetotelluric method was first described by Tikhonov [142] and Cagniard [23] independently. Using the assumption of a plane wave source, the ratio of observed

horizontal electric field ( $E_x$  or  $E_y$ ) and the orthogonal magnetic field component ( $H_y$  or  $H_x$ ), is called the impedance;

$$Z = \frac{E_x}{H_y} = -\frac{E_y}{H_x}. \quad (2.6.1)$$

The impedance values are used to define the commonly used MT response function as apparent resistivity, which may be defined as the resistivity of equivalent fictitious half space. The apparent resistivity,  $\rho_a$ , and the impedance phase,  $\phi$ , are respectively given by the relation

$$\rho_a = \frac{1}{\omega\mu_0} |Z|^2, \quad (2.6.2)$$

and

$$\phi = \tan^{-1} \left\{ \frac{\text{Im}(Z)}{\text{Re}(Z)} \right\}. \quad (2.6.3)$$

For a homogeneous half space, phase is always  $45^\circ$ . For a conductive body in half space phase is in the range  $45^\circ - 90^\circ$ , while for a resistive body it is in the range  $0^\circ - 45^\circ$ .

The variation of resistivity in the earth is rarely one-dimensional, therefore above definition of apparent resistivity and phase has only limited utility. To describe higher dimensionality or anisotropy, Cantwell [24] introduced a rank 2 impedance tensor ( $\mathbf{Z}$ ). The MT impedance tensor ' $\mathbf{Z}$ ' describes the linear relation between horizontal electric and magnetic field components.  $\mathbf{Z}$  can be written as

$$\begin{pmatrix} E_x \\ E_y \end{pmatrix} = \begin{Bmatrix} Z_{xx} & Z_{xy} \\ Z_{yx} & Z_{yy} \end{Bmatrix} \begin{bmatrix} H_x \\ H_y \end{bmatrix}. \quad (2.6.4)$$

The electric field components are calculated for a current system which flows in N-S (first mode) or in E-W (second mode) direction. To obtain the same electric field components, however, for another orientation of the current system, we can rotate the model by  $90^\circ$ , to construct the equations system (2.52) and solving it again for

x (Weaver [157]). The need for computing the electric field components using two orientations of the current system is based on the fact that the model responses in 3D MT are the full impedance tensor. Thus, to construct the full impedance tensor we need two orientations of current system and hence, the equation (2.6.4) can be rewritten as

$$\begin{pmatrix} E_{x1} & E_{x2} \\ E_{y1} & E_{y2} \end{pmatrix} = \begin{Bmatrix} Z_{xx} & Z_{xy} \\ Z_{yx} & Z_{yy} \end{Bmatrix} \begin{bmatrix} H_{x1} & H_{x2} \\ H_{y1} & H_{y2} \end{bmatrix}, \quad (2.6.5)$$

where subscripts 1 and 2 indicate two polarizations respectively. Further, the complex impedance tensor ( $\mathbf{Z}$ ) in equation (2.6.5) can be converted into apparent resistivity and phase as

$$\rho_{ij} = \frac{1}{\omega\mu_0} |Z_{ij}|^2, \quad (2.6.6)$$

$$\phi_{ij} = \tan^{-1}\{Im(Z_{ij})/Re(Z_{ij})\}. \quad (2.6.7)$$

## 2.7 Solution of Boundary Value Problem

The governing partial differential equations (2.4.8 and 2.4.9) along with the boundary conditions define the complete MT BVP. Analytic solution of 3D MT problem does not exist, hence, the problem is solved using numerical methods. Any numerical method transforms the MT BVP to a system of linear equations (matrix equation) as

$$\mathbf{A}\mathbf{E}_s = \mathbf{b}, \quad (2.7.1)$$

where  $\mathbf{A}$  is the system matrix whose sparsity structure depends on the numerical method used,  $\mathbf{E}_s$  is a vector containing unknown internal secondary electric fields, and  $\mathbf{b}$  is obtained from boundary conditions. Now, matrix equation (2.7.1) is solved using iterative matrix solver method.



### 2.7.1 Static Divergence Correction

The main problem while solving equation 2.7.1 is that at long periods, i.e.,  $\omega \rightarrow 0$  or in the region where  $\sigma = 0$ , the condition of current conservation ( $\nabla \cdot \mathbf{E}$ ) is not satisfied due to the computational round off errors in the iterative process. To this effect the equation (2.7.2) is not satisfied.

$$\begin{aligned} i\omega\mu_0 \nabla \cdot (\sigma \mathbf{E}_s) &= \nabla \cdot (-i\omega\mu_0\sigma_s \mathbf{E}_p), \\ \nabla \cdot (\sigma \mathbf{E}_s) &= -\frac{i}{\omega\mu_0} \nabla \cdot \mathbf{b}. \end{aligned} \quad (2.7.2)$$

Thus, to get rid of this problem, following Smith [134] the gradient of an unknown scalar  $\phi$  is added to the iterative solution ( $\mathbf{E}_s^n$ ) after  $n^{th}$  iteration. Now, the corrected electric field  $\mathbf{E}_s^C = \mathbf{E}_s^n + \nabla\phi$  satisfy the equation

$$\nabla \cdot (\sigma \mathbf{E}_s^C) = -\frac{i}{\omega\mu_0} \mathbf{b}. \quad (2.7.3)$$

The unknown scalar  $\phi$  is calculated by solving the scalar boundary value problem

$$\nabla \cdot (\sigma \nabla \phi) = -\frac{i}{\omega\mu_0} \nabla \cdot \mathbf{b} - \nabla \cdot (\sigma \mathbf{E}_s^n), \quad (2.7.4)$$

with the boundary condition  $\phi|_{bound} = 0$ .

## 2.8 Closure

The governing differential equations along with the boundary conditions define an EM boundary value problem which is solved using some numerical technique. The solution of this BVP provides the field values which do not contain direct information about the resistivity structure of earth, therefore, response functions are derived from these field values. The derived response functions are then used as data for inversion as

discussed in Chapter 3. The complete details of numerical method implementation while developing **3DINV\_FD** algorithm are discussed in Chapter 4.



# FORMULATION OF MAGNETOTELLURIC INVERSE PROBLEM

### 3.1 Introduction

Data inversion is an educated interpretation exercise where the ultimate goal is to provide a mathematical framework to transform measured data from the data space to the model space in order to estimate model parameters. Solving such inverse problems arises in many branches of the medical, physical and geophysical sciences. It is more objective than the quantitative data interpretation where interest is in a model whose computed response fits the observed response. In geophysics, solving the inverse problem is aimed to determine the structure of the earth. Depending on which geophysical method is used, the structure of the earth can be explained by the distribution of the electrical resistivity (geoelectric and electromagnetic methods), acoustic velocity (seismic method), density (gravitational method), etc. These physical

properties of the rocks give information of the geological formations, which define the structure of the earth.

The aim of geophysical inversion is not only to deduce, from a given set of observations, as much information about the earth system as possible, but also to evaluate the quality of inference together with its level of confidence. For doing parametric inversion, the system is defined in terms of the data and an operator. The latter is described by physics of the problem and distribution of physical parameters of the model. The inter-relationship of data and operator governs the system characteristics.

For the case of MT methods, resistivity within the earth is a function  $\rho(x,y,z)$ . As a result, in general, infinite parameters are required to describe it precisely (Parker [101]). The retrieval of general 3D variation of resistivity, from the 2-D data procured over the air-earth surface, is not viable. Moreover, the observations will always be finite in number, consequently, the MT inverse problem becomes a grossly underdetermined one. This infers that there may exist an infinite number of models whose response will match the observed data equally well. Such a case is termed as 'non-uniqueness'.

In practice, there is natural, observational and instrumental noise in the observations. These noisy observations may lead to inconsistency and instability in the system. The inconsistency arises as a result of incompatibility of the chosen model with the noisy data set. For an inconsistent system, the exact solution does not exist. The instability is a characteristic of the operator which gets highlighted in the presence of erroneous data. Due to instability, small errors in data may lead to large errors in estimated parameters. Therefore, the non-uniqueness, inconsistency and instability of the inverse problem suggest that the system under study is a degenerate one.

On every count, suggested by Hadamard [48] to define a well-posed problem, the MT inverse problem is an ill-posed one due to insufficient and inaccurate data (Jackson [55]). The goal of data inversion is to design algorithms which can mitigate this ill-posedness and provide reasonable solution of such problems. Some of the techniques, used for this purpose, are discussed here.

## 3.2 Mitigation of Ill-posedness

The exact solution of an ill-posed EM inverse problem does not exist. If it is so, the next best step is to look for schemes which can provide an approximate solution having essential features of the exact solution. In such schemes an attempt is made to regularize the problem. For regularization the ill-posed problem is replaced by an equivalent well-posed one which possesses a solution that can be treated as an approximate but reasonable solution of the original problem. Techniques used for the regularization are widely discussed in literature, particularly in the standard references like Backus and Gilbert [9, 8], Sabatier [116], Parker and Whaler [102], Oldenburg [98], Raiche [107], Meju [80], Oldenburg [99], Tarantola [138], Menke [81], Twomey [147], Tikhonov and Arsenin [143], Parker [100], Newman and Hoversten [95], Zhdanov [164], Newman and Boggs [93], Zhdanov [165] and Abubakar et al. [1]. A good review of the techniques used for solving EM inverse problem is given by Sarkar et al. [117], Avdeev [4], Abubakar et al. [2] and Siripunvaraporn [125].

Various schemes developed for solving ill-posed problem are, in general, introduced in matrix notations. For a given problem, let  $n$  and  $p$  be the number of observations and unknown parameters respectively. The inverse problem can be expressed in matrix

form as

$$\mathbf{G}\mathbf{P} = \mathbf{D}. \quad (3.2.1)$$

Here,  $\mathbf{G}$  is the  $n \times p$  coefficient matrix which simulates physics of the problem,  $\mathbf{P}$  is the  $p \times 1$  unknown parameter vector and  $\mathbf{D}$  is the  $n \times 1$  known observation vector. The equation (3.2.1) can be interpreted as the mapping, by the matrix operator  $\mathbf{G}$ , of a  $p$ -dimensional parameter vector  $\mathbf{P}$  to the  $n$ -dimensional data vector  $\mathbf{D}$ . The solution of this problem seeks the operator  $\hat{\mathbf{G}}^{-1}$  which would map the right hand side vector  $\mathbf{D}$  to an  $p$ -dimensional vector  $\mathbf{P}$  as

$$\mathbf{P} = \hat{\mathbf{G}}^{-1}\mathbf{D}. \quad (3.2.2)$$

The inverse problem can be solved when its inconsistency, non-uniqueness and instability are controlled. These negative characteristics of the system may exist either concurrently or one at a time. The means that can be employed to handle these features are discussed one by one.

### 3.2.1 Inconsistency

The inconsistency present in a system is basically an interplay of the coefficient matrix  $\mathbf{G}$  and the data vector  $\mathbf{D}$ . If the vector  $\mathbf{D}$  can not be expressed as a linear superposition of the column vectors of the matrix  $\mathbf{G}$  then inconsistency arises. To handle it, all one can do is to lower the acceptance level or quality of acceptable solution.

### 3.2.2 Non-uniqueness

The quality of inversion largely depends on parametrization, i.e. on the choice of model parameters and the derived data needed to represent the model. The choice of model is always made on the basis of a priori information. The a priori knowledge in EM

data inversion is derived from the geological information or from the results of other geophysical methods. This helps in better approximation of real earth models and, in turn, in improved interpretation (Jackson [56], Whittall [159]). The non-uniqueness of EM inverse problem can be rendered by restricting the complexity of earth models. A class of simplified models, like a layered earth or the regular well shaped body, can be used as an approximation of the real structures. The parametrization of real earth in terms of finite dimensional models helps in reducing the non-uniqueness.

### **3.2.3 Instability**

The instability in a system implies that small changes in data may lead to large changes in parameter values. Basically, the root cause of instability is ill-conditioning of the coefficient matrix. An ill-conditioned matrix has a large condition number, defined as the ratio of the largest to smallest eigenvalue. It may be emphasized here that although instability is inherent in the system, yet it is reflected only in the presence of errors in computations and/or data.

In geoelectromagnetics, the equivalence is a commonly encountered problem for layered earth models. Under equivalence, one can not determine the layer resistivity and thickness independently, however, their product can accurately be estimated. Due to this layer parameter coupling, the poor resolvability of individual parameters leads to instability. However, the resolution of product itself, which represents a bulk parameter, reduces both the non-uniqueness and instability.

Some of these measures of alleviating ill-posedness of the inverse problem have been employed in the formulations of the 3D MT inverse problem presented here.



### 3.3 Types of Inverse Problems

The rank,  $k$ , is defined as the maximum number of independent rows or columns of the matrix. The system defined by equation (3.2.1) can be classified on the basis of rank of the matrix  $\mathbf{G}$ .

1. If the rank ' $k$ ' is equal to the minimum of  $n$  and  $p$ , i.e.

$$k = \min (n,p),$$

the system is called 'full ranked'.

2. If the rank ' $k$ ' is less than the minimum of  $n$  and  $p$ , i.e.

$$k < \min (n,p),$$

the system is called 'rank deficient'.

An alternative classification of the system (3.2.1) can be given in terms of the relative values of  $m$  and  $n$ . The categorisation can be listed as

1. Evendetermined if  $n = p$ ,
2. Overdetermined if  $n > p$  and
3. Underdetermined if  $n < p$ .

For a full ranked system the evendetermined, overdetermined and underdetermined cases are termed as 'evendetermined', 'perfectly overdetermined' and 'perfectly underdetermined' respectively. Since the exact solution exists only for the perfectly evendetermined case, one has to look for approximate solutions for the remaining cases. For the perfectly overdetermined and underdetermined cases, operationally one has to look for operators which can transform the rectangular coefficient matrix to a full

ranked square one. Instead of listing the operational steps of various inverses, the logical sequence of obtaining these inverses is presented here.

### 3.3.1 Least Square Inverse

A perfectly overdetermined system may suffer from inconsistency. The inconsistency may be ascertained by determining the rank of augmented matrix  $[\mathbf{G} \mid \mathbf{D}]$ . If it is smaller than the rank of matrix  $\mathbf{G}$  then the system is inconsistent. In such a case, instead of looking for zero misfit, a minimum error solution is sought. The model parameter vector, which minimizes the misfit between the model response and the observations, is accepted as the desired solution. For this purpose, the norm,  $\Phi_l$  of the residual vector,  $\mathbf{r}$ , is minimized. This minimization problem can be stated as

$$\text{minimize } \Phi_l = \mathbf{r}^T \mathbf{r}, \quad (3.3.1)$$

$$\text{where } \mathbf{r} = \mathbf{D} - \mathbf{G}\mathbf{P}. \quad (3.3.2)$$

The least square solution of equation (3.2.1), obtained by minimization of  $\Phi$ , with respect to the unknown vector  $\mathbf{P}$ , can be written as

$$\mathbf{P} = \hat{\mathbf{G}}_l^{-1} \mathbf{D}, \quad (3.3.3)$$

$$\text{where } \hat{\mathbf{G}}_l^{-1} = (\mathbf{G}^T \mathbf{G})^{-1} \mathbf{G}^T. \quad (3.3.4)$$

The operator  $\hat{\mathbf{G}}_l$  is termed as ‘Least Square Inverse’ of matrix  $\mathbf{G}$  and the superscript T and -1 stand for the matrix transpose and inverse operations respectively. Generally the  $L_2$  norm is used as it results in a linear system of equations. Further, it produces the best estimate when the error in data follows Gaussian distribution. It may be emphasized again that the least square solution is a consequence of lowering the acceptable level for accuracy of the solution.

### 3.3.2 Minimum Norm Inverse

For the perfectly underdetermined system, the observations do not provide enough information for unique determination of all the model parameters. As a result, an infinity of solutions will exist for such a system. Therefore, some extraneous constraints need be applied to seek a unique solution. For this purpose, the length  $\Phi_m$  of the solution vector  $\mathbf{x}$  is commonly minimized, subject to the constraint that the solution satisfies the matrix equation (3.2.1). This constrained minimization problem can be stated as

$$\text{minimize } \Phi_m = \mathbf{P}^T \mathbf{P}, \quad (3.3.5)$$

$$\text{such that } \mathbf{P} \text{ satisfy, } \mathbf{G}\mathbf{P} = \mathbf{D}. \quad (3.3.6)$$

The minimum norm solution is obtained as

$$\mathbf{P} = \hat{\mathbf{G}}_m^{-1} \mathbf{D}, \quad (3.3.7)$$

$$\text{where } \hat{\mathbf{G}}_m^{-1} = \mathbf{G}^T (\mathbf{G}\mathbf{G}^T)^{-1}. \quad (3.3.8)$$

The operator  $\hat{\mathbf{G}}_m^{-1}$  is the 'Minimum Norm Inverse' of matrix  $\mathbf{G}$ . For the constrained minimization of the objective function,  $\Phi_m$ , the Lagrange's method of undetermined multipliers is used. The obtained solution is unique with respect to the chosen objective function.

### 3.3.3 Regularized Inverse

The above two solutions exist only for the full ranked systems for which the respective coefficient matrix products,  $\mathbf{G}^T \mathbf{G}$  and  $\mathbf{G}\mathbf{G}^T$ , appearing in their definitions, are non-singular.

A rank deficient system is overdetermined or underdetermined, depending upon the values of  $n$  and  $p$ . However, inherently it is underdetermined as  $k < p$ . As a result, the inverse problem is neither completely overdetermined nor completely underdetermined. It may be termed as a 'mixed determined' problem for which one can neither seek the least square nor the minimum norm solution. For its solution, a new objective function,  $\Phi_r$  is defined, which is a combination of the norms of misfit and solution vectors, This regularized inverse problem is defined as

$$\begin{aligned} \text{minimize } \Phi_r &= \varepsilon\Phi_l + (1 - \varepsilon)\Phi_m \text{ i.e.,} \\ \Phi_r &= \varepsilon(\mathbf{r}^T \mathbf{r}) + (1 - \varepsilon)(\mathbf{P}^T \mathbf{P}). \end{aligned} \quad (3.3.9)$$

In equation (3.3.9),  $\varepsilon$  is a trade-off parameter that determines the relative weight being given to minimization of misfit or solution vector norms.  $\varepsilon$  lies between 0 and 1, leading to the minimum norm and the least square solutions for the two extreme values respectively. The objective function (3.10) can be rewritten as

$$\Phi_{rl} = (\mathbf{r}^T \mathbf{r}) + \lambda^2(\mathbf{P}^T \mathbf{P}), \quad (3.3.10)$$

or

$$\Phi_{rm} = v^2(\mathbf{r}^T \mathbf{r}) + (\mathbf{P}^T \mathbf{P}), \quad (3.3.11)$$

where  $\lambda^2 = \frac{1 - \varepsilon}{\varepsilon}$  and  $v^2 = \frac{\varepsilon}{1 - \varepsilon}$ .

Equation (3.2.1), when solved using either of these objective functions, provides a solution for the overdetermined and underdetermined cases respectively, as

$$\mathbf{P} = (\mathbf{G}^T \mathbf{G} + \lambda^2 \mathbf{I})^{-1} \mathbf{G}^T \mathbf{D}, \quad (3.3.12)$$

or

$$\mathbf{P} = \mathbf{G}^T (\mathbf{G} \mathbf{G}^T + v^2 \mathbf{I})^{-1} \mathbf{D}. \quad (3.3.13)$$

In the above expressions the parameter  $\lambda$  or  $\nu$  play the role of a damping factor which prevents the unbounded oscillations in the solution. Therefore, the method is also known as 'Damped Least Square' or 'Damped Minimum Norm' method. This method was independently developed by Tikhonov, Phillips, Twomey and Marquardt in early sixties and is popularly known as 'Ridge-regression' or 'Marquardt method' in geophysical literature with  $\lambda$  or  $\nu$  being termed 'Marquardt parameter' (Marquardt [78]).

The ridge-regression method can also be used for full rank systems when the coefficient matrix is ill-conditioned. The impact of small eigenvalues gets reduced by the addition of Marquardt parameter  $\lambda$  or  $\nu$  to these. The enhanced eigenvalues result in improved stability.

### 3.3.4 Weighted Inverse

Some observations are, in general, more accurate than the others. This a priori knowledge can be used in assigning weights to scale the observations accordingly. The more accurate observations will be assigned higher weights in comparison to the less accurate ones. The model parameters can be obtained by introducing weighting matrices,  $\mathbf{W}_r$  for misfit and  $\mathbf{W}_m$  for solution respectively. The inverse of data error co-variance matrix, whenever available, is the most widely used weighting matrix  $W_r$ . If not available, one may employ a diagonal matrix with inverse of data errors as the diagonal entries. The  $W_m$  is constructed on the basis of the smoothness or other constraints imposed on the solution vector. The new objective functions, weighted

misfit or weighted length, are respectively defined as

$$\Phi_{wl} = \mathbf{r}^T \mathbf{W}_r \mathbf{r}, \quad (3.3.14)$$

or

$$\Phi_{wm} = \mathbf{P}^T \mathbf{W}_m \mathbf{P}. \quad (3.3.15)$$

The solution corresponding to these objective functions, termed as the 'weighted least square' and the 'weighted minimum norm', are given as

$$\mathbf{P} = (\mathbf{G}^T \mathbf{W}_r \mathbf{G})^{-1} \mathbf{G}^T \mathbf{W}_r \mathbf{D}, \quad (3.3.16)$$

and

$$\mathbf{P} = \mathbf{W}_m \mathbf{G}^T (\mathbf{G} \mathbf{W}_m \mathbf{G}^T)^{-1} \mathbf{D}. \quad (3.3.17)$$

Analogous to the weighted least square and weighted minimum norm solutions for the perfectly overdetermined and underdetermined cases, the weighting can also be applied to the regularized inverse case. The solutions for these two cases, depending on the values of n and p, will be

$$\mathbf{P} = (\mathbf{G}^T \mathbf{W}_r \mathbf{G} + \lambda^2 \mathbf{W}_m)^{-1} \mathbf{G}^T \mathbf{W}_r \mathbf{D}, \quad (3.3.18)$$

or

$$\mathbf{P} = \mathbf{W}_m^{-1} \mathbf{G}^T (\mathbf{G} \mathbf{W}_m^{-1} \mathbf{G}^T + \lambda^2 \mathbf{W}_r^{-1})^{-1} \mathbf{D}. \quad (3.3.19)$$

The special smoothness features desired in solution can be achieved by minimizing the norm of higher order differences of x components. Higher the order of difference, smoother the solution. The trade-off then is between smoothness and finer details of the solution. For example, in Occam's inversion, the norm of first order differences are minimized (Constable et al. [29]). Tikhonov regularization provides the flexibility that any a priori knowledge of system can also be translated in terms of a function and

used as a constraint. All these inverses are termed as 'generalized inverses' of matrix  $\mathbf{G}$  (Rao and Mitra [108]). The approach adopted to solve the 3D MT inverse problem in the present work is discussed next.

### 3.4 3D MT Inverse Problem Solution

The electric and magnetic field values, and therefore the response functions derived from them, are non-linear functions of resistivity. Hence, the inverse problem, which is evaluation of model resistivity parameters from a given set of observations, is a non-linear problem. The most common and widespread inversion approaches can be classified in two main categories:

1. Quasi-linearized inversion: A non linear function mapping the model parameters from model space to data space (the forward modeling operator) is first linearized before the inverse problem is solved.(Broyden [20], Zhdanov et al. [166], Lin et al. [70], Li et al. [69])
2. Non linear inversion: The inverse problem is solved directly using the non linear forward modelling operator.(McGillivray and Oldenburg [79], Commer and Newman [27, 28], Kelbert et al. [60])

Each of the above inversion schemes can be solved in model or in data space. In the present work, while developing the **3DINV\_FD** algorithm we have adopted the quasi-linearized inversion scheme in model space.

### 3.4.1 3DINV\_FD Algorithm: Linearized Inversion in Model Space

In MT we have some measured/synthetic data in form of horizontal and/or vertical transfer functions or apparent resistivities and phases for which we find model parameters (resistivities) that can explain the measured data. Before discussing the mathematical formulations for the inversion process, a few notations are set that will be used:

- The elements of data vector  $\mathbf{D}$  are the 'n' measured/synthetic data, i.e.

$$\mathbf{D} = [d_1, d_2, d_3, \dots, d_n]^T.$$

The n-dimensional data vector resides in the data space.

- The model  $\mathbf{P}$  we are seeking contains p model parameters and can be presented as

$$\mathbf{P} = [P_1, P_2, P_3, \dots, P_p]^T.$$

The p-dimensional model vector resides in the data space.

- Projecting a vector from model space to data space is accomplished by the forward modeling operator  $\mathbf{F}$ , which is function of  $\mathbf{P}$ . The operator  $\mathbf{F}(\mathbf{P})$  generates the synthetic data. The model parameter vector  $\mathbf{P}$  and the data vector  $\mathbf{D}$  are related to each other as:

$$\mathbf{F}(\mathbf{P}) = \mathbf{D} + \mathbf{e}.$$

We have approximated the original non-linear 3D MT inverse problem by a linear one, using quasi-linearization of the actual problem. Towards this end, the



field/response vector is expressed by its Taylor series around a parameter vector  $\mathbf{P}^k$  as

$$F^i(\mathbf{P}^a) = F^i(\mathbf{P}^k) + \sum_{j=1}^p \frac{\partial F^i}{\partial P_j^k} (P_j^a - P_j^k) + \frac{1}{2} \sum_{j=1}^p \sum_{l=1}^p \frac{\partial^2 F^i}{\partial P_j^k \partial P_l^k} (P_j^a - P_j^k)(P_l^a - P_l^k) + \dots$$

$$\text{where } i = 1, 2, 3, \dots, n. \quad (3.4.1)$$

Now, after writing equation (3.4.1) for all  $i$ , it can be written in matrix form as

$$\mathbf{F}(\mathbf{P}^a) = \mathbf{F}(\mathbf{P}^k) + \mathbf{J}^k \cdot \Delta \mathbf{P} + \frac{1}{2} \widehat{\Delta \mathbf{P}} \cdot \mathbf{H}^k \cdot \widetilde{\Delta \mathbf{P}} + \dots \quad (3.4.2)$$

Here,  $\mathbf{P}^a$ ,  $\mathbf{P}^k$ ,  $\mathbf{J}^k$  and  $\mathbf{H}^k$  are the true/actual parameter vector, guess model parameter vector, Jacobian and Hessian matrices respectively. As shown in equations (3.4.3 and 3.4.4), the elements of  $\mathbf{J}^k$  and  $\mathbf{H}^k$  are the first and second derivative of the calculated data with respect to the model parameters respectively

$$\mathbf{J}^k = \begin{pmatrix} \frac{\partial F^1(P^k)}{\partial P_1^k} & \frac{\partial F^1(P^k)}{\partial P_2^k} & \dots & \frac{\partial F^1(P^k)}{\partial P_p^k} \\ \frac{\partial F^2(P^k)}{\partial P_1^k} & \ddots & \dots & \vdots \\ \vdots & \dots & \ddots & \vdots \\ \frac{\partial F^n(P^k)}{\partial P_1^k} & \dots & \dots & \frac{\partial F^n(P^k)}{\partial P_p^k} \end{pmatrix}, \quad (3.4.3)$$

$$\mathbf{H}^k = \text{diag}\{\mathbf{H}^k_1, \mathbf{H}^k_2, \dots, \mathbf{H}^k_n\} \text{ where,}$$

$$\mathbf{H}^k_j = \begin{pmatrix} \frac{\partial^2 F^j(P^k)}{\partial P_1^k} & \frac{\partial^2 F^j(P^k)}{\partial P_1^k \partial P_2^k} & \dots & \frac{\partial^2 F^j(P^k)}{\partial P_1^k \partial P_p^k} \\ \frac{\partial^2 F^j(P^k)}{\partial P_2^k \partial P_1^k} & \ddots & \dots & \vdots \\ \vdots & \dots & \ddots & \vdots \\ \frac{\partial^2 F^j(P^k)}{\partial P_p^k \partial P_1^k} & \dots & \dots & \frac{\partial^2 F^j(P^k)}{\partial P_p^k} \end{pmatrix}. \quad (3.4.4)$$

For quasi - linearization, the guess model  $\mathbf{P}^k$  is assumed to be sufficiently close to the unknown true/actual parameter vector  $\mathbf{P}^a$ , so that only the linear terms of the parameter correction vector need be retained in the Taylor's series expansion, which

reduces equation (3.4.2) to

$$\mathbf{F}(\mathbf{P}^a) \approx \mathbf{F}(\mathbf{P}^k) + \mathbf{J}^k \cdot \Delta \mathbf{P}, \quad (3.4.5)$$

$$\mathbf{J}^k \cdot \Delta \mathbf{P} = \Delta \mathbf{R}, \quad (3.4.6)$$

Adding  $\mathbf{J}^k \cdot (\mathbf{P}^k - \mathbf{P}^0)$  on both sides, we get,

$$\mathbf{J}^k \cdot (\mathbf{P}^{k+1} - \mathbf{P}^0) = \Delta \mathbf{R} + \mathbf{J}^k \cdot (\mathbf{P}^k - \mathbf{P}^0). \quad (3.4.7)$$

Here,  $\mathbf{P}^0$  is the prior model. The equation (3.4.7) is the mathematical representation of our quasi - linearized inverse problem.

### 3.4.2 Optimization using Gauss-Newton with Conjugate Gradient Method

Now, for solving the MT inverse problem in equation (3.4.7), the function to be minimised is known as misfit-function, cost-function, objective function or penalty function (Tikhonov and Arsenin [143]),  $\psi(\mathbf{P}, \lambda)$ , is defined as:

$$\psi(\mathbf{P}, \lambda) = \psi_d(\mathbf{P}) + \lambda \psi_m(\mathbf{P}, \mathbf{P}^0), \quad (3.4.8)$$

where  $\psi_d$  defined as the scalar product of weighted misfit between observed data and predicted data, as given in the theory of Tikhonov, the penalty function has a regularization (stabilizer) part  $\psi_m$ . There are many ways of defining this stabilizer (see, for example, Farquharson and Oldenburg [36]). In the present work this regularization functional is defined to obtain smooth models, hence misfit  $\psi_d$  and regularization(stablizer) functional  $\psi_m$  are defined as

$$\psi_d(\mathbf{P}) = (\mathbf{D} - \mathbf{F}[\mathbf{P}])^T \mathbf{C}_d^{-1} (\mathbf{D} - \mathbf{F}[\mathbf{P}]), \quad (3.4.9)$$

$$\psi_m(\mathbf{P}, \mathbf{P}^0) = (\mathbf{P} - \mathbf{P}^0)^T \mathbf{C}_m^{-1} (\mathbf{P} - \mathbf{P}^0). \quad (3.4.10)$$

Using equations (3.4.9),(3.4.10) in equation (3.4.8), objective function becomes

$$\psi(\mathbf{P}, \lambda) = \{(\mathbf{D} - \mathbf{F}[\mathbf{P}])^T \mathbf{C}_d^{-1}(\mathbf{D} - \mathbf{F}[\mathbf{P}])\} + \lambda\{(\mathbf{P} - \mathbf{P}^0)^T \mathbf{C}_m^{-1}(\mathbf{P} - \mathbf{P}^0)\}, \quad (3.4.11)$$

where  $\mathbf{F}[\mathbf{P}]$  is the model response, the positive -definite matrix  $\mathbf{C}_d$  is a diagonal matrix with diagonal entries as variance of error in data, termed as data covariance matrix,  $\mathbf{C}_m$  is the model covariance matrix, and  $\lambda$  is the Lagrange multiplier or trade off parameter, controlling the stabilizer part.

The optimization of cost function defined, in equation 3.4.11, is nonlinear because model response is a nonlinear function of model parameters. We have used the Gauss-Newton with conjugate gradient(GN-CG) iterative method for solving optimization problem, which is based on quasi-linearization of the objective function. For the  $(k + 1)^{th}$  iteration, the forward response  $\mathbf{F}[\mathbf{P}_{k+1}]$  is expressed around the parameters obtained in  $k^{th}$  iteration by a Taylor series expansion and discarding the second or higher order derivatives as,

$$\mathbf{F}[\mathbf{P}_{k+1}] = \mathbf{F}[\mathbf{P}_k + \Delta\mathbf{P}] = \mathbf{F}[\mathbf{P}_k] + \mathbf{J}_k(\mathbf{P}_{k+1} - \mathbf{P}_k), \quad (3.4.12)$$

where the subscript k in the equation is the iteration number,  $\mathbf{J}_k$  is the Jacobian matrix defined in equation (3.4.22). By using equation (3.4.12) in (3.4.11), the cost function becomes

$$\psi(\mathbf{P}_{k+1}, \lambda) = (\mathbf{D}' - \mathbf{J}_k \Delta\mathbf{P})^T \mathbf{C}_d^{-1}(\mathbf{D}' - \mathbf{J}_k \Delta\mathbf{P}) + \lambda(\mathbf{P}_k + \Delta\mathbf{P} - \mathbf{P}^0)^T \mathbf{C}_m^{-1}(\mathbf{P}_k + \Delta\mathbf{P} - \mathbf{P}^0), \quad (3.4.13)$$

where,

$$\mathbf{D}' = \mathbf{D} - \mathbf{F}[\mathbf{P}_k], \quad (3.4.14)$$

describes the misfit between observed/synthetic and calculated data and  $\Delta\mathbf{P}$  is given by

$$\mathbf{P}_{k+1} = \mathbf{P}_k + \Delta\mathbf{P}. \quad (3.4.15)$$

Now, the extremal stationary point (minimum or maximum) of the cost function  $\psi(\mathbf{P}, \lambda)$  can be found by taking the derivative of equation (3.4.13) with respect to  $\Delta\mathbf{P}$ , and setting the result equal to zero as

$$\begin{aligned} \frac{\partial\psi(\mathbf{P}_k + \Delta\mathbf{P}, \lambda)}{\partial\Delta\mathbf{P}} &= \frac{\partial}{\partial\Delta\mathbf{P}} [(\mathbf{D}' - \mathbf{J}_k\Delta\mathbf{P})^T \mathbf{C}_d^{-1} (\mathbf{D}' - \mathbf{J}_k\Delta\mathbf{P})] \\ &+ \frac{\partial}{\partial\Delta\mathbf{P}} [\lambda(\mathbf{P}_k + \Delta\mathbf{P} - \mathbf{P}^0)^T \mathbf{C}_m^{-1} (\mathbf{P}_k + \Delta\mathbf{P} - \mathbf{P}^0)] = 0 \\ &= \frac{\partial}{\partial\Delta\mathbf{P}} [\mathbf{D}'^T \mathbf{C}_d^{-1} \mathbf{D}' - \mathbf{D}'^T \mathbf{C}_d^{-1} \mathbf{J}_k \Delta\mathbf{P} - \Delta\mathbf{P}^T \mathbf{J}_k^T \mathbf{C}_d^{-1} \mathbf{D}' \\ &+ \Delta\mathbf{P}^T \mathbf{J}_k^T \mathbf{C}_d^{-1} \mathbf{J}_k \Delta\mathbf{P}] + \frac{\partial}{\partial\Delta\mathbf{P}} [\lambda \mathbf{P}_k^T \mathbf{C}_m^{-1} \mathbf{P}_k + 2\lambda \Delta\mathbf{P}^T \mathbf{C}_m^{-1} \mathbf{P}_k \\ &- 2\lambda \mathbf{P}_k^T \mathbf{C}_m^{-1} \mathbf{P}^0 - 2\lambda \Delta\mathbf{P}^T \mathbf{C}_m^{-1} \mathbf{P}^0 + \lambda \Delta\mathbf{P}^T \mathbf{C}_m^{-1} \Delta\mathbf{P} - \lambda \mathbf{P}^{0T} \mathbf{C}_m^{-1} \mathbf{P}^0] = 0 \\ &= 2\mathbf{J}_k^T \mathbf{C}_d^{-1} \mathbf{J}_k \Delta\mathbf{P} - 2\mathbf{J}_k^T \mathbf{C}_d^{-1} \mathbf{D}' + 2\lambda \mathbf{C}_m^{-1} [\mathbf{P}_k - \mathbf{P}^0 + \Delta\mathbf{P}] = 0 \\ &\equiv \mathbf{J}_k^T \mathbf{C}_d^{-1} \mathbf{J}_k \mathbf{P}_{k+1} - \mathbf{J}_k^T \mathbf{C}_d^{-1} \mathbf{J}_k \mathbf{P}_k + \lambda \mathbf{C}_m^{-1} (\mathbf{P}_{k+1} - \mathbf{P}^0) = \mathbf{J}_k^T \mathbf{C}_d^{-1} \mathbf{D}'. \end{aligned} \quad (3.4.16)$$

Now adding  $-\mathbf{J}_k^T \mathbf{C}_d^{-1} \mathbf{J}_k \mathbf{P}^0$  on both sides, in equation (3.4.16) we get

$$\begin{aligned} \mathbf{J}_k^T \mathbf{C}_d^{-1} \mathbf{J}_k (\mathbf{P}_{k+1} - \mathbf{P}^0) + \lambda \mathbf{C}_m^{-1} (\mathbf{P}_{k+1} - \mathbf{P}^0) &= \mathbf{J}_k^T \mathbf{C}_d^{-1} \{\mathbf{D}' + \mathbf{J}_k (\mathbf{P}_k - \mathbf{P}^0)\}, \\ \mathbf{P}_{k+1} &= (\mathbf{J}_k^T \mathbf{C}_d^{-1} \mathbf{J}_k + \lambda \mathbf{C}_m^{-1})^{-1} \mathbf{J}_k^T \mathbf{C}_d^{-1} \{\mathbf{D}' + \mathbf{J}_k (\mathbf{P}_k - \mathbf{P}^0)\} + \mathbf{P}^0. \end{aligned} \quad (3.4.17)$$

The iterative sequence of normal equations (3.4.17) is simply a matrix equation and is solved using iterative matrix solver to obtain the updated model parameters  $\mathbf{P}_{k+1}$ , which is used as the current model for next iteration. The equation (3.4.17) can be written in matrix form as

$$\mathbf{P}_{k+1} - \mathbf{P}^0 = \hat{\mathbf{G}}^{-1} \mathbf{r}, \quad (3.4.18)$$

where  $\hat{\mathbf{G}} = [\mathbf{J}_k^T \mathbf{C}_d^{-1} \mathbf{J}_k + \lambda \mathbf{C}_m^{-1}]$ , and

$$\mathbf{r} = \mathbf{J}_k^T \mathbf{C}_d^{-1} \{\mathbf{D}' + \mathbf{J}_k (\mathbf{P}_k - \mathbf{P}^0)\}.$$

From the inverse problem formulation, it is clear that the basic steps of each inversion iteration are the solution of forward problem and the generation of Jacobian matrix. Hence, for an efficient algorithm, saving in computational cost or storage in any of these steps can significantly improve the algorithm.

### 3.4.3 Calculation of Jacobian

The direct calculation of Jacobian ( $\mathbf{J}$ ) using finite differences

$$J_{ij} = \frac{F_i[P_1, \dots, P_j + \delta P_j, \dots, P_p] - F_i[P_1, \dots, P_j, \dots, P_p]}{\delta P_j}, \quad (3.4.19)$$

requires solution of  $p+1$  forward problems. In the approach for computing  $\mathbf{J}$ , selection of  $\delta P_j$  is very critical for the numerical stability of the inverse problem. To avoid this difficulty,  $\mathbf{J}$  can be computed by differentiating the forward problem equation (2.7.1) with respect to model parameter ( $\mathbf{P}$ ), we get

$$\mathbf{A} \frac{\partial \mathbf{E}}{\partial P_j} = -\frac{\partial \mathbf{A}}{\partial P_j} \mathbf{E}, \quad (3.4.20)$$

$$\mathbf{A} J_j = Y_j. \quad (3.4.21)$$

Writing equation 3.4.21 for all  $P_j$  ( $j=1,2,\dots,p$ ), we get

$$\mathbf{J} = \mathbf{A}^{-1} \mathbf{Y}, \quad (3.4.22)$$

where  $J_j = \frac{\partial \mathbf{E}}{\partial P_j}$  and  $Y_j = -\frac{\partial \mathbf{A}}{\partial P_j} \mathbf{E}$  are the  $j^{th}$  columns of matrices  $\mathbf{J}$  and  $\mathbf{Y}$  respectively. However, for large problems, where, the number of parameters 'p' is very large, it becomes computationally very costly and requires large memory for storage. The inverse problem solution can be speeded up significantly by avoiding the direct computation of Jacobian.

## 3.5 Closure

The solution of ill-posed MT inverse problem is obtained through regularization. The non-linear 3D inverse problem is solved iteratively by quasi-linearization. Numerical implementation of 3D forward and inverse problem in **3DINV\_FD** algorithm, based on finite difference method, is discussed next.



# NUMERICAL IMPLEMENTATION OF FINITE DIFFERENCE METHOD

## 4.1 Introduction

The MT data inversion algorithm efficiency crucially depends upon the accuracy and efficiency with which one can solve the forward problem. This, in effect, means getting solution of the boundary value problem. The analytical solution of the 3D partial differential equations, derived from Maxwell's equations does not exist. To overcome this limitation, numerical methods are used for modeling of 3D MT problems.

The complex real earth can be modeled using any one of the available numerical techniques that translate the partial differential equation into a matrix equation. These numerical methods can be grouped into two broad classes - Integral Equation Methods (IEMs) and Differential Equation Methods (DEMs). Both these classes have identified merits and demerits in terms of their respective applicability. Preference of one method over the other is dictated by the complexity of the model and the available computational resources.



In IEM, the integral operator is transformed, through quadrature formulae, to a matrix operator. Here, only the anomalous region is modeled. This results in a small but full coefficient matrix. In fact much of the earlier work in 3D modelling was done using IEM only (Weidelt [158], Wannamaker et al. [153, 154], Eaton [32], Wannamaker [152], Zhdanov and Fang [168] and Kaufman and Eaton [59]). However, inspite of these positive features the use of IEM is restricted to the modeling of confined bodies in a layered earth. It is so because this method is constrained by the necessity of efficient computation of Green's functions and the easily computable Green's functions exist only for the layered earth primary model.

The DEMs, Finite Element Method (FDM) or Finite Difference Method (FEM), are popular in simulating arbitrarily shaped geometries. In these methods the whole domain of study need be discretized. This results in a large but grossly sparse coefficient matrices. Earlier, their use was limited because of paucity of efficient large matrix solvers. Recent advances in iterative solution techniques have helped in establishing their superiority over IEM. In FEM differential operator is reduced to a matrix operator through a functional minimization. Moreover, FEM is very useful in solving problems with complex geometries having curved boundaries (Coggon [25], Reddy et al. [110], Wannamaker et al. [155], Travis and Chave [144], Livelybrooks [71] and Mogi [87]). The differential operator is reduced to a matrix operator through difference approximation in case of FDM. The mathematics of FDM is much simpler and easier to implement than that of FEM. In geophysics, where the main emphasis is on the solution of inverse problem, any inversion method would have limited resolution because of erroneous observations. Therefore, it may not be economically viable to model refined curved boundaries instead of the simple linear boundaries. Moreover, the matrix solvers for

FDM are more efficient than those commonly used for FEM.

Besides the methods belonging to the above two classes, there exist some Hybrid methods where positive features of IEM and DEM are amalgamated e.g. Vachirastienchai et al. [148], Rung-Arunwan and Siripunvaraporn [113]. But these methods are again applicable only to confined structures (Lee et al. [67]). The comparative studies of different numerical modeling methods is also available in the literature (Zhdanov et al. [167], Han et al. [49] among others).

Therefore, after looking in to merits and disadvantages of different numerical methods, in the present work FDM is used to solve the forward problem defined by equations (2.4.8) and (2.4.9).

## 4.2 Implementing Finite Difference Method

In FDM the derivatives of a function are replaced by the appropriate difference formula, obtained from the Taylor series expansion of the function as

First order derivative approximation:

$$\frac{\partial F(x, y, z)}{\partial x} \simeq \frac{F(x + \Delta x, y, z) - F(x, y, z)}{\Delta x}, \quad (4.2.1)$$

Second order derivative approximation:

$$\frac{\partial^2 F(x, y, z)}{\partial x^2} \simeq \frac{F(x + \Delta x, y, z)}{\Delta x^2} - \frac{2F(x, y, z)}{\Delta x^2} + \frac{F(x - \Delta x, y, z)}{\Delta x^2}. \quad (4.2.2)$$

The detailed explanation of FDM is available in the standard text e.g. Forsythe and Wasow [38], Hildebrand [52], Mitchell and Griffiths [85] and Tafflove et al. [137].

### 4.2.1 Staggered Grid

In order to implement the FDM for solving the forward problem defined by equations (2.4.8 and 2.4.9), the modeling domain is discretized into cells/cuboids by straight grid lines parallel to the three co-ordinate axes ( $\mathbf{X}, \mathbf{Y}, \mathbf{Z}$ ). In the present work, the staggered grid is used for implementing the FDM. The staggered grid was first used in electrical engineering problems by Yee [162], and now it is widely used in EM FDM modeling. In staggered grid implementation, the components of  $\mathbf{E}$  are defined at the center of cell edges and components of  $\mathbf{H}$  are defined at the center of cell faces as shown in Figure (4.1).

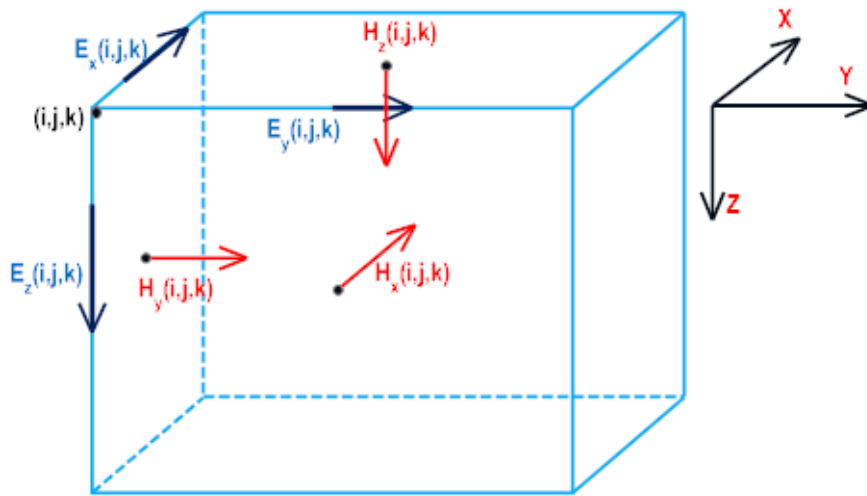


Figure 4.1: Staggered grid used for implementing FDM

The advantage of implementing staggered grid over normal grid where all six field components are defined at the nodes, is that in spite of computational roundoff errors  $\nabla \cdot \mathbf{H}$  is implicit zero. Thus the field computation is more accurate than those obtained from normal grid.

### 4.2.1.1 Grid Specifications

The number of cells in the grid are specified by  $nx$ ,  $ny$  and  $nz$  in  $\mathbf{X}$ ,  $\mathbf{Y}$  and  $\mathbf{Z}$  directions respectively. Conductivity of the cell  $(i,j,k)$  is represented as  $\sigma(i,j,k)$  and its volume as  $vol(i,j,k) = a(i).b(j).c(k)$ , where  $a(i)$ ,  $b(j)$  and  $c(k)$  are the distances between two adjacent nodes in  $\mathbf{X}$ ,  $\mathbf{Y}$  and  $\mathbf{Z}$  directions respectively (Figure 4.2). The edges of the cube are  $(x(i), x(i+1))$ ,  $(y(j), y(j+1))$  and  $(z(k), z(k+1))$ . The cell edge centers are defined as  $x_c(i)$ ,  $y_c(j)$  and  $z_c(k)$  with

$$\begin{aligned} x_c(i) &= \frac{x(i+1) + x(i)}{2}, \\ y_c(j) &= \frac{y(j+1) + y(j)}{2}, \\ z_c(k) &= \frac{z(k+1) + z(k)}{2}. \end{aligned} \quad (4.2.3)$$

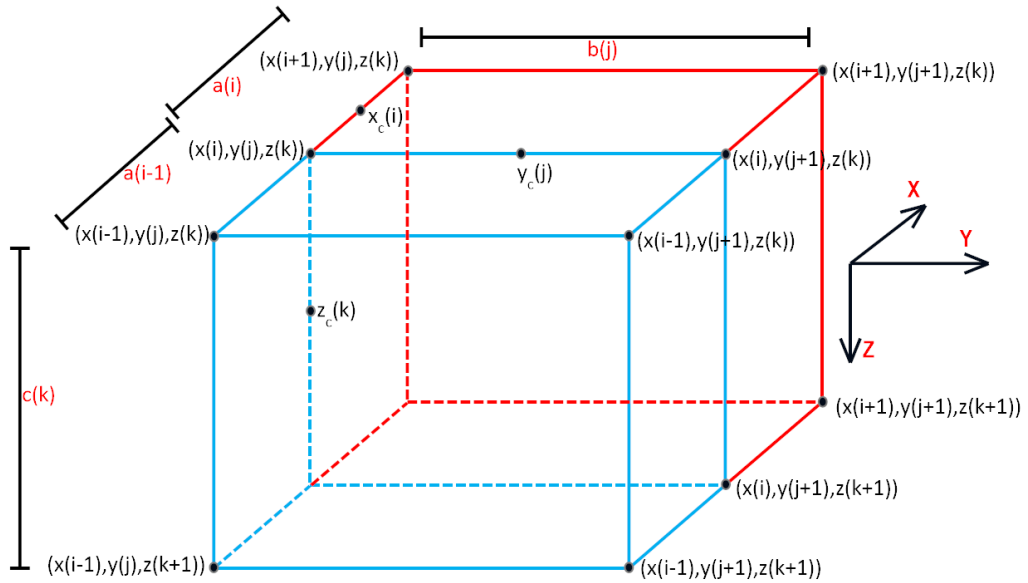


Figure 4.2: Staggered grid used for implementing FDM

## 4.2.2 Weighted Average Conductivity

While employing FDM to solve the problem, the spatial average of conductivity at a node is required (Brewitt-Taylor and Weaver [19]). The average conductivities,  $\sigma_x(i, j, k)$ ,  $\sigma_y(i, j, k)$  and  $\sigma_z(i, j, k)$  at the center of cell edges where electric field components,  $E_x(i, j, k)$ ,  $E_y(i, j, k)$  and  $E_z(i, j, k)$  are defined respectively, are computed as

$$\begin{aligned}
 \sigma_x(i, j, k) &= \frac{a(i)}{4.vol_x(i, j, k)} \left[ b(j-1)c(k-1)\sigma(i, j-1, k-1) + b(j)c(k-1)\sigma(i, j, k-1) \right. \\
 &\quad \left. + b(j-1)c(k)\sigma(i, j-1, k) + b(j)c(k)\sigma(i, j, k) \right], \\
 \sigma_y(i, j, k) &= \frac{b(j)}{4.vol_y(i, j, k)} \left[ a(i-1)c(k-1)\sigma(i-1, j, k-1) + a(i)c(k-1)\sigma(i, j, k-1) \right. \\
 &\quad \left. + a(i-1)c(k)\sigma(i-1, j, k) + a(i)c(k)\sigma(i, j, k) \right], \\
 \sigma_z(i, j, k) &= \frac{c(k)}{4.vol_z(i, j, k)} \left[ a(i-1)b(j-1)\sigma(i-1, j-1, k) + a(i)b(j-1)\sigma(i, j-1, k) \right. \\
 &\quad \left. + a(i-1)b(j)\sigma(i-1, j, k) + a(i)b(j)\sigma(i, j, k) \right]. \quad (4.2.4)
 \end{aligned}$$

Here,

$$\begin{aligned}
 vol_x(i, j, k) &= a(i)bh(j)ch(k), \\
 vol_y(i, j, k) &= ah(i)b(j)ch(k), \\
 vol_z(i, j, k) &= ah(i)bh(j)c(k), \quad (4.2.5)
 \end{aligned}$$

are volume of the prisms  $p_x$ ,  $p_y$  and  $p_z$  with conductivity  $\sigma_x$ ,  $\sigma_y$  and  $\sigma_z$  (Figures 4.3, 4.4 and 4.5) respectively.

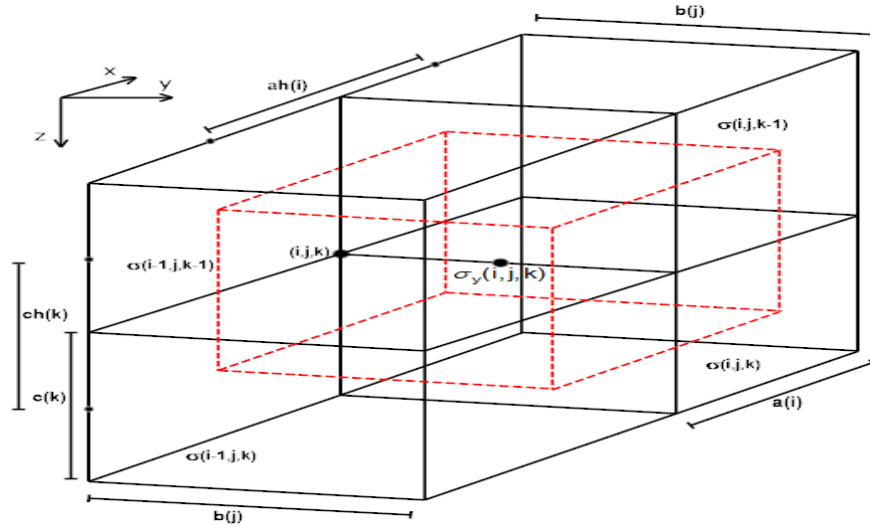


Figure 4.4: Grid cells and associated spacing parameters. The red dotted prism is of average conductivity  $\sigma_y(i, j, k)$

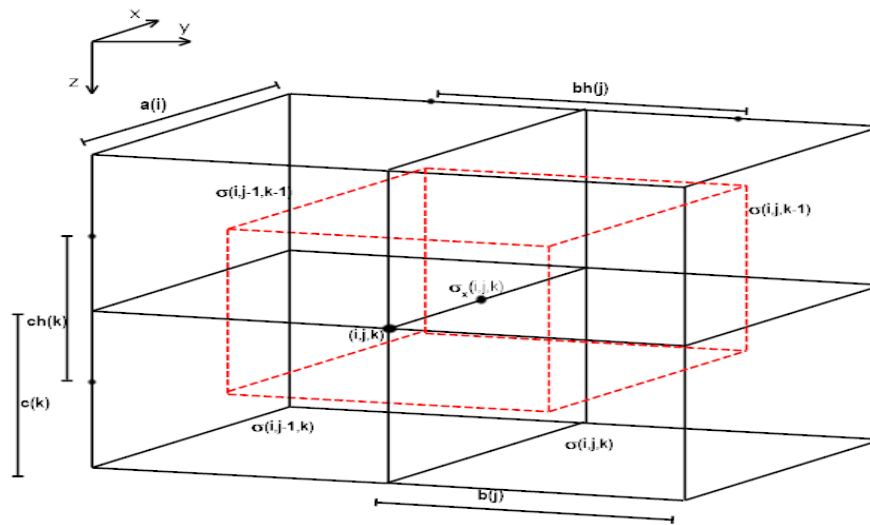


Figure 4.3: Grid cells and associated spacing parameters. The red dotted prism is of average conductivity  $\sigma_x(i, j, k)$

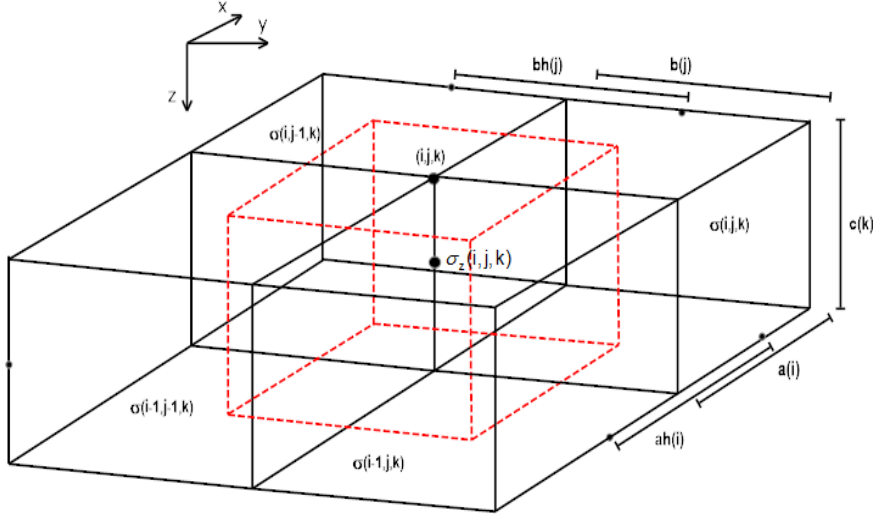


Figure 4.5: Grid cells and associated spacing parameters. The red dotted prism is of average conductivity  $\sigma_z(i, j, k)$

### 4.2.3 Staggered Finite Difference Equation

The system equation (2.4.9) for electric field components  $E_x^s, E_y^s$  and  $E_z^s$  approximated using the finite differences, for  $(i,j,k)$  cell can be written as

$$\begin{aligned}
& \left[ \frac{a(i)ch(k)}{b(j)} + \frac{a(i)ch(k)}{b(j-1)} + \frac{a(i)bh(j)}{c(k)} + \frac{a(i)bh(j)}{c(k-1)} + \omega\mu_0\sigma_x^{i,j,k}vol_x(i, j, k) \right] E_x^s(i, j, k) \\
& + \frac{a(i)ch(k)}{b(j-1)} E_x^s(i, j-1, k) + \frac{a(i)ch(k)}{b(j)} E_x^s(i, j+1, k) + \frac{a(i)bh(j)}{c(k-1)} E_x^s(i, j, k-1) \\
& + \frac{a(i)bh(j)}{c(k)} E_x^s(i, j, k+1) + ch(k)E_y^s(i, j-1, k) - ch(k)E_y^s(i+1, j-1, k) \\
& - ch(k)E_y^s(i, j, k) + ch(k)E_y^s(i+1, j, k) + bh(j)E_z^s(i, j, k-1) - bh(j)E_z^s(i+1, j, k-1) \\
& - bh(j)E_z^s(i, j, k) + bh(j)E_z^s(i+1, j, k) = -\omega\mu_0(\sigma_x^{i,j,k} - \sigma^p)vol_x(i, j, k)E_x^p(i, j, k),
\end{aligned} \tag{4.2.6}$$

$$\begin{aligned}
& \left[ \frac{ah(i)b(j)}{c(k)} + \frac{ah(i)b(j)}{c(k-1)} + \frac{b(j)ch(k)}{a(i)} + \frac{b(j)ch(k)}{a(i-1)} + \iota\omega\mu_0\sigma_y^{i,j,k}vol_y(i,j,k) \right] E_y^s(i,j,k) \\
& + \frac{ah(i)b(j)}{c(k-1)} E_y^s(i,j,k-1) + \frac{ah(i)b(j)}{c(k)} E_y^s(i,j,k+1) + \frac{b(j)ch(k)}{a(i-1)} E_y^s(i-1,j,k) \\
& + \frac{b(j)ch(k)}{a(i)} E_y^s(i+1,j,k) + ah(i)E_z^s(i,j,k-1) - ah(i)E_z^s(i,j+1,k-1) \\
& - ah(i)E_z^s(i,j,k) + ah(i)E_z^s(i,j+1,k) + ch(k)E_x^s(i-1,j,k) - ch(k)E_x^s(i-1,j+1,k) \\
& - ch(k)E_x^s(i,j,k) + ch(k)E_x^s(i,j+1,k) = -\iota\omega\mu_0(\sigma_y^{i,j,k} - \sigma^p)vol_y(i,j,k)E_y^p(i,j,k),
\end{aligned} \tag{4.2.7}$$

$$\begin{aligned}
& \left[ \frac{bh(j)c(k)}{a(i)} + \frac{bh(j)c(k)}{a(i-1)} + \frac{ah(i)c(k)}{b(j)} + \frac{ah(i)c(k)}{b(j-1)} + \iota\omega\mu_0\sigma_z^{i,j,k}vol_z(i,j,k) \right] E_z^s(i,j,k) \\
& + \frac{bh(j)c(k)}{a(i-1)} E_z^s(i-1,j,k) + \frac{bh(j)c(k)}{a(i)} E_z^s(i+1,j,k) + \frac{ah(i)c(k)}{b(j-1)} E_x^s(i,j-1,k) \\
& + \frac{ah(i)c(k)}{b(j)} E_x^s(i,j+1,k) + bh(j)E_x^s(i-1,j,k) - bh(j)E_x^s(i-1,j,k+1) \\
& - bh(j)E_x^s(i,j,k) + bh(j)E_x^s(i,j,k+1) + ah(i)E_y^s(i,j-1,k) - ah(i)E_y^s(i,j-1,k) \\
& - ah(i)E_y^s(i,j,k) + ah(i)E_y^s(i,j,k+1) = -\iota\omega\mu_0(\sigma_z^{i,j,k} - \sigma^p)vol_z(i,j,k)E_z^p(i,j,k).
\end{aligned} \tag{4.2.8}$$

Now, staggered finite difference (SFD) equations 4.2.6, 4.2.7 and 4.2.8 are written for all non-trivial components of electric field.

#### 4.2.3.1 System Matrix Description

After writing these FD approximation equations for all field components, these are assembled in form of a matrix equation as

$$\mathbf{E}^s = \mathbf{A}^{-1}\mathbf{b}. \tag{4.2.9}$$

Here,  $\mathbf{E}^s$  is a vector containing unknown non-trivial electric field components, and  $\mathbf{b}$  is obtained from boundary conditions. There are numerous ways of arranging the algebraic



equations (4.2.6-4.2.8), whose coefficients constitute the matrix  $\mathbf{A}$ . In the present work, first  $E_x^s$  and  $E_y^s$  components are arranged first and then the  $E_z^s$  components are arranged (Figures 4.6 and 4.7) to constitute the system matrix. The system matrix is highly sparse matrix (Figure 4.8), with maximum 13 nonzero elements in a row, and it is stored in Compact Sparse Row (CSR) format. The total number of electric field components determine the size of the system matrix. The number of non-trivial electric field components are,

- non-trivial  $E_x^s$  components =  $nx.nym.nzm$ ,
- non-trivial  $E_y^s$  components =  $nxm.ny.nzm$ ,
- non-trivial  $E_z^s$  components =  $nxm.nym.nz$ .

Here,  $nxm = (nx - 1)$ ,  $nym = (ny - 1)$  and  $nzm = (nz - 1)$ . So, the system matrix is of dimension  $(nef \times nef)$ , and  $nef$  is defined as

$$\begin{aligned} nef &= nzm(nx.nym + nxm.ny) + nxm.nym.nz \\ &= nzm.nxy + nxm.nym.nz \end{aligned}$$

#### 4.2.4 Divergence Correction

As explained in chapter 2, to improve convergence at low frequencies, static divergence correction is applied to the iterative solution. The SFD equations for calculating the

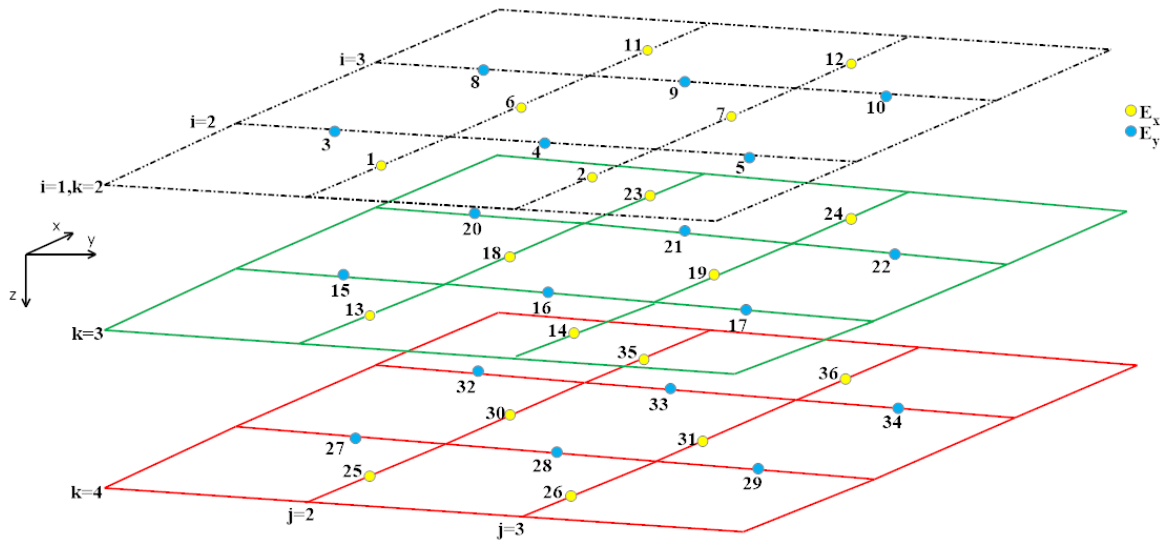


Figure 4.6: Numbering scheme  $E_x$  and  $E_y$  components in system matrix  $\mathbf{A}$  associated with grid  $(3 \times 3 \times 4)$ .

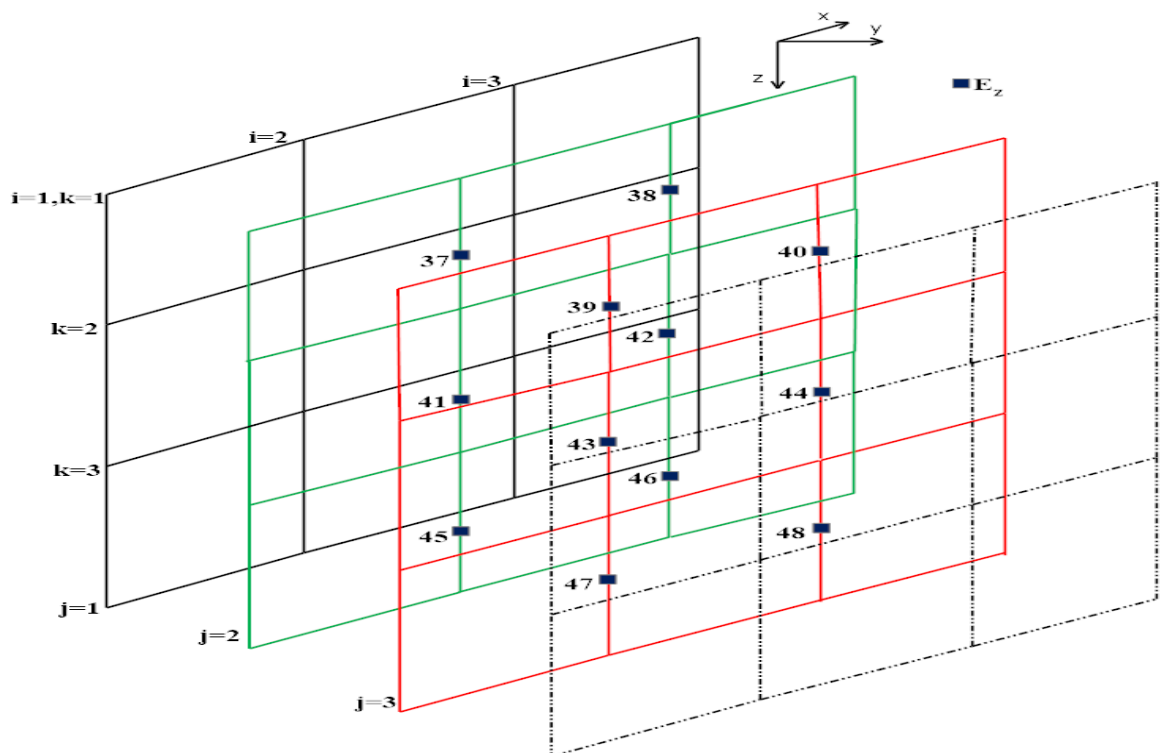


Figure 4.7: Numbering scheme  $E_z$  components in system matrix  $\mathbf{A}$  associated with grid  $(3 \times 3 \times 4)$ .

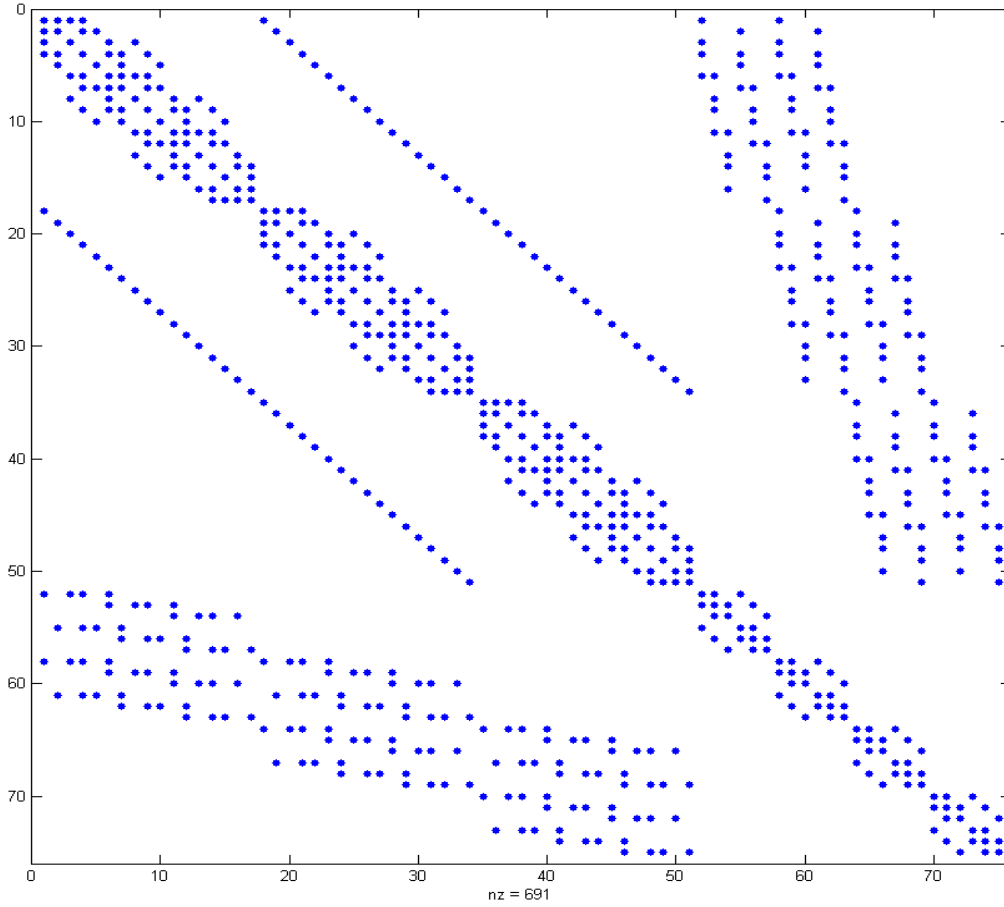


Figure 4.8: Structure of system matrix  $\mathbf{A}$  associated with grid  $(4 \times 3 \times 4)$ .

unknown scalar  $\phi$  is obtained by approximating the derivatives in equation (2.7.4)

by the difference formula. The SFD equation for  $\phi$  is

$$\begin{aligned}
 & a1\phi(i, j, k - 1) + a2\phi(i - 1, j, k) + a3\phi(i, j - 1, k) - a4\phi(i, j, k) + a5\phi(i, j + 1, k) + \\
 & a6\phi(i + 1, j, k) + a7\phi(i, j, k + 1) = b1E^p(i, j, k) - b2E^p(i - 1, j, k) + b3E^p(i, j, k) - \\
 & b4E^p(i, j - 1, k) - c1E_x^s(i, j, k) + c2E_x^s(i - 1, j, k) - c3E_y^s(i, j, k) + c4E_y^s(i, j - 1, k) \\
 & - c5E_z^s(i, j, k) + c6E_z^s(i, j, k - 1).
 \end{aligned}$$

(4.2.10)

Here,

$$\begin{aligned}
a1 &= \frac{ah(i)bh(j)\sigma_z(i, j, k-1)}{c(k-1)} & a2 &= \frac{bh(j)ch(k)\sigma_x(i-1, j, k)}{a(i-1)} \\
a3 &= \frac{ah(i)ch(k)\sigma_y(i, j-1, k)}{b(j-1)} & a5 &= \frac{ah(i)ch(k)\sigma_y(i, j+1, k)}{b(j)} \\
a6 &= \frac{bh(j)ch(k)\sigma_x(i+1, j, k)}{a(i)} & a7 &= \frac{ah(i)bh(j)\sigma_z(i, j, k+1)}{c(k)} \\
a4 &= a1 + a2 + a3 + a5 + a6 + a7,
\end{aligned}$$

$$\begin{aligned}
b1 &= bh(j)ch(k)\sigma_x^a(i, j, k) & b2 &= bh(j)ch(k)\sigma_x^a(i-1, j, k) \\
b3 &= ah(i)ch(k)\sigma_y^a(i, j, k) & b4 &= ah(i)ch(k)\sigma_y^a(i, j-1, k),
\end{aligned}$$

and

$$\begin{aligned}
c1 &= bh(j)ch(k)\sigma_x(i, j, k) & c2 &= bh(j)ch(k)\sigma_x(i-1, j, k) \\
c3 &= ah(i)ch(k)\sigma_y(i, j, k) & c4 &= ah(i)ch(k)\sigma_y(i, j-1, k) \\
c5 &= ah(i)bh(j)\sigma_z(i, j, k) & c6 &= ah(i)bh(j)\sigma_z(i, j, k-1).
\end{aligned}$$

Writting equation (4.2.10) for all non-trivial (i,j,k), arranging them we get a matrix equation system as

$$\mathbf{C}\Phi = \mathbf{d} \tag{4.2.11}$$

Now, equation (4.2.11) is solved to get value of  $\Phi$  on all the nodes and from which  $\nabla\phi$  is computed at the center of cell edges, where electric field components are defined, to correct the iterative solution.

## 4.2.5 Forward Matrix Solver

Now, to solve equation (4.2.9), iterative bi-conjugate gradient stabilized 'BICGSTAB' method (Van der Vorst [149]) along with DILU preconditioner (Barrett et al. [11]) is

implemented. Furthermore, to improve the efficiency, OpenMP platform is used to compute the response of different frequencies in parallel.

#### 4.2.6 Transformation and Interpolation

After computing electric field  $\mathbf{E}$ , we need to calculate the magnetic field  $\mathbf{H}$  for computing the different MT response functions. As described in Chapter 2,  $\mathbf{H}$  is calculated from the finite difference approximation of the equation (2.4.2) as

$$\begin{aligned} H_x(i, j, k) &= \frac{i}{\omega\mu_0} \left[ \frac{E_z(i, j+1, k) - E_z(i, j, k)}{b(j)} - \frac{E_y(i, j, k+1) - E_y(i, j, k)}{c(k)} \right] \\ H_y(i, j, k) &= \frac{i}{\omega\mu_0} \left[ \frac{E_x(i, j, k+1) - E_x(i, j, k)}{c(k)} - \frac{E_z(i+1, j, k) - E_z(i, j, k)}{a(i)} \right] \end{aligned} \quad (4.2.12)$$

As, these magnetic field values are defined at the center of cell faces, for calculating their values at observation points/site location we first compute field values in the first two layers at air earth interface i.e.  $k = z_{air\_earth\_int}$  and  $k = z_{air\_earth\_int}+1$ . So, to compute magnetic field we design a transformation matrix using equation (4.2.12) as

$$\mathbf{h} = \mathbf{T}'\mathbf{E} \quad (4.2.13)$$

where

- $\mathbf{h}$  is the vector containing horizontal components of magnetic field for two layers. The dimension of  $\mathbf{h}$  is  $(2nxy \times 1)$ ,  $nxy = nx(ny - 1) + (nx - 1)ny$ ,
- $\mathbf{E}$  is the vector containing all non-trivial electric field components. The dimension of  $\mathbf{E}$  is  $(nef \times 1)$ ,
- $\mathbf{T}'$  is the transformation matrix and its dimension is  $(2nxy \times nef)$ .

$\mathbf{T}'$  is a highly sparse matrix with at most 4 non-zero elements in each row. So, only the non-zero elements are stored in a  $(nxy3 \times 4)$ array and their corresponding position

is also stored in a  $(nxy3 \times 4)$  array. The non-zero elements and their column position in a row are

For  $H_y$ :

$$T'_{l,1} = -\frac{\iota}{\omega\mu_0 c(k)}, \text{ col}_{l,1} = (k-2)nxy + k$$

$$T'_{l,2} = \frac{\iota}{\omega\mu_0 c(k)}, \text{ col}_{l,2} = (k-1)nxy + k$$

$$T'_{l,3} = \frac{\iota}{\omega\mu_0 a(i)}, \text{ col}_{l,3} = nzm.nxy + (k-1)nxm.nym + (j-2).nxm + i - 1$$

$$T'_{l,4} = -\frac{\iota}{\omega\mu_0 a(i)}, \text{ col}_{l,4} = nzm.nxy + (k-1)nxm.nym + (j-2).nxm + i$$

For  $H_x$ :

$$T'_{l,1} = \frac{\iota}{\omega\mu_0 c(k)}, \text{ col}_{l,1} = (k-2)nxy + k$$

$$T'_{l,1} = -\frac{\iota}{\omega\mu_0 c(k)}, \text{ col}_{l,2} = (k-1)nxy + k$$

$$T'_{l,1} = -\frac{\iota}{\omega\mu_0 b(j)}, \text{ col}_{l,3} = nzm.nxy + (k-1)nxm.nym + (j-1)nxm + i - nxm$$

$$T'_{l,1} = \frac{\iota}{\omega\mu_0 b(j)}, \text{ col}_{l,4} = nzm.nxy + (k-1)nxm.nym + (j-1)nxm + i$$

After computing the magnetic field at face center of the cells in two layers, its value is extrapolated at the cell edge center where electric fields are defined. Both these operations are combined for computation of magnetic field values at the edge center of the grid block and are represented by matrix operator  $\mathbf{T}$ .

In order to compute the field response at the observation points from the field values at grid points, we have adopted bi-linear interpolation from Press et al. [106]. We have designed two interpolation matrices  $\mathbf{Ip}_1$  for interpolating  $E_x$  and  $H_y$ , and  $\mathbf{Ip}_2$  for interpolating  $E_y$  and  $H_x$ .

### 4.3 Inverse Formulation

The non-linear MT problem, after quasi-linearization, is solved iteratively starting with an initial guess model. In general, since the location and extent of the anomalous body can be roughly guessed from the observed response, there is no need for inverting the whole modeling domain. A good initial guess helps in faster convergence of the iterative process. The data recorded at surface sites or the synthetically generated data, constitute the observation vector. The parameter vector  $\mathbf{P}$  consists of the resistivities ( $\rho$ ) of the cells enclosed in the inversion domain. The initial guess values are the current value of  $\rho_{i,j,k}$  of the  $(i, j, k)^{th}$  block. For numerical accuracy, instead of  $\rho_{i,j,k}$ , its logarithm given below is considered as parameter,

$$P_l = \log \rho_{i,j,k} = -\log \sigma_{i,j,k}. \quad (4.3.1)$$

It is more efficient to work with the logarithmic parameters because out of all the model parameters, the  $\rho$  varies over the widest range. Using  $\log \rho$  as the parameters, not only scales this large variation in parameter values but also guarantees that the  $\rho$  has only positive values.

In order to solve the inverse problem matrix equation (3.4.17), the Jacobian matrix  $\mathbf{J}$  need to be calculated using equation (3.4.22) which is rewritten as

$$\mathbf{J} = \mathbf{A}^{-1}\mathbf{Y},$$

where  $Y_l = -\frac{\partial \mathbf{A}}{\partial P_l} \mathbf{E}$  is the  $l^{th}$  column of matrix  $\mathbf{Y}$ . So to construct matrix  $\mathbf{Y}$ , we need the differentiation of system matrix  $\mathbf{A}$  with respect to the parameters.

### 4.3.1 Matrix Solver for Inverse Problem

In the present work, we are inverting the impedance tensor  $\mathbf{Z}$ , so we need the corresponding Jacobian  $\mathbf{K}$ . For the derived Jacobian  $\mathbf{K}$ , the inverse problem defined in equation (3.4.18) is rewritten as

$$\mathbf{P}_{k+1} - \mathbf{P}^0 = \hat{\mathbf{G}}^{-1} \mathbf{r}, \quad (4.3.2)$$

where  $\hat{\mathbf{G}} = [\mathbf{K}_k^T \mathbf{C}_d^{-1} \mathbf{K}_k + \lambda \mathbf{C}_m^{-1}]$ , and

$$\mathbf{r} = \mathbf{K}_k^T \mathbf{C}_d^{-1} \{\mathbf{D}' + \mathbf{K}_k(\mathbf{P}_k - \mathbf{P}^0)\}.$$

It may be stated here that equation (4.3.2) is valid for real matrices. But in **3DINV\_FD** algorithm we are working with complex variables so, we have converted our problem to one involving complex matrices following the work of Rodi and Mackie [112], which is discussed next.

### 4.3.2 Real to Complex Algebra

Let  $\hat{\mathbf{D}}$  be a complex vector such that elements of  $\mathbf{D}$  are either real or imaginary part of a unique element of  $\hat{\mathbf{D}}$ :

$$\mathbf{D} = Re\{\hat{\mathbf{T}}\hat{\mathbf{D}}\}, \quad (4.3.3)$$

where

$$\hat{T}_{ij} = \begin{cases} 1, & \text{if } p_i = Re\{\hat{p}_j\} \\ -\iota, & \text{if } p_i = Im\{\hat{p}_j\} \\ 0, & \text{otherwise} \end{cases}$$

So, the forward modeling operator  $\mathbf{F}$  can be written as

$$\mathbf{F}(\mathbf{P}) = Re\{\hat{\mathbf{T}}\mathbf{F}(\hat{\mathbf{P}})\}, \quad (4.3.4)$$



where  $\hat{\mathbf{F}}$  is the complex forward modeling operator. Now, Jacobian  $\mathbf{K}$  can also be written as

$$\mathbf{K} = Re\{\hat{\mathbf{T}}\hat{\mathbf{K}}\}, \quad (4.3.5)$$

where,  $\hat{\mathbf{K}}$  is the complex derived Jacobian.

### 4.3.3 Derivative of System Matrix

The derivative of a system matrix element is zero unless its expression contains  $\rho$ . Since the conductivity of a (i,j,k) cell  $\sigma(i, j, k)$  contributes to 12 weighted average conductivities, namely  $(\sigma_x(i, j, k), \sigma_x(i, j + 1, k), \sigma_x(i, j, k + 1), \sigma_x(i, j + 1, k + 1), \sigma_y(i, j, k), \sigma_y(i+1, j, k), \sigma_y(i, j, k+1), \sigma_x(i+1, j, k), \sigma_z(i, j, k), \sigma_z(i+1, j, k), \sigma_z(i, j+1, k)$  and  $\sigma_z(i + 1, j + 1, k))$ . As a result, the derivative of the  $\mathbf{A}$  is a diagonal matrix with 12 nonzero elements and hence, the matrix  $\mathbf{Y}$  of dimension  $(nef \times p)$ , is grossly sparse with each column having at most 12 non-zero entries in row positions corresponding to the non-zero element in  $\hat{\mathbf{A}} = -\frac{\partial \mathbf{A}}{\partial P_l}$ . The derivative with respect to the logarithmic parameter is defined as

$$\frac{\partial}{\partial P_l} = -\frac{1}{\rho_{i,j,k}} \frac{\partial}{\partial \sigma_{i,j,k}}. \quad (4.3.6)$$

After differentiating with  $-\log \sigma_{i,j,k}$ , all 12 non-zero elements along the diagonal of  $\hat{\mathbf{A}}$  have value

$$val = \frac{i\omega\mu_0}{4.\rho_{i,j,k}} [a(i).b(j).c(k)], \quad (4.3.7)$$

and their position along the diagonal are

- For  $\sigma_x(i, j, k)$ :  $n = (k + l - 3) \cdot \{nx \cdot (ny - 1) + (nx - 1) \cdot ny\} + (i - 1) \cdot (2ny - 1) + (j - 1) + (m - 1)$  where  $l, m = 1, 2$ ,

- For  $\sigma_y(i, j, k)$ :  $n = (k + l - 3) \cdot \{nx \cdot (ny - 1) + (nx - 1) \cdot ny\} + (i + m - 2) \cdot (2ny - 1) + (j - 1) - (ny - 1)$  where  $l, m = 1, 2$ ,
- For  $\sigma_z(i, j, k)$ :  $n = (k + nz - 2) \cdot \{nx \cdot (ny - 1) + (nx - 1) \cdot ny\} + (i - 1) + (j + l - 3) \cdot (nx - 1) + (m - 1)$  where  $l, m = 1, 2$ .

Now, matrix  $\mathbf{Y}$  is computed as

$$Y_l = -\frac{\partial \mathbf{A}}{\partial P_l} \mathbf{E} \quad (4.3.8)$$

To save space, instead of storing full sparse matrix  $\mathbf{Y}$ , only the non zero elements are stored and their position in the column of  $\mathbf{Y}$ , are stored. As there are modes of polarization, so two matrices  $\mathbf{Y}_1$  and  $\mathbf{Y}_2$  are constructed for each polarization mode. During inversion we need the Jacobian corresponding to the response function which is being inverted. The details for calculating derived Jacobian for  $\mathbf{Z}$  is discussed here.

#### 4.3.4 Derived Jacobian

The Jacobian computed from equation (3.4.22) is for the electric field  $\mathbf{E}$  components. The derived Jacobian  $\mathbf{K}$  can be derived by considering that the first order perturbation of  $\mathbf{Z}$  are the result of perturbation to the computed EM fields  $(\frac{\partial \mathbf{E}}{\partial \mathbf{P}}, \frac{\partial \mathbf{B}}{\partial \mathbf{P}})$ , such that

$$\begin{aligned} \frac{\partial \mathbf{Z}}{\partial \mathbf{P}} &= \frac{\partial}{\partial \mathbf{P}} \left( \frac{\mathbf{E}}{\mathbf{H}} \right), \\ &= \frac{\partial \mathbf{E}}{\partial \mathbf{P}} \mathbf{H}^{-1} - \mathbf{Z} \frac{\partial \mathbf{B}}{\partial \mathbf{P}} \mathbf{H}^{-1} \end{aligned} \quad (4.3.9)$$

Now, consider  $i^{th}$  observation point,  $\mathbf{H}^{-1}$  is

$$\begin{bmatrix} H_{x1}^i & H_{x2}^i \\ H_{y1}^i & H_{y2}^i \end{bmatrix}^{-1} = \begin{bmatrix} \frac{H_{y2}^i}{D} & -\frac{H_{y1}^i}{D} \\ -\frac{H_{x2}^i}{D} & \frac{H_{x1}^i}{D} \end{bmatrix} = \begin{bmatrix} \bar{H}_1^i & \bar{H}_3^i \\ \bar{H}_2^i & \bar{H}_4^i \end{bmatrix} \quad (4.3.10)$$

where,  $D = H_{x1}^i H_{y2}^i - H_{x2}^i H_{y1}^i$ .

So, equation (4.3.9 at  $i^{th}$  observation point becomes,

$$\begin{aligned} \begin{Bmatrix} \partial_{P_j} Z_{xx}^i & \partial_{P_j} Z_{xy}^i \\ \partial_{P_j} Z_{yx}^i & \partial_{P_j} Z_{yy}^i \end{Bmatrix} &= \begin{pmatrix} \partial_{P_j} E_{x1}^i & \partial_{P_j} E_{x2}^i \\ \partial_{P_j} E_{y1}^i & \partial_{P_j} E_{y2}^i \end{pmatrix} \begin{bmatrix} \bar{H}_1^i & \bar{H}_3^i \\ \bar{H}_2^i & \bar{H}_4^i \end{bmatrix} - \\ &\begin{Bmatrix} Z_{xx}^i & Z_{xy}^i \\ Z_{yx}^i & Z_{yy}^i \end{Bmatrix} \begin{pmatrix} \partial_{P_j} H_{x1}^i & \partial_{P_j} H_{x2}^i \\ \partial_{P_j} H_{y1}^i & \partial_{P_j} H_{y2}^i \end{pmatrix} \begin{bmatrix} \bar{H}_1^i & \bar{H}_3^i \\ \bar{H}_2^i & \bar{H}_4^i \end{bmatrix}. \end{aligned} \quad (4.3.11)$$

The calculated electric and magnetic fields can be interpolated at the observation point.

Thus, for  $i^{th}$  observation point we can write

$$\begin{aligned} E_{x1}^i &= Ip_1^i \cdot \mathbf{E}^1, & E_{x2}^i &= Ip_1^i \cdot \mathbf{E}^2, & E_{y1}^i &= Ip_2^i \cdot \mathbf{E}^1, & E_{y2}^i &= Ip_2^i \cdot \mathbf{E}^2, \\ H_{x1}^i &= Ip_2^i \cdot \mathbf{T} \cdot \mathbf{E}^1, & H_{x2}^i &= Ip_2^i \cdot \mathbf{T} \cdot \mathbf{E}^2, & H_{y1}^i &= Ip_1^i \cdot \mathbf{T} \cdot \mathbf{E}^1, & H_{y2}^i &= Ip_1^i \cdot \mathbf{T} \cdot \mathbf{E}^1. \end{aligned} \quad (4.3.12)$$

Using equations(4.3.11 and 4.3.12), we can write

$$\begin{aligned} \partial_{P_j} Z_{xx}^i &= \bar{H}_1^i \{Ip_1^i - Z_{xx}^i Ip_2^i \mathbf{T} - Z_{xy}^i Ip_1^i \mathbf{T}\} \partial_{m_k} \mathbf{E}^1 \\ &+ \bar{H}_2^i \{Ip_1^i - Z_{xx}^i Ip_2^i \mathbf{T} - Z_{xy}^i Ip_1^i \mathbf{T}\} \partial_{m_k} \mathbf{E}^2. \end{aligned} \quad (4.3.13)$$

After writing equation (4.3.13) for all observation points and parameters, they can be assembled in matrix form as

$$\begin{aligned} K_1 &= \text{diag}(\bar{H}_1) \{\mathbf{Ip}_1 - \text{diag}(Z_{xx})\mathbf{Ip}_2\mathbf{T} - \text{diag}(Z_{xy})\mathbf{Ip}_1\mathbf{T}\} \mathbf{A}^{-1} \mathbf{Y}_1 \\ &+ \text{diag}(\bar{H}_2) \{\mathbf{Ip}_1 - \text{diag}(Z_{xx})\mathbf{Ip}_2\mathbf{T} - \text{diag}(Z_{xy})\mathbf{Ip}_1\mathbf{T}\} \mathbf{A}^{-1} \mathbf{Y}_2. \end{aligned} \quad (4.3.14)$$

Similarly writing for  $Z_{xy}$ ,  $Z_{yx}$  and  $Z_{yy}$

$$\begin{aligned} K_2 &= \text{diag}(\bar{H}_3) \{ \mathbf{I}_{\mathbf{p}_1} - \text{diag}(Z_{xx})\mathbf{I}_{\mathbf{p}_2}\mathbf{T} - \text{diag}(Z_{xy})\mathbf{I}_{\mathbf{p}_1}\mathbf{T} \} \mathbf{A}^{-1}\mathbf{Y}_1 \\ &+ \text{diag}(\bar{H}_4) \{ \mathbf{I}_{\mathbf{p}_1} - \text{diag}(Z_{xx})\mathbf{I}_{\mathbf{p}_2}\mathbf{T} - \text{diag}(Z_{xy})\mathbf{I}_{\mathbf{p}_1}\mathbf{T} \} \mathbf{A}^{-1}\mathbf{Y}_2, \end{aligned} \quad (4.3.15)$$

$$\begin{aligned} K_3 &= \text{diag}(\bar{H}_1) \{ \mathbf{I}_{\mathbf{p}_2} - \text{diag}(Z_{yx})\mathbf{I}_{\mathbf{p}_2}\mathbf{T} - \text{diag}(Z_{yy})\mathbf{I}_{\mathbf{p}_1}\mathbf{T} \} \mathbf{A}^{-1}\mathbf{Y}_1 \\ &+ \text{diag}(\bar{H}_2) \{ \mathbf{I}_{\mathbf{p}_2} - \text{diag}(Z_{yx})\mathbf{I}_{\mathbf{p}_2}\mathbf{T} - \text{diag}(Z_{yy})\mathbf{I}_{\mathbf{p}_1}\mathbf{T} \} \mathbf{A}^{-1}\mathbf{Y}_2, \end{aligned} \quad (4.3.16)$$

$$\begin{aligned} K_4 &= \text{diag}(\bar{H}_3) \{ \mathbf{I}_{\mathbf{p}_2} - \text{diag}(Z_{yx})\mathbf{I}_{\mathbf{p}_2}\mathbf{T} - \text{diag}(Z_{yy})\mathbf{I}_{\mathbf{p}_1}\mathbf{T} \} \mathbf{A}^{-1}\mathbf{Y}_1 \\ &+ \text{diag}(\bar{H}_4) \{ \mathbf{I}_{\mathbf{p}_2} - \text{diag}(Z_{yx})\mathbf{I}_{\mathbf{p}_2}\mathbf{T} - \text{diag}(Z_{yy})\mathbf{I}_{\mathbf{p}_1}\mathbf{T} \} \mathbf{A}^{-1}\mathbf{Y}_2. \end{aligned} \quad (4.3.17)$$

So, combining equations (4.3.14-4.3.17), the derived Jacobian  $\mathbf{K}$  is written as

$$\begin{aligned} \mathbf{K}_{(4nobs \times p)} &= \begin{pmatrix} K_1 \\ K_2 \\ K_3 \\ K_4 \end{pmatrix} = \begin{pmatrix} L_{xx}^1 & L_{xx}^2 \\ L_{xy}^1 & L_{xy}^2 \\ L_{yx}^1 & L_{yx}^2 \\ L_{yy}^1 & L_{yy}^2 \end{pmatrix}_{(4nobs \times 2nef)} \cdot \begin{pmatrix} \mathbf{A}^{-1} & \mathbf{0} \\ \mathbf{0} & \mathbf{A}^{-1} \end{pmatrix}_{(2nef \times 2nef)} \cdot \begin{pmatrix} \mathbf{Y}_1 \\ \mathbf{Y}_2 \end{pmatrix}_{(2nef \times p)} \\ &= \begin{pmatrix} L_{xx}^1 \\ L_{xy}^1 \\ L_{yx}^1 \\ L_{yy}^1 \end{pmatrix} \mathbf{A}^{-1}\mathbf{Y}_1 + \begin{pmatrix} L_{xx}^2 \\ L_{xy}^2 \\ L_{yx}^2 \\ L_{yy}^2 \end{pmatrix} \mathbf{A}^{-1}\mathbf{Y}_2 \\ &= \mathbf{L}^1 \mathbf{A}^{-1} \mathbf{Y}_1 + \mathbf{L}^2 \mathbf{A}^{-1} \mathbf{Y}_2 \end{aligned} \quad (4.3.18)$$

### 4.3.5 Bypassing Explicit Jacobian Computation

The matrix equation (4.3.2) is solved using CG method, and in CG method the matrix  $\hat{\mathbf{G}}$  is only required in matrix vector product (Appendix A). This property of CG is used to bypass the direct/explicit computation of Jacobian ( $\mathbf{K}$ ), as now matrix  $\mathbf{K}$  is

only employed in the computation of quantities  $\mathbf{K} \cdot \mathbf{s}$  and  $\mathbf{K}^T \cdot \mathbf{t}$  for particular vectors  $\mathbf{s}$  and  $\mathbf{t}$ . It is evident from equations (4.3.5 and 4.3.18) that the required matrix-vector products ( $\mathbf{K}\mathbf{s}$  and  $\mathbf{K}^T\mathbf{t}$ ) can be computed as

$$\begin{aligned}\mathbf{K}\mathbf{s} &= Re\{\hat{\mathbf{T}}\hat{\mathbf{K}}\mathbf{s}\} \\ &= Re\{\hat{\mathbf{T}}\mathbf{L}^1\mathbf{A}^{-1}\mathbf{Y}_1\mathbf{s} + \hat{\mathbf{T}}\mathbf{L}^2\mathbf{A}^{-1}\mathbf{Y}_2\mathbf{s}\}\end{aligned}\quad (4.3.19)$$

$$\begin{aligned}\mathbf{K}^T\mathbf{t} &= Re\{\hat{\mathbf{K}}^T\hat{\mathbf{T}}^T\mathbf{t}\} \\ &= Re\{\hat{\mathbf{K}}^T\bar{\mathbf{t}}\} \\ &= Re\{\mathbf{Y}_1^T\mathbf{A}^{-1}\mathbf{L}^{1T}\bar{\mathbf{t}} + \mathbf{Y}_2^T\mathbf{A}^{-1}\mathbf{L}^{2T}\bar{\mathbf{t}}\}\end{aligned}\quad (4.3.20)$$

where  $\bar{\mathbf{t}}$  is the complex conjugate of vector  $\mathbf{t}$ . It is evident from equations (4.3.19 and 4.3.20) that 4 pseudo forward problems are solved in 1 CG iteration to avoid the direct computation of the Jacobian matrix.

## 4.4 Solution of Inverse Problem

During, the numerical implementation for solving the inverse problem, there are two levels of iterations. The outer loop for quasi-linearizing the inverse problem, whereas the inner loop is for the iterations of the CG used to obtain the corrected logarithmic parameters. From, the obtained parameter vector  $\mathbf{P}'$ , the updated resistivity of the blocks in the inversion domain is obtained as

$$\mathbf{P}_{k+1} = \mathbf{P}^0 \exp(\mathbf{P}'). \quad (4.4.1)$$

The use logarithmic parameters works well for large variations in the model parameter resulting from larger dynamic range in the signals and hence, stabilizing the inversion procedure. The updated parameter vector  $\mathbf{P}_{k+1}$  is used as initial guess for the next

iteration. After each iteration in the outer loop the solution is checked for convergence. The convergence of iterative process is determined by two criteria,

- The misfit between the updated model response and observed/synthetic data is less than the desired tolerance level.
- The improvement in the parameter vector in successive iterations is not significant.

Moreover, the inversion process stops when misfit after the current update is greater than that of previous iteration or when the iteration number exceeds a given limit. The obtained model is accepted as one of the possible solution of the inverse problem.

## 4.5 Closure

The FDM having simple mathematics and easy implementation is preferred over other numerical methods for solving MT inverse problem. The forward problem is solved using BICGSTAB method while CG method is used for solving inverse problem. The algorithm **3DINV\_FD**, where the different aspects of finite difference implementation have been programmed in FORTRAN90, is discussed in Chapter 5.



# DEVELOPMENT AND DETAILS OF 3DINV\_FD ALGORITHM

## 5.1 Introduction

The ultimate goal of any EM inversion algorithm is to find an optimum resistivity model by employing a cost-effective technique. At the time when this study was started there were only a few 3D EM inversion algorithms available, therefore, in the present research work, an effort has been made to develop an efficient 3D MT data inversion algorithm **3DINV\_FD**, by numerically implementing the forward and inverse formulations discussed in Chapter 4. The sequence of development, highlighting the difficulties faced and the manner in which these were overcome, is presented below.

## 5.2 Sequence of Development

The present study was carried out over a period of about five years. Like any major exercise, the algorithm **3DINV\_FD** was also developed in various stages. For understanding the discrete inversion, we started with the development of a primitive



2D algorithm for MT data inversion. and finally developed the 3D algorithm **3DINV\_FD**. It may be stressed here that 2D algorithm development took only 30% of the time spent on the development of **3DINV\_FD**. During the course of time, the different versions of inversion algorithm were developed. Some features of these intermediate versions have survived in the final version, while others have been dropped out. The outcome of this thorough and extensive research is an efficient 3D MT data inversion algorithm, **3DINV\_FD**.

### 5.2.1 2D Algorithm Version I

Initially, the 2D forward modeling algorithm for TE mode was developed using the same methodology as was to be used in 3D case i.e. FDM. The Dirichlet boundary condition was applied on the two vertical sides and at the bottom boundary and following the work of Stuntebeck [136], Kumar [64] field continuation boundary conditions were applied at the air-earth interface. Preconditioned BICGSTAB with Jacobi preconditioner was used as matrix solver. The inversion algorithm was also developed using the same methodology as was to be used in 3D i.e. quasi-linearized inversion. The sensitivity matrix was computed explicitly by perturbing the parameters. Although, this approach was computationally costly and required space for storage, the reason for doing so was to develop a base algorithm to which further improvements can be matched. For solving the matrix equation in inversion algorithm CG method was used. Moreover, in this version the starting value of regularization parameter,  $\lambda$ , was selected by hit and trial approach and then its value was decreased during the iterative process.

### **5.2.2 2D Algorithm Version II**

After the results of this algorithm were found satisfactory the process of making the algorithm efficient started. To this end, the first improvement done in version-I was that the selection of regularization parameter and its cooling during the iterative process was done as proposed by Newman and Alumbaugh [91]. Moreover, the main objective was to avoid explicit Jacobian matrix computation, and for achieving that we needed the derivative of system matrix with respect to the parameters. So, in this version the Jacobian matrix was constructed explicitly by differentiating the system matrix with respect to the model parameters and then multiplying it by the electric field values. The reason for doing so was to confirm that the derivative of the system matrix is computed correctly. This is confirmed by matching the Jacobian computed using two methods.

After establishing the correctness of derivative of system matrix, we developed the 2D TE mode inversion algorithm in which the Jacobian computations were bypassed by using the CG method to our advantage.

### **5.2.3 Version III**

After successfully developing the 2D inversion algorithm, as per the objective of this research work, development of the 3D inversion algorithm was started. For this purpose, the main ideas from the 2D algorithm were carried forward to the 3D forward modeling algorithm. Boundary conditions used were same as used in 2D algorithm. But instead of nodal grid, staggered grid were used in 3D algorithm. The first difficulty faced in this algorithm was that, due to field continuation boundary conditions at the air-earth interface, the forward modeling algorithm took long time for computing

the field responses because while implementing this boundary condition matrix vector product is required and for 3D case this operation took most of the time and more storage was required to store a full matrix of dimension  $(nxy \times nxy)$  which is part of the system matrix. Second difficulty faced was that the BICGSTAB along with jacobi preconditioner was used for matrix equation solution and it showed very poor convergence results.

So, to overcome these difficulties, the field continuation boundary condition was dropped, and 7 layers were added in the air and Dirichlet boundary condition was also applied to the top boundary. This resulted in large system matrix but a lot was saved on computation time. Furthermore, the jacobi preconditioner was replaced by ILU(0) preconditioner which also resulted in very fast convergence. For developing 3D inversion program, the algorithm successfully tested for 2D case was accordingly implemented and successfully tested for noise free synthetic data.

#### 5.2.4 Final Version

The final version of the inversion algorithm **3DINV\_FD** was achieved after the ILU(0) preconditioner was replaced by DILU preconditioner which is mathematically same as ILU(0) (Barrett et al. [11]) but easy to implement and requires less computation time. Moreover, the more efficiently forward problem is solved, it will result in a more efficient inversion algorithm. So, various features of the algorithm to achieve this objective are discussed below.

## **5.3 Saleent Features of 3DINV\_FD Algorithm**

The **3DINV\_FD** algorithm has various features for improving its efficiency and versatility. Since the algorithm has a compact modular structure, so to add further features to the algorithm, a subroutine can be plugged in or removed easily without affecting the remaining program. The special features result in a cost effective algorithm providing good quality inversion. The various features, which enhance versatility or efficiency, are discussed below

### **5.3.1 Source Term**

The program is structured in such a way that first the computations are carried out in terms of secondary fields. Later on, the primary fields are added to secondary fields, for the total field computations. Therefore, in order to incorporate the source effect only a subroutine, computing the response of primary layered earth model in presence of source, is to be added replacing the existing output'1d subroutine which computes 1-D primary field due to a plane wave source.

### **5.3.2 Optimal Parameters for Static Divergence Correction**

The main feature of the forward modeling algorithm, controlling its convergence at low frequency is ststic divergence correction. After rigorous testing on synthetic models, the parameters for applying divergence correction are fixed to optimal values for fast convergence.

### 5.3.3 Multi-frequency Response in Parallel

In the inversion algorithm **3DINV\_FD** the forward problem for obtaining the response for different frequencies and solving pseudo forward problems during CG iterations are solved in parallel using the OpenMP parallel programming platform on shared memory architecture.

### 5.3.4 Field and Synthetic Data

The inversion algorithm **3DINV\_FD** can handle both field and synthetic data. For synthetic models, first the forward response is generated, next, if desired, corrupted with noise and then inverted. In order to simulate erroneous characteristic of real data, the synthetic data is corrupted with Gaussian noise.

### 5.3.5 CG Method

The inverse matrix equation (4.3.2) is solved using the conjugate gradient method. This particular choice of matrix solver is governed by the fact that CG method does not need explicit computation of Jacobian matrix. All it needs is the product of this matrix or its transpose with a vector. Moreover, for each CG inversion iteration the pseudo forward problem is solved 4 times, in contrast to other matrix solvers where it has to be solved as many times as the number of unknown parameters. So, till the number of CG iterations is less than  $1/4^{th}$  the number of unknown parameters, the CG will be more efficient than other methods.

## 5.4 Details of Algorithm

The algorithm, **3DINV\_FD**, employs FDM for solving forward and inverse problems. The algorithm comprises 6887 lines and 44 subroutines. It works in double precision arithmetic. In order to avoid stack overflows, it uses dynamic memory allocation and the memory is freed by deallocating the arrays if not required further in the program. The description and features of algorithm are highlighted in the Figure 5.1.

Total 9 input/output (I/O) units are opened in the program. The parameters and data controls are read from the 4 different input files. The remaining 5 output files are used for different outputs which are helpful in analyzing the results. Sample I/O files are given in Appendix B.

## 5.5 Structure of Algorithm

The main program of the inversion algorithm **3DINV\_FD** provides the infrastructure and the run controls. In the main program input and output files are opened and two basic subroutines (**frwd\_modlmg** and **inversion**) are called depending on the control parameter 'problem\_counter'. The main program gets the control parameters by calling the subroutine **frwd\_input** and then decides to which subroutine it should get directed to. The control parameters are read in **frwd\_input** namely 'response\_counter' and 'problem\_counter'. The possible values of these parameters and their purpose are listed in Table 5.1. Flow chart of the main program is given in Figure 5.2.

### **Basic Algorithm Statistics**

3DINV\_FD : 6887 Lines

Main program : 146 Lines

Subroutines : 6741 Lines (# 44)

### **Methodology**

- Finite Difference Method.
- Quasi-Linear Inversion.
- Conjugate Gradient matrix solver for inverse problem.

### **Forward Modeling Features**

- Optimal parameters for static divergence correction.
- BICGSTAB with DILU preconditioner.
- Gaussian noise addition to synthetic data.
- Multi frequency response computation in parallel.

### **Inversion Features**

- In-built computation of regularization parameter.
- Computation and storage of sensitivity matrix not required.
- Logarithmic parameters.
- Synthetic/Field data Inversion

Figure 5.1: 3D MT inversion algorithm 3DINV\_FD in nutshell

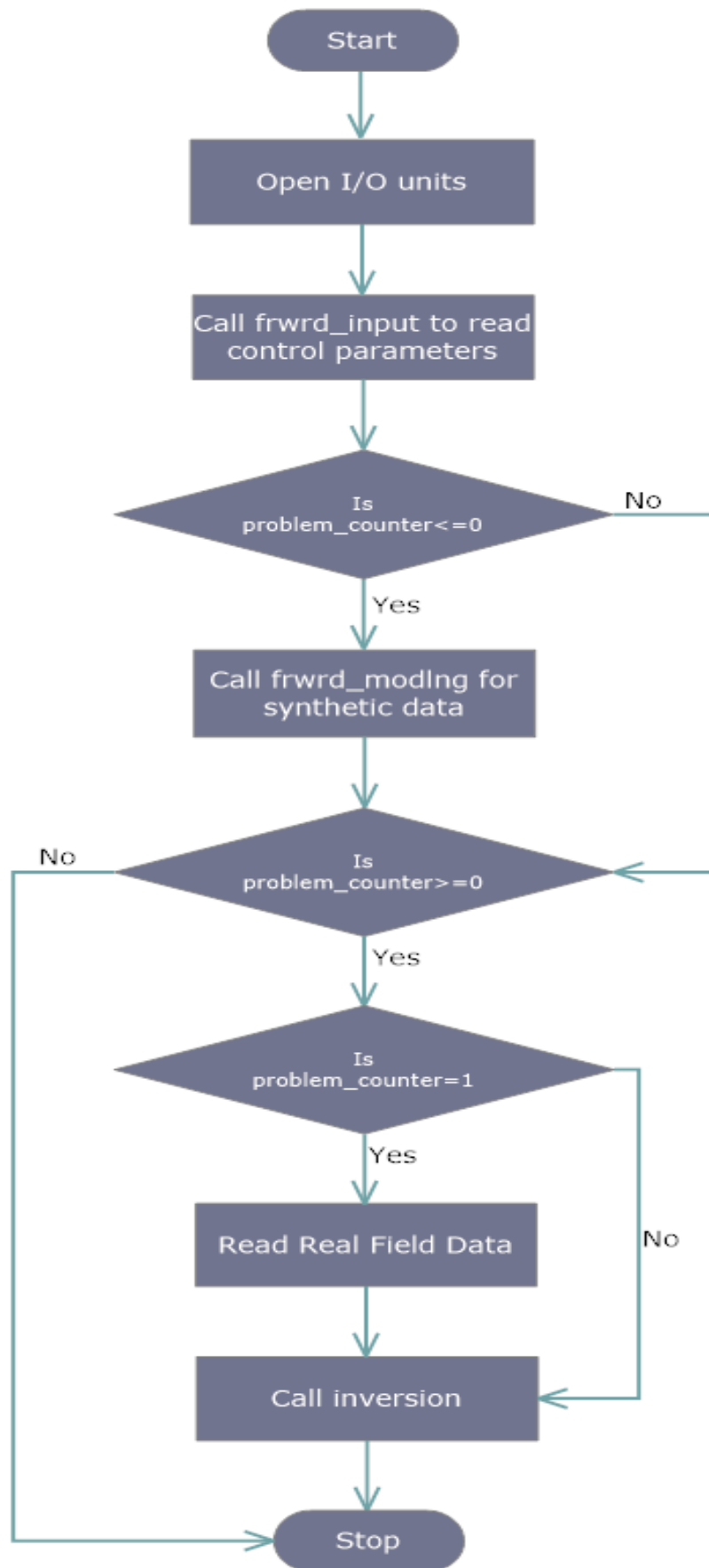


Figure 5.2: Flow chart of main program



Table 5.1: Control parameters description

Parameter	Controls	Values	Description
response_counter	Response	1	Invert off-diagonal $\mathbf{Z}$
	Function	2	Invert full $\mathbf{Z}$
problem_counter	Problem Type	-1	Only Forward Modeling
		0	Forward Modeling and Inversion
		1	Only Inversion
matvec_mul_flag	Matrix Vector	1	Multiply a matrix with a vector
	Multiplication	2	Multiply matrix transpose with vector
polarization_flag	Two Current	1	Calculations for one polarization
	Polarizations	2	Calculations for other polarization

### 5.5.1 Subroutines in 3DINV\_FD

In the development of **3DINV\_FD** all 44 subroutines, categorized as forward subroutines or inversion subroutines according to the module in which these are called, are developed by us. All the subroutines are discussed below one by one. Grid parameters and other parameters required during run time used in different subroutines are described in Table 5.2.

Table 5.2: Grid parameters and other run-time control parameters

Parameter	Description
nx	Number of blocks in X-direction
ny	Number of blocks in Y-direction
Continued on next page	

Table 5.2 - continued from previous page

nz	Number of blocks in Z-direction
$nxy=nx(ny-1)+(nx-1)ny$	Number of $E_x$ and $E_y$ components in one plane
$nef=nxy(nz-1)+(nx-1)(ny-1)nz$	Total number of non-trivial electric field components in modeling domain
ix	Running index of blocks in X-direction
iy	Running index of blocks in Y-direction
iz	Running index of blocks in Z-direction
nt	Number of time periods
nobs	Number of site locations
nobspt	Total number of data
nbl	Total number of blocks in inversion domain
bicg_tol	Tolerances level for forward problem
inv_iter	Maximum number of inversion iterations
eps	Threshold value for misfit
lambda	Regularization parameter

### 5.5.1.1 Forward Modeling Subroutines

The subroutines which are called from the subroutine **response**, which is called for synthetic model response computation in **frwrdd\_modlmg** or during the solution of pseudo forward problem are termed as forward subroutines. For synthetic response computation, the model specifications and other parameters are read in the subroutine **frwrdd\_input**. The tree structure of various subroutines, called in **response**, is shown in Figure 5.3. Few important forward subroutines are briefly described here.

Subroutine **frwrdd\_input** is called in the main program to read information about control parameters 'problem'counter' and 'response'counter' from file 'inp'frwrdd'. Depending on the value of 'problem'counter', it also contain information about the synthetic model i.e. time periods, grid lines and resistivity structure information, using which synthetic data is obtained for inversion. After reading model information, the resistivity array *reg* is constructed which contains resistivity of every block in modeling domain. The number of observation points and their coordinate values are read from file 'site'coordinates'.

Subroutine **response** computes the model response for frequency values read in subroutine **frwrdd\_input**. First, subroutine **construct\_sigma** is called for computing volume weighted average conductivity at points where field values are to be calculated using equations (4.2.4). Then in a Do loop over number of frequencies, model response computations are performed. The subroutine **weight** is called to construct the system matrix **A** only for first frequency using equations (4.2.6 - 4.2.8), for rest of the frequencies only diagonal terms are computed and stored. Next, subroutine **div\_weight** is called to construct the matrix **C** defined in equation (4.2.11). As matrix **C** is independent of frequency, this subroutine is also called only once. Then in subroutine **output\_1d** 1-D boundary field is computed which will be used for computing secondary field and then finally added to secondary field to compute total electric field.

For each frequency, secondary field is computed for two polarizations. For this purpose in an inner Do loop over polarization inside the frequency loop, first of all subroutine **righthandvec** is called, in which righthand side vector **b** defined in equation (4.2.9), is constructed. Then forward problem is solved using Krylov's

subspace iterative method BICGSTAB by calling subroutine **bicgstab**. As explained in Chapter 3, for faster convergence at low frequencies, iterative solution after every few BICGSTAB iteration must be corrected by applying static divergence correction.

For implementing divergence correction, first subroutine **div\_righthand** is called to construct vector **d** defined in equation (4.2.11). The subroutine **div\_solver** is called to solve the matrix equation using CG method, to obtain the values of scalar  $\Phi$  at grid nodes. Next, subroutine **div\_correction** is called to calculate  $\nabla\Phi$  and correct the iterative solution. Finally, primary field is added to secondary field to compute total electric field values at staggered grid points.

In order to compute MT response functions, i.e. impedance **Z**, apparent resistivity  $\rho_a$  and phase  $\phi$ , we calculate magnetic field values by calling subroutine **output3d\_mfield** and then the response functions are calculated at site locations in subroutine **output3d\_response**. If the observation points do not coincide with staggered grid points then the response is interpolated by calling **bilin\_interpolate\_matrix** and **inpv** in subroutine **output3d\_response**. The flow chart of subroutine **response** is shown in Figure 5.4.

For completeness, a table of various subroutines, with their purpose, the subroutines they are called from and subroutines they call is given in Table 5.3.

Table 5.3: Description of various forward subroutines.

<b>Subroutine</b>	<b>Purpose</b>	<b>Called in</b>	<b>Calls</b>
<b>construct_</b> <b>sigma</b>	Weighted conductivity at edge center	<b>response</b>	×
<b>weight</b>	System matrix formation	<b>response</b>	×
Continued on next page			

Table 5.3 continued from previous page

<b>output_1d</b>	Computation of primary field	<b>response</b>	×
<b>righthandvec1</b>	For polarization 1 compute vector <b>b</b>	<b>response</b>	×
<b>righthandvec2</b>	For polarization 1 compute vector <b>b</b>	<b>response</b>	×
<b>bicgstab</b>	Matrix solver for forward problem	<b>response</b>	<b>preconditioner_3d, ae1</b>
<b>div_weight</b>	Construct matrix for divergence correction	<b>response</b>	×
<b>div_righthand1</b>	Formation right hand side for divergence correction	<b>response</b>	×
<b>div_solver</b>	Divergence matrix equation solver (CG)	<b>k_matvec_ mul,</b> <b>kt_matvec_ mul</b>	<b>div_ preconditioner,</b> <b>div_matvec</b>
<b>div_correction</b>	Correct iterative solution by adding Gradient of scalar	<b>response,</b> <b>k_matvec_ mul,</b> <b>kt_matvec_ mul</b>	×
Continued on next page			

Table 5.3 continued from previous page

<b>output3d_ mfield</b>	Compute $\mathbf{H}$ at edge center of blocks	<b>response</b>	<b>transformation_ matrix,</b> <b>t_nodes_mat,</b> <b>transformation_ matv, t_ nodes_ matv</b>
<b>output3d_ response</b>	Compute $\mathbf{Z}$ , $\rho_a$ and $\phi$ at site locations	<b>response</b>	<b>bilin_ interpolate_ matrix, inpv</b>
<b>preconditioner_ 3d</b>	Preconditioning of ill - conditioned system matrix	<b>bicgstab</b>	×
<b>ae1</b>	Matrix vector product during matrix solver	<b>bicgstab</b>	×
<b>div_ preconditioner</b>	Preconditioning of ill - conditioned matrix $\mathbf{C}$	<b>div_ solver</b>	×
<b>div_matvec</b>	Matrix vector product during matrix equation solution	<b>div_ solver</b>	×
<b>transformation_ matrix</b>	Construct matrix for $\mathbf{E}$ to $\mathbf{H}$ transformation at face center	<b>output3d_ mfield</b>	×
Continued on next page			

Table 5.3 continued from previous page

<b>t_nodes_mat</b>	Construct matrix for calculating <b>H</b> at edge center	<b>output3d_mfield</b>	×
<b>transformation_matv</b>	Compute <b>H</b> at face center	<b>output3d_mfield,</b> <b>l_matvec_mul,</b> <b>lt_matvec_mul</b>	×
<b>t_nodes_matv</b>	Compute <b>H</b> at edge center	<b>output3d_mfield,</b> <b>l_matvec_mul,</b> <b>lt_matvec_mul</b>	×
<b>bilin_interpolate_matrix</b>	Construct interpolation matrices	<b>output3d_response</b>	×
<b>inpv</b>	Product of interpolation matrix with a vector	<b>output3d_response,</b> <b>l_matvec_mul,</b> <b>lt_matvec_mul</b>	×

### 5.5.1.2 Inversion Subroutines

The inversion subroutines are called in subroutine **inversion** which is called for computation of inverse problem solution. For reading the input data from file **inv\_inp**, pertaining to the initial guess model, the inversion domain geometry and other inversion parameters, the subroutine **inversion\_input** is called. The misfit between the observed

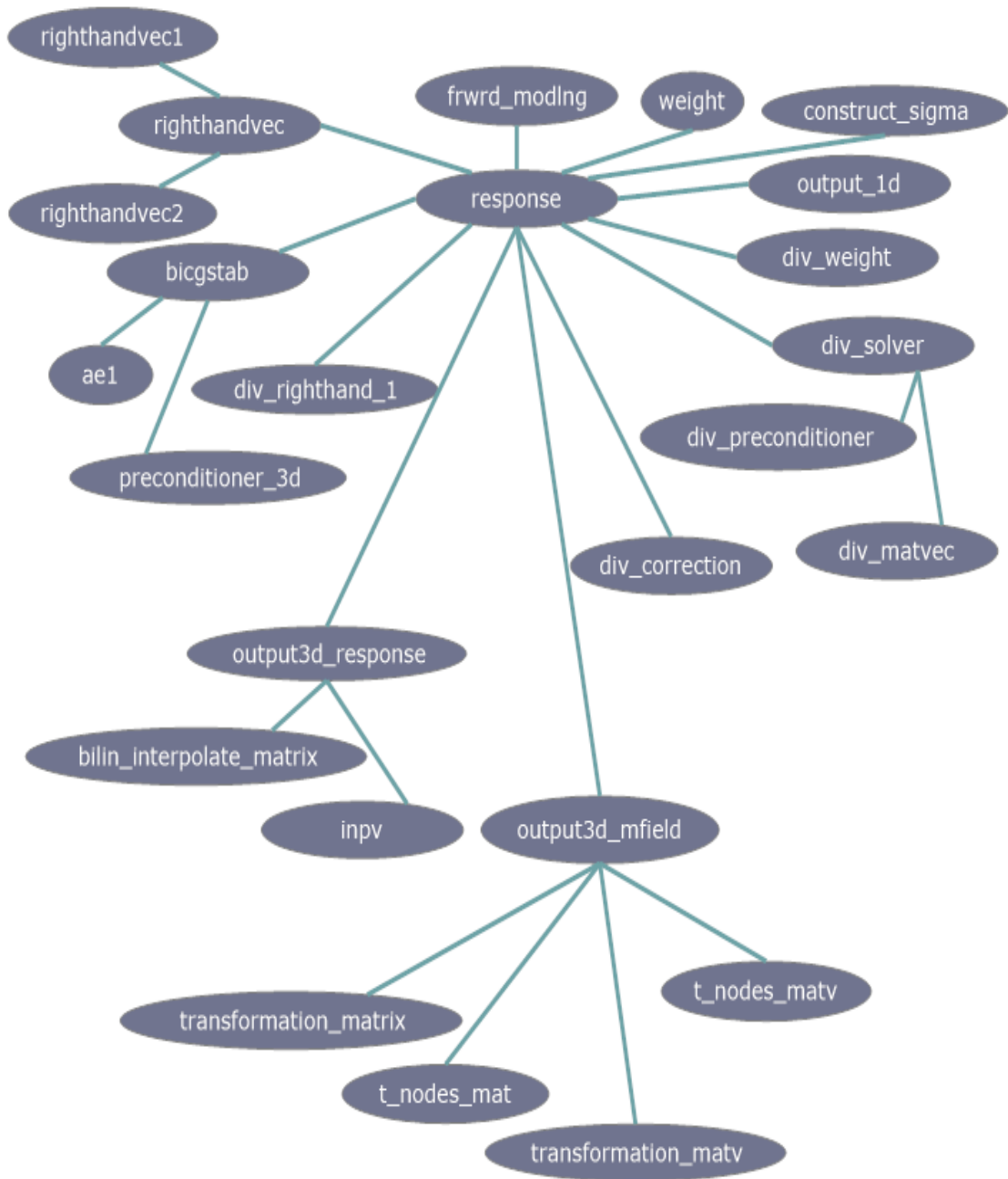


Figure 5.3: Tree structure of forward subroutines



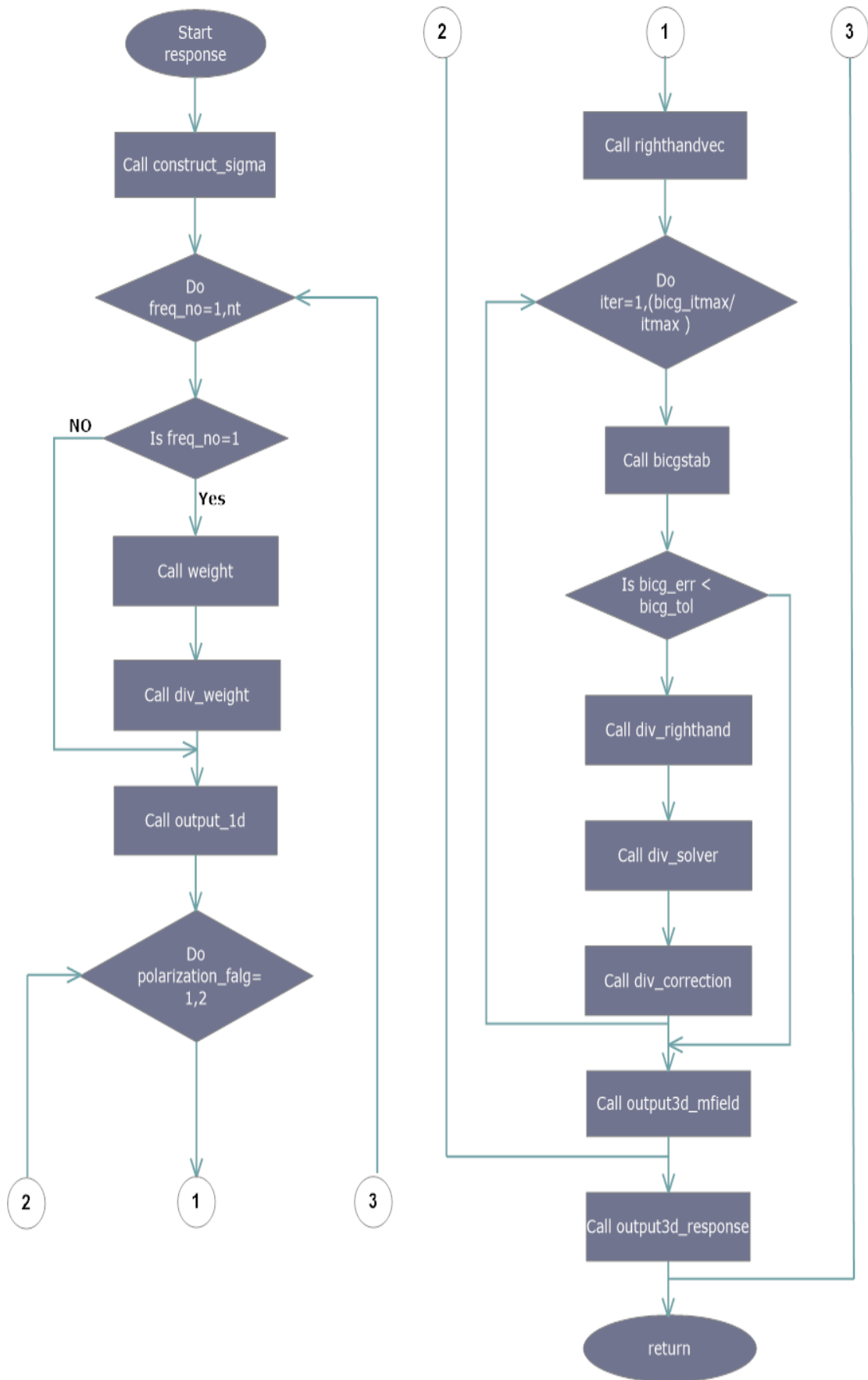


Figure 5.4: Flow chart of **response** subroutine

and predicted response is expressed in terms of root mean square (rms) error and the convergence is checked. The tree structure of subprograms used in subroutine **inversion** is given in Figure 5.5. The important inversion subprograms are also discussed in brief.

In subroutine **inversion\_input** first the parameters of the initial guess model, on the basis of observed response, are read. Next, the iteration and convergence parameters, 'inv\_iter', 'eps' and 'cg\_itmax' and 'cg\_tol' are read for inversion and the CG iterations respectively. The inversion domain is chosen to encompass the anomaly. The left and right corner coordinates of inversion domain in X- direction 'xlc', 'xrc', in Y- direction 'ylc' and 'yrc' and the top and bottom corner coordinates in Z- direction 'zuc' and 'zdc' are read. The rho0, the initial guess of resistivity, within the inhomogeneity is read. For field problem, field data is read from file **data**.

After reading input data, for determining the running index in X,Y and Z direction (ibl, ibr, jbl, jbr, zbu and zbd) for identifying the inversion domain and the number of parameters 'nbl' in inversion domain, subroutine **invdom** is called. Then, subroutine **model.covariance** is called to construct the roughness matrix, which will be used while solving equation (4.3.2).

For each inversion iteration, first the model responses are computed for all frequencies in parallel by calling the subroutine **response**. Subroutine **rhsmat** is called for computation of the matrix **Y** using equation (4.3.8) which is the product of field vector with the system matrix derivative with respect to resistivity parameters and is needed for avoiding the explicit Jacobian construction for Jacobian based computations.

Subroutine **conjugate\_gradient** solves the inverse matrix equation (4.3.2) using

conjugate gradient matrix solver which is implemented through splitting of real and imaginary parts. The main steps of this subroutine calculate the product of matrix  $\hat{\mathbf{G}}$  with arbitrary vectors converting real computations to complex as explained in Chapter 4 by calling subroutine **cg\_matmul**.

In subroutine **cg\_matmul**, first the product of matrix  $\mathbf{K}$  with the given input vector is computed by calling subroutine **k\_matvec\_mul** then the product of inverse of data covariance matrix  $\mathbf{C}_d^{-1}$  with the output vector is computed and the resulting vector is multiplied by matrix  $\mathbf{K}^T$  in the subroutine **kt\_matvec\_mul**. Then, this vector is added to the vector obtained by multiplying  $\lambda\mathbf{C}_m^{-1}$  with the given input vector and the final result is returned to the calling subroutine.

The subroutine **k\_matvec\_mul** computes the product of matrix  $\mathbf{K}$  with a vector using the equation (4.3.19). To perform this task a number of subroutines are called, subroutines **rhsv1** and **rhsv2** are called to multiply vector with matrices  $\mathbf{Y}_1$  and  $\mathbf{Y}_1$  respectively. Subroutine **jacobian\_solver** is called to solve the pseudo forward problems using BICGSTAB method and divergence correction is also applied. Subroutine **l\_matvec\_mul** is called to multiply vector with matrices  $\mathbf{L}^1$  and  $\mathbf{L}^2$ . Same subroutines are also called in subroutine **kt\_matvec\_mul** after setting the value of **matvec\_mul\_flag** to 2. This value of **matvec\_mul\_flag** signifies that transpose of a matrix is multiplied by a vector.

The flow chart of subroutine **inversion** is given in Figure 5.6 and for completeness a brief description of inversion subprograms, along with their purpose(s), subroutines they are called in and subroutines they call, is given in Table 5.4.

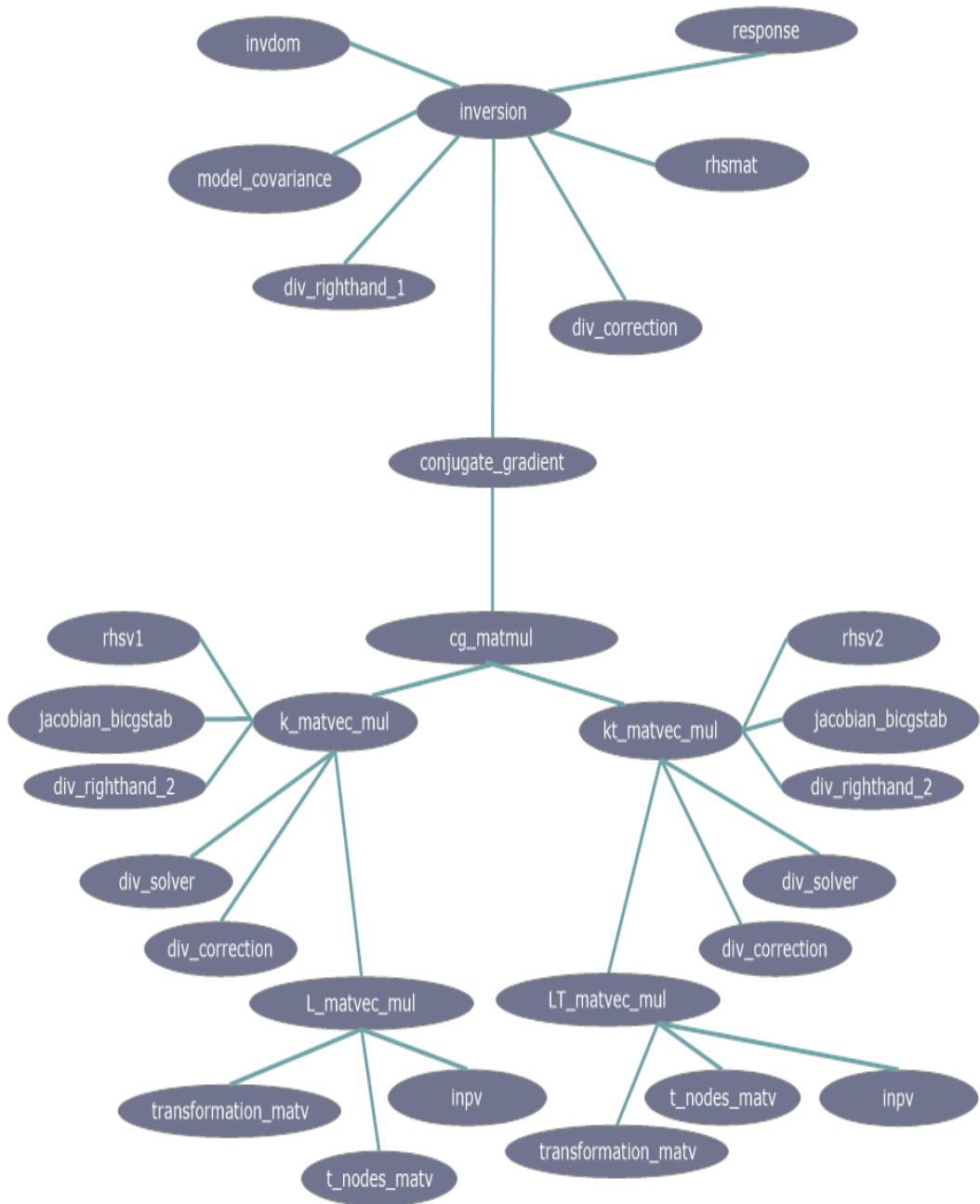


Figure 5.5: Tree structure of inversion subroutines

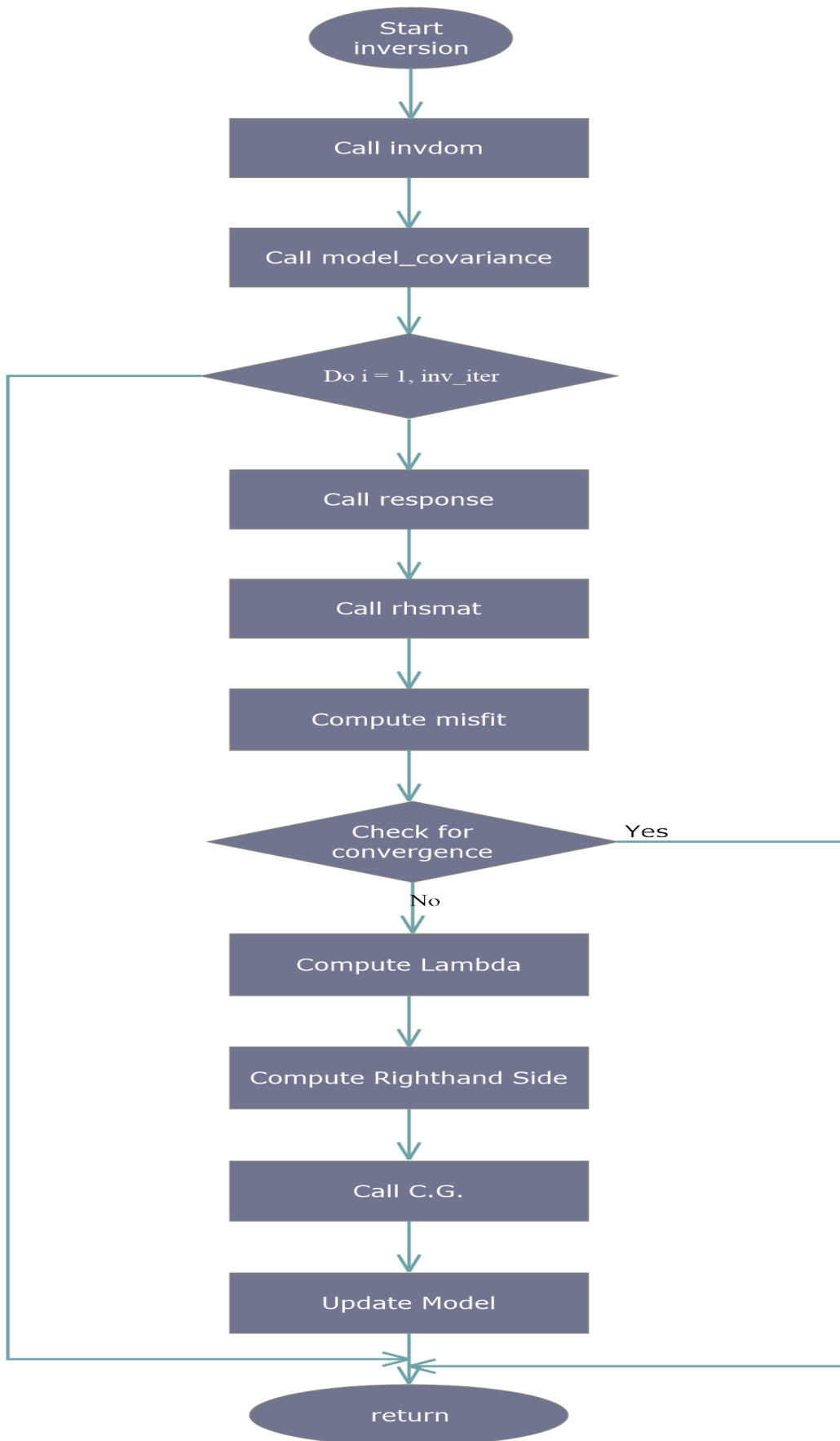


Figure 5.6: Flow chart of inversion modeling subroutine

Table 5.4: Description of various inversion subroutines.

<b>Subroutine</b>	<b>Purpose</b>	<b>Called in</b>	<b>Calls</b>
<b>invdom</b>	Define inversion domain index	<b>inversion</b>	×
<b>model_ covariance</b>	Construct model covariance matrix	<b>inversion</b>	×
<b>response</b>	Compute response of updated models	<b>inversion</b>	See Table 5.3
<b>rhsmat</b>	Construct matrix <b>Y</b>	<b>inversion</b>	×
<b>conjugate_ gradient</b>	Matrix solver for inverse problem	<b>inversion</b>	<b>cg_matmul</b>
<b>cg_matmul</b>	Running index of blocks in Y-direction	<b>conjugate_ gradient</b>	<b>k_matvec_mul</b> , <b>kt_matvec_mul</b>
<b>rhsv1</b>	Number of time periods	<b>k_matvec_mul</b> , <b>kt_matvec_mul</b>	×
<b>rhsv2</b>	Number of site locations	<b>k_matvec_mul</b> , <b>kt_matvec_mul</b>	×
<b>jacobian_bicg_ solver</b>	Total number of data	<b>k_matvec_mul</b> , <b>kt_matvec_mul</b>	×
<b>t_nodes_matv</b>	See Table 5.3	<b>l_matvec_mul</b> , <b>lt_matvec_mul</b>	×
<b>invp</b>	See Table 5.3	<b>l_matvec_mul</b> , <b>lt_matvec_mul</b>	×

Continued on next page

Table 5.4 continued from previous page

<b>div_righthand2</b>	Total number of blocks in inversion domain	<b>k_matvec_mul</b> , <b>kt_matvec_mul</b>	×
<b>div_solver</b>	Tolerances level for forward problem	<b>k_matvec_mul</b> , <b>kt_matvec_mul</b>	×
<b>div_correction</b>	Maximum number of inversion iterations	<b>k_matvec_mul</b> , <b>kt_matvec_mul</b>	×
<b>l_matvec_mul</b>	Threshold value for misfit	<b>k_matvec_mul</b>	×
<b>lt_matvec_mul</b>	Regularization parameter	<b>kt_matvec_mul</b>	×
<b>transformation_matv</b>	See Table 5.3	<b>l_matvec_mul</b> , <b>lt_matvec_mul</b>	×
<b>k_matvec_mul</b>	Running index of blocks in Z-direction	<b>cg_matmul</b>	<b>rhsv1</b> , <b>rhsv2</b> , <b>jacobian_bicg_solver</b> , <b>div_righthand2</b> , <b>div_solver</b> , <b>div_correction</b> , <b>l_matvec_mul</b>
<b>kt_matvec_mul</b>	Total number non-trivial electric field components in modeling domain	<b>cg_matmul</b>	-Do-

## 5.6 Closure

Since algorithm **3DINV\_FD** is based on quasi-linearization it needs judicious choice of convergence criterion. In its present version, the inversion domain should encompass all the in-homogeneities. As a result the algorithm is found to be more efficient for confined anomalous body.

The developed inversion algorithm **3DINV\_FD** for 3D MT data is the final result of this research work. Its validity and applicability are tested through various theoretical exercises designed especially for this purpose. The validation exercises and results are discussed in Chapter 6 and Chapter 7.





# FORWARD MODELING ALGORITHM OPTIMIZATION AND VALIDATION

## 6.1 Introduction

Once the development of the software is completed, it is essential to validate its accuracy and then work towards improving its efficiency. The accuracy of **3DINV\_FD** is validated by comparing its result with the published results and to improve the efficiency of the forward modeling algorithm and hence, the inversion algorithm, the computational parameters for divergence correction are optimally chosen after testing on synthetically designed experiments. Comparison of results for validation and findings of experiments designed to improve the efficiency of **3DINV\_FD** algorithm are discussed here.

## 6.2 Validation of **3DINV\_FD**

The **3DINV\_FD** inversion algorithm is based on quasi-linearization approach and hence, it requires the solution of forward problem a number of times in one inversion iteration. Therefore, to establish the accuracy of the developed software, forward

modeling algorithm has to be validated first.

## 6.2.1 Forward Algorithm Validation

The best check to establish the accuracy of any newly developed algorithm is the reproduction of results available in literature. The developed forward modeling algorithm is validated on different standard models.

### 6.2.1.1 Single Block Model

The first model to validate the algorithm is taken from COMMEMI paper (Zhdanov et al. [167]). In COMMEMI paper the results of different algorithms based on Finite Difference, Finite Element and Integral Equation Methods are compiled together. The model 3D-1(B) of COMMEMI paper is reproduced in Figure 6.1.

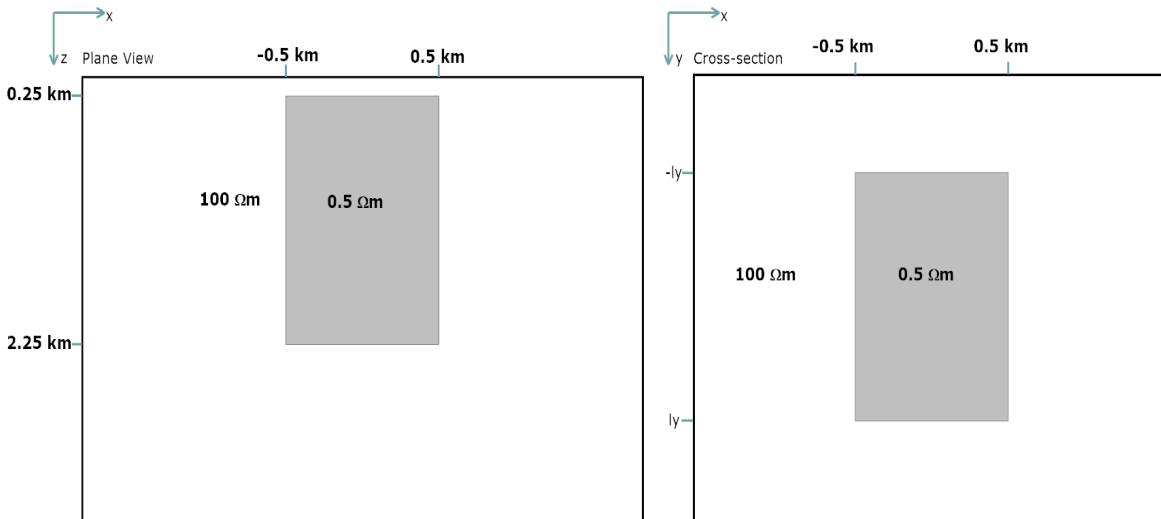


Figure 6.1: Single Block Model

The model 3D-1(B) consists of a rectangular conducting block embedded in a homogeneous half-space. The resistivity of the block is  $0.5 \Omega\text{-m}$  while that of the half space is  $100 \Omega\text{-m}$  and is placed at a depth of 250 m below the earth surface. The block is elongated along Y axis ( $l_y = 5 \text{ km}$ ) and its dimensions are 1 km, 10 km and 2

km along X,Y and Z axis respectively. The response is calculated for time period 10 sec along two profiles. The profile 1 is along the X axis at X = 0 km and stations along this profile are at Y = 0, 2.5, 3.75, 5, 6.25, 7.5 and 10 km and the profile 2 is along the Y axis at Y = 0 km and stations along this profile are at X = 0, 0.25, 0.5, 0.75, 1, 1.5, 2 and 4 km. The comparison of  $\rho_{xy}$  and  $\rho_{yx}$  along the two profiles with the results provided in COMMEMI paper are shown in Figures 6.2a - 6.2d.

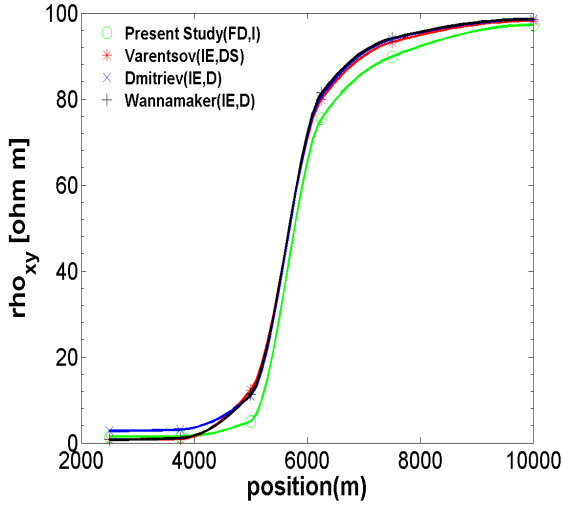
### 6.2.1.2 Two Block Model

The second model (3D-2) for validating the developed algorithm is also chosen from COMMEMI paper. This standard model was used by various researchers (Wannamaker [152], Mackie et al. [74], Avdeev et al. [6], Siripunvaraporn et al. [129]) to validate their algorithms. The model consists of two rectangular blocks, of which one is conducting and other is resistive, in the upper layer of a three-layer model (Figure 6.3). The resistivities of the layers are  $10\Omega\text{-m}$ ,  $100\Omega\text{-m}$  and  $0.1\Omega\text{-m}$  and the dimensions and resistivities of the embedded blocks are given in Table 6.1. The response is computed

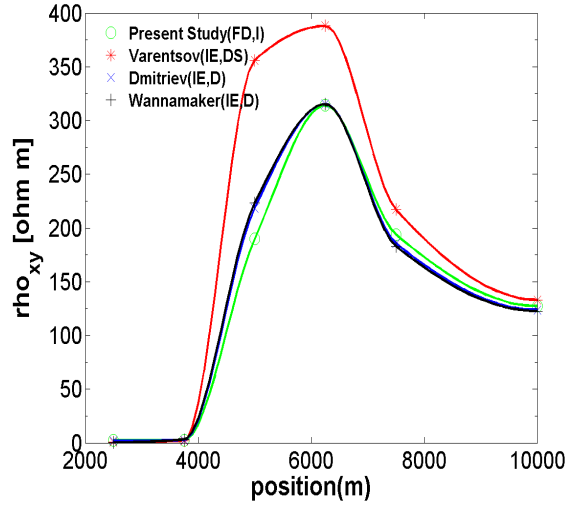
Table 6.1: Dimensions and resistivities of the anomalous bodies in 3D-2 model.

	x (km)	y (km)	z (km)	resistivity ( $\Omega\text{-m}$ )
block 1	-20 to 20	-20 to 0	0 to 10	$1(\rho_1)$
block 2	-20 to 20	0 to 20	0 to 10	$100(\rho_2)$

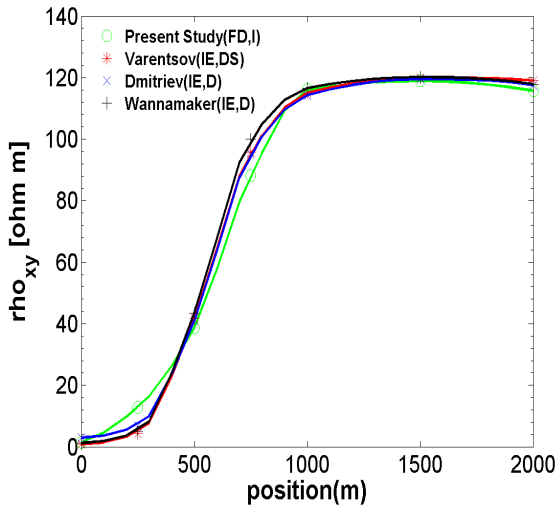
for time period 100 sec along three profiles A, B and C (Figure.6.3b). The results (responses) of **3DINV\_FD** algorithm are compared with the results of Siripunvaraporn et al. [129], the numerical values of the responses for the algorithm of Siripunvaraporn



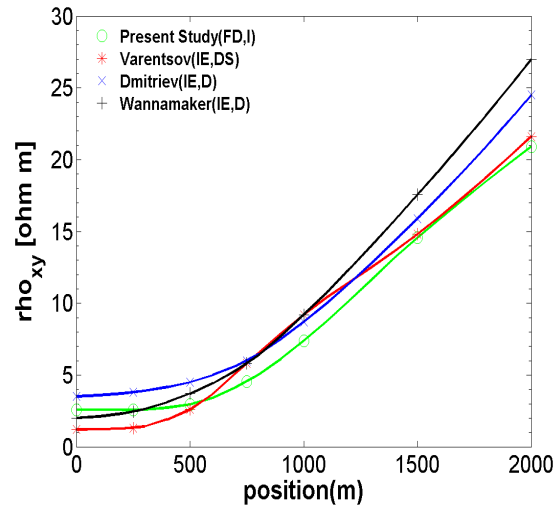
(a)  $\rho_{xy}$  along profile 1



(b)  $\rho_{yx}$  along profile 1



(c)  $\rho_{xy}$  along profile 2



(d)  $\rho_{yx}$  along profile 2

Figure 6.2: Comparison of **3DINV\_FD** and published results in COMMEMI paper (Zhdanov et al. [167]) for model 3D-1(B). Abbreviations: FD = finite difference method, IE = integral equation method, D = direct solution, S = stationary field approximation, I = iterative solution.

et al. [129] are obtained by discretizing the plots given in the paper. The comparison of apparent resistivity and phase along three profiles is shown in Figures 6.4 - 6.9

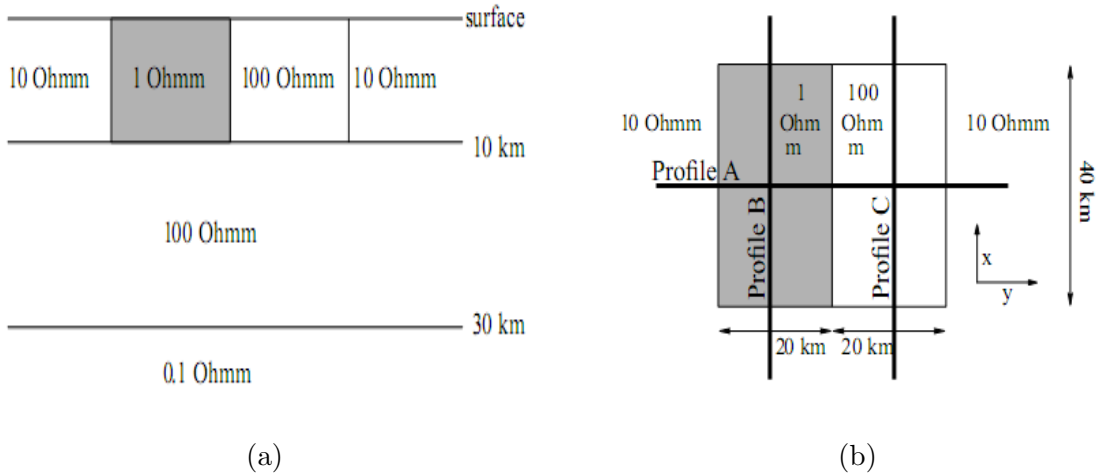


Figure 6.3: (a) Cross-section view of the synthetic model and (b) Profiles where data are generated.

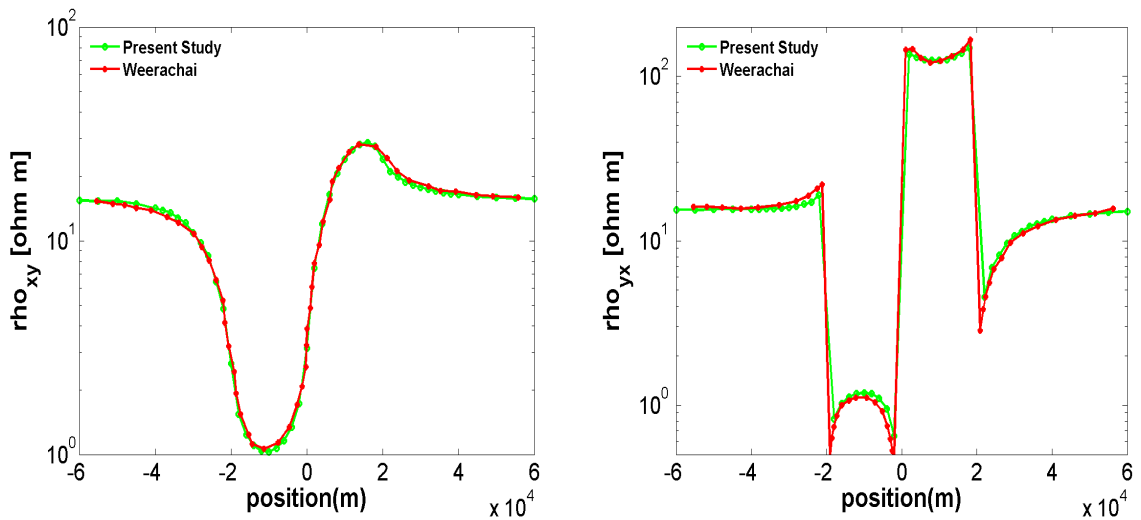


Figure 6.4: Comparison of apparent resistivities in  $Z_{xy}$  and  $Z_{yx}$  modes between results from 3DINV\_FD algorithm and Siripunvaraporn et al. [129] along profile A.

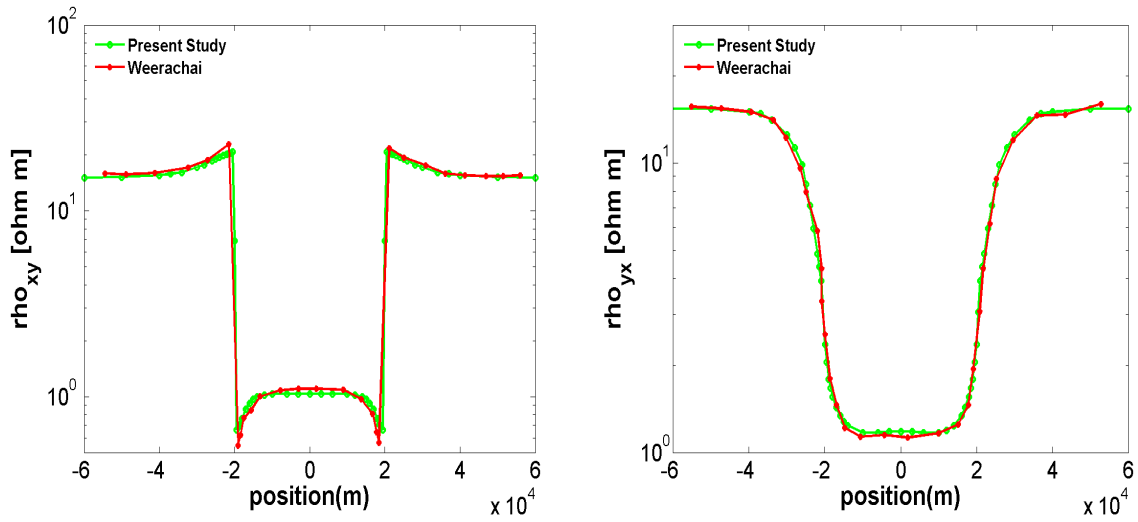


Figure 6.5: Comparison of apparent resistivities in  $Z_{xy}$  and  $Z_{yx}$  modes between results from **3DINV\_FD** algorithm and Siripunvaraporn et al. [129] along profile B.

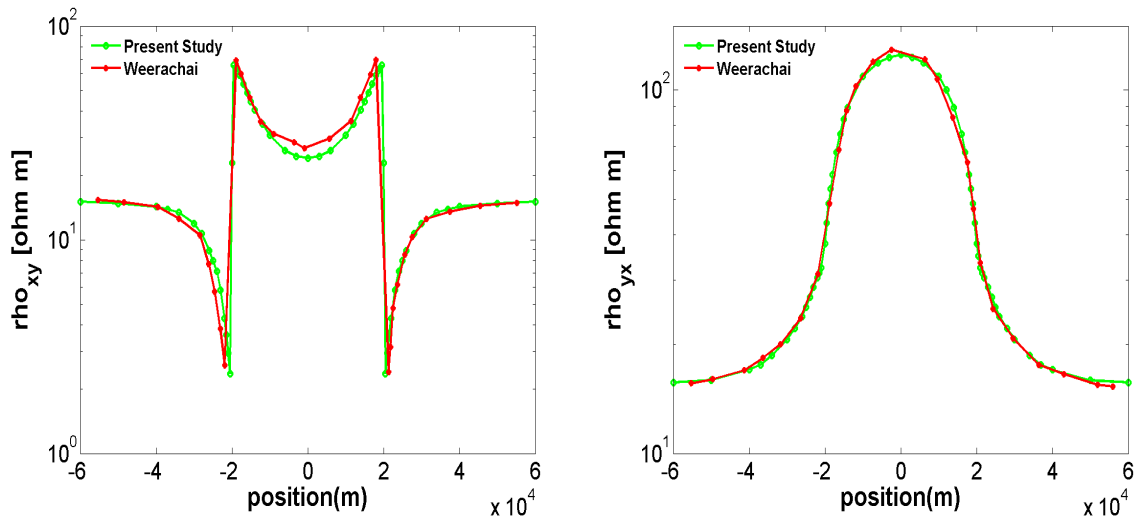


Figure 6.6: Comparison of apparent resistivities in  $Z_{xy}$  and  $Z_{yx}$  modes between results from **3DINV\_FD** algorithm and Siripunvaraporn et al. [129] along profile C.

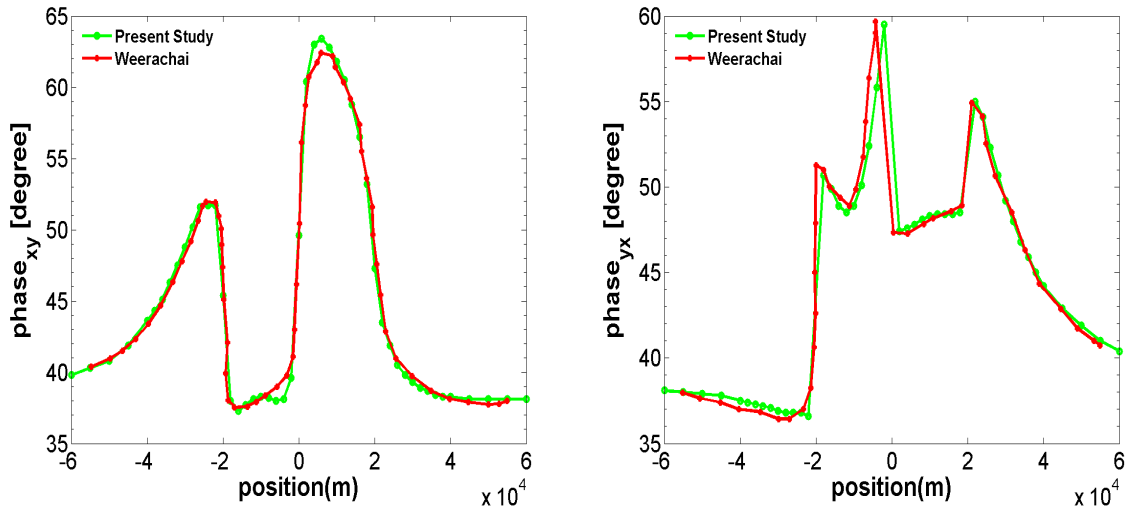


Figure 6.7: Comparison of phase in  $Z_{xy}$  and  $Z_{yx}$  modes between results from **3DINV\_FD** algorithm and Siripunvaraporn et al. [129] along profile A.

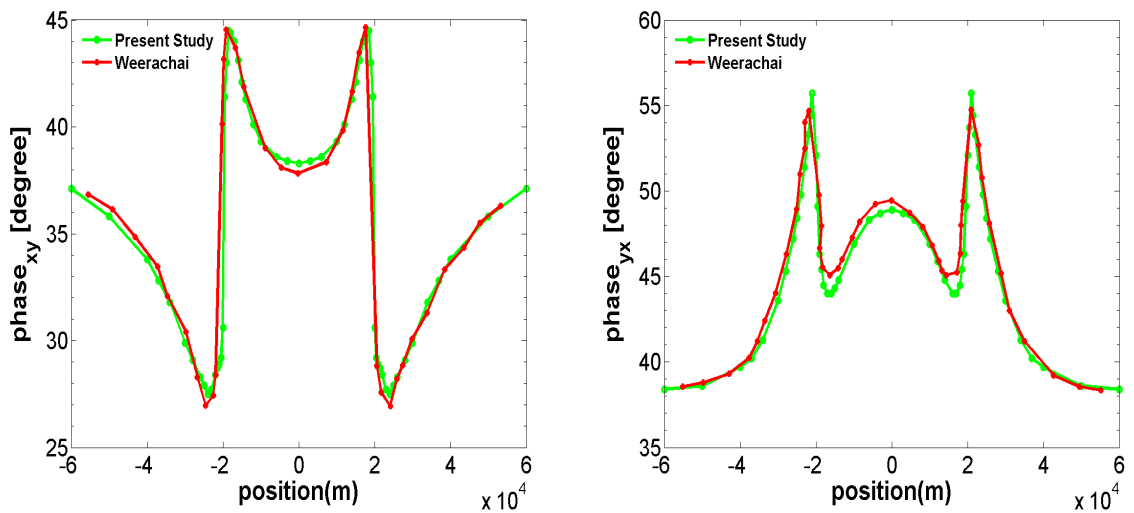


Figure 6.8: Comparison of phase in  $Z_{xy}$  and  $Z_{yx}$  modes between results from **3DINV\_FD** algorithm and Siripunvaraporn et al. [129] along profile B.



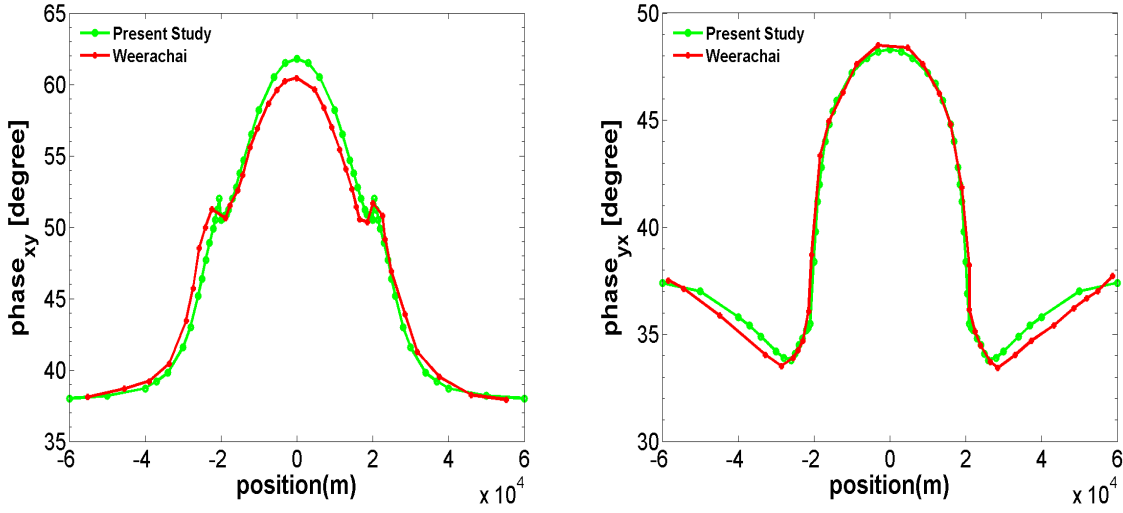


Figure 6.9: Comparison of phase in  $Z_{xy}$  and  $Z_{yx}$  modes between results from 3DINV\_FD algorithm and Siripunvaraporn et al. [129] along profile C.

### 6.2.1.3 Dublin Test Model 1

The third model chosen for validating the forward algorithm is taken from Miensoopust et al. [83]. This model termed as Dublin Test Model 1 (DTM1), was proposed in MT 3D Inversion Workshop 2008 and was aimed at comparison of results of different modeling codes. The model consists of three blocks of different resistivities in an homogeneous half-space of resistivity 100  $\Omega$ -m. The dimensions and the resistivities of the blocks

Table 6.2: Dimensions and resistivities of the anomalous bodies in DTM1.

	x (km)	y (km)	z (km)	resistivity ( $\Omega$ -m)
block 1	-20 to 20	-2.5 to 2.5	5 to 20	10 ( $\rho_1$ )
block 2	-15 to 0	-2.5 to 22.5	20 to 25	1 ( $\rho_2$ )
block 3	0 to 15	-22.5 to 2.5	20 to 50	10,000 ( $\rho_3$ )

are given in Table 6.2. In Figure 6.10, the sketches of the cross-section and plan view of

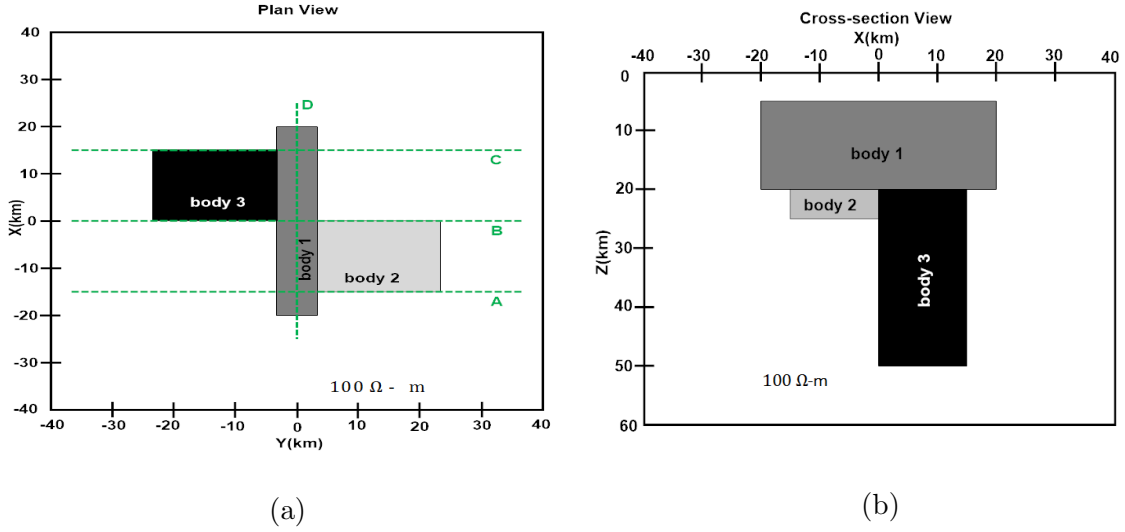


Figure 6.10: Plan and cross-section view of Dublin test model ( $\rho_1 = 10 \Omega \text{ m}, \rho_2 = 1 \Omega \text{ m}, \rho_3 = 10000 \Omega \text{ m}$ ).

the model are shown. The response is computed for 4 time periods (1 s, 10 s, 100 s and 1000 s) at 59 observations points located on 4 profiles, 3 profiles (A, B and C) parallel to Y axis at  $X = -15 \text{ km}$ ,  $X = 0 \text{ km}$  and  $X = 15 \text{ km}$  and each having 16 equally spaced observation points with 5 km spacing (from  $Y = -37.5 \text{ km}$  to  $Y = 37.5 \text{ km}$ ) and the 4<sup>th</sup> profile (D) parallel to X axis at  $Y = 0 \text{ km}$  has 11 equally spaced observation points with 5 km spacing (from  $X = -25 \text{ km}$  to  $X = 25 \text{ km}$ ). For validating the algorithm, the numerical values of the responses from different algorithms are downloaded from Miensoyust and Jones [82]. In Figures 6.11 to 6.14 the  $\rho_{xy}$  and  $\rho_{yx}$  obtained from **3DINV\_FD** and published results for time period 100 sec along all 4 profiles and the relative error with respect to the published results are shown and similarly the comparison of results along profile X2 for all periods is shown in Figures 6.15 to 6.18. The relative error is upto 5% and is within the acceptable range.

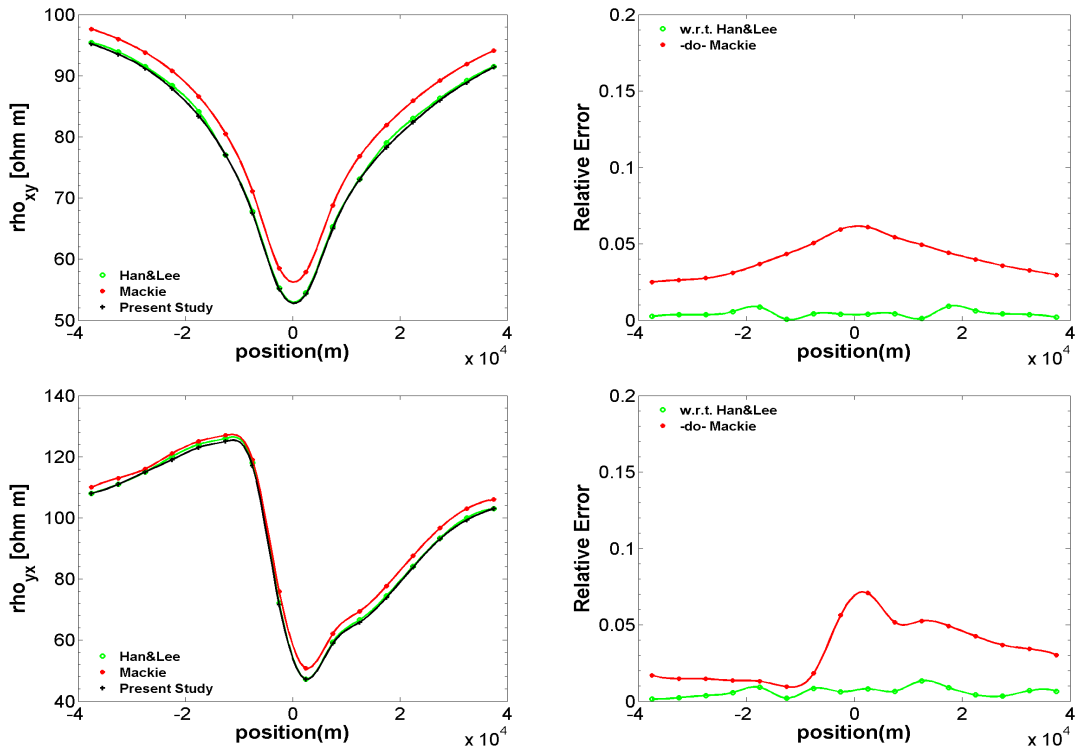


Figure 6.11: Comparison of Apparent resistivities in  $Z_{xy}$  and  $Z_{yx}$  modes for time period 100 sec along profile A.

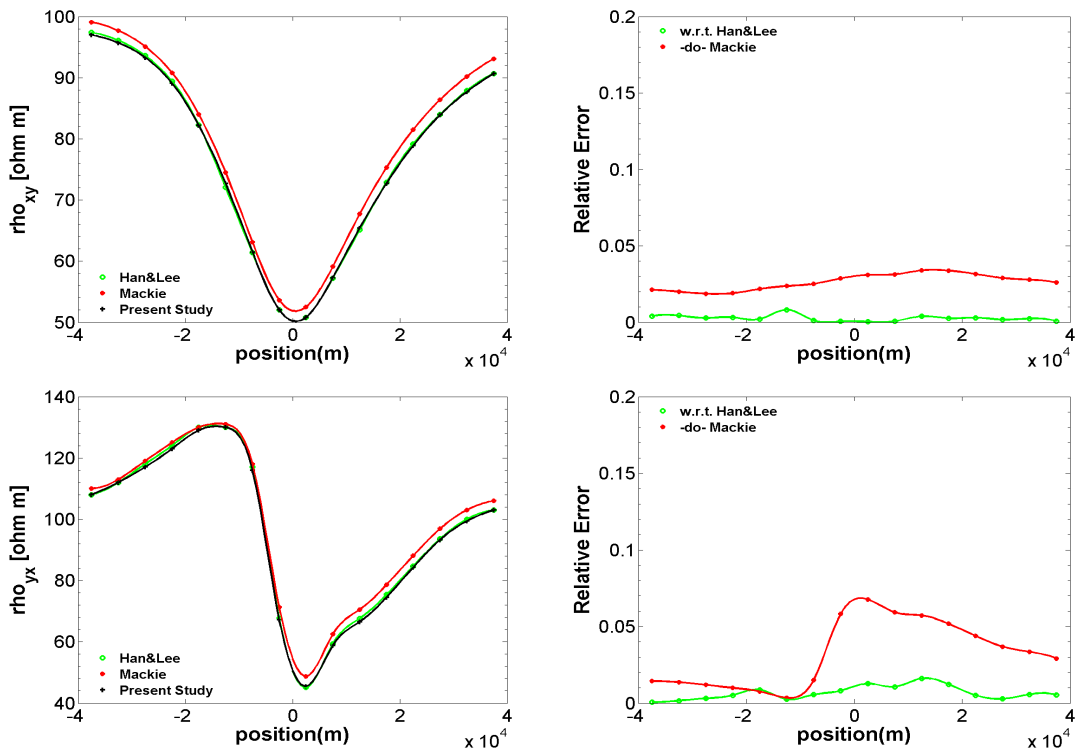


Figure 6.12: Comparison of Apparent resistivities in  $Z_{xy}$  and  $Z_{yx}$  modes for time period 100 sec along profile B.

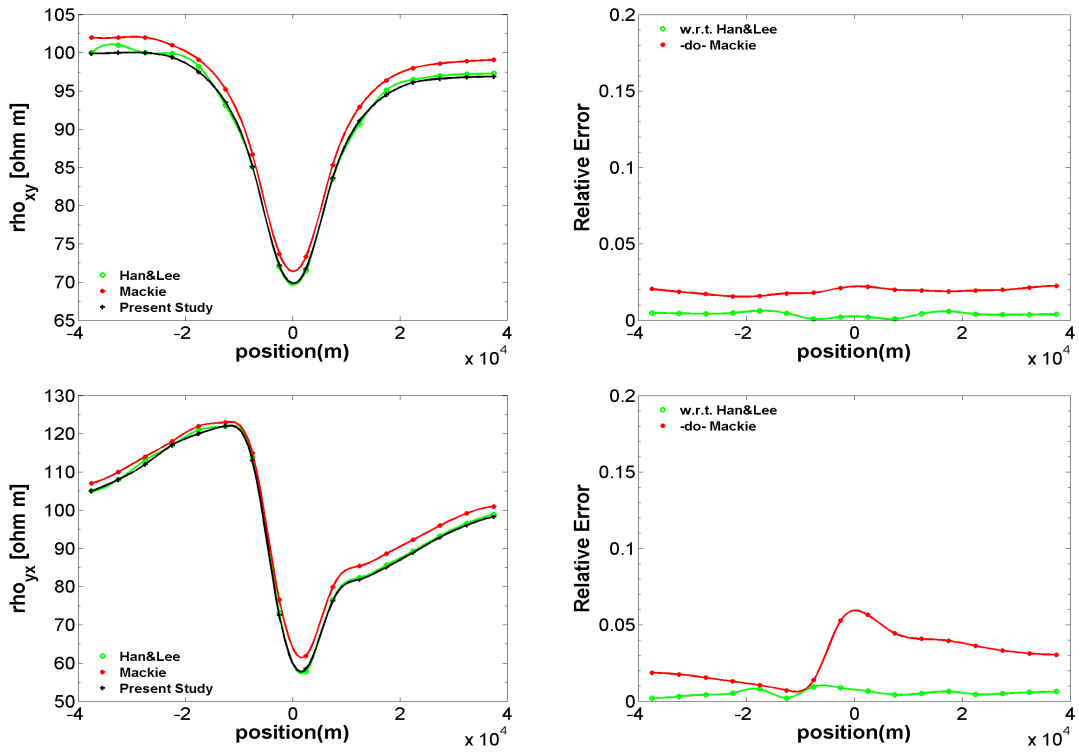


Figure 6.13: Comparison of Apparent resistivities in  $Z_{xy}$  and  $Z_{yx}$  modes for time period 100 sec along profile C.

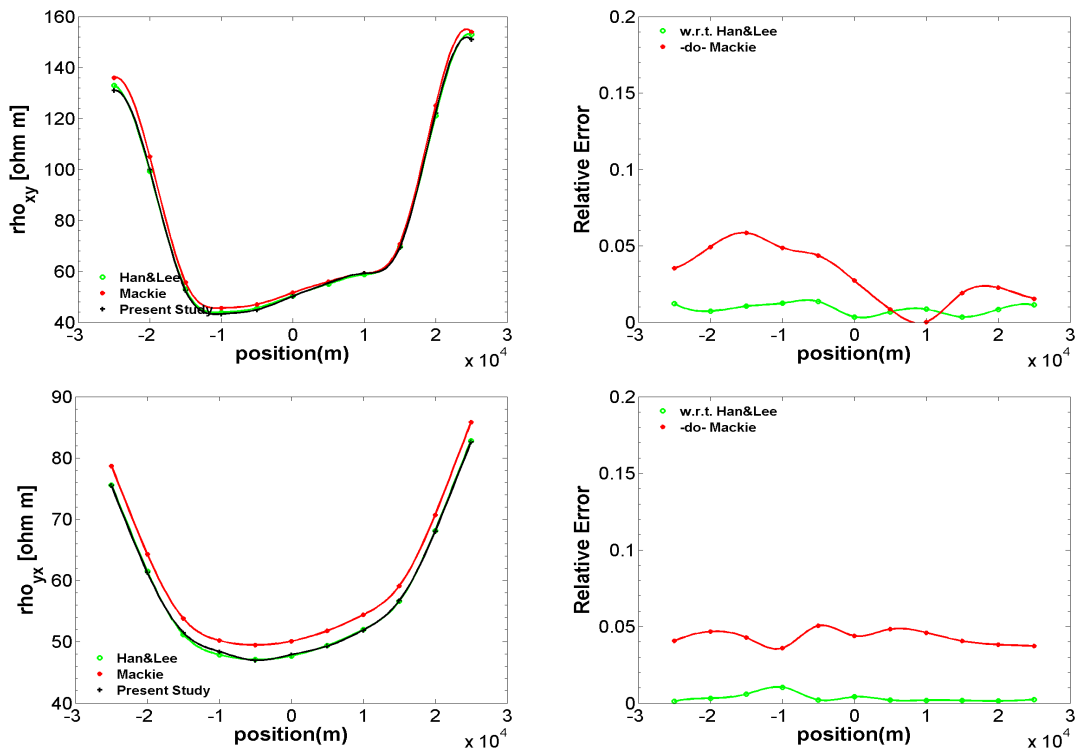


Figure 6.14: Comparison of Apparent resistivities in  $Z_{xy}$  and  $Z_{yx}$  modes for time period 100 sec along profile D.

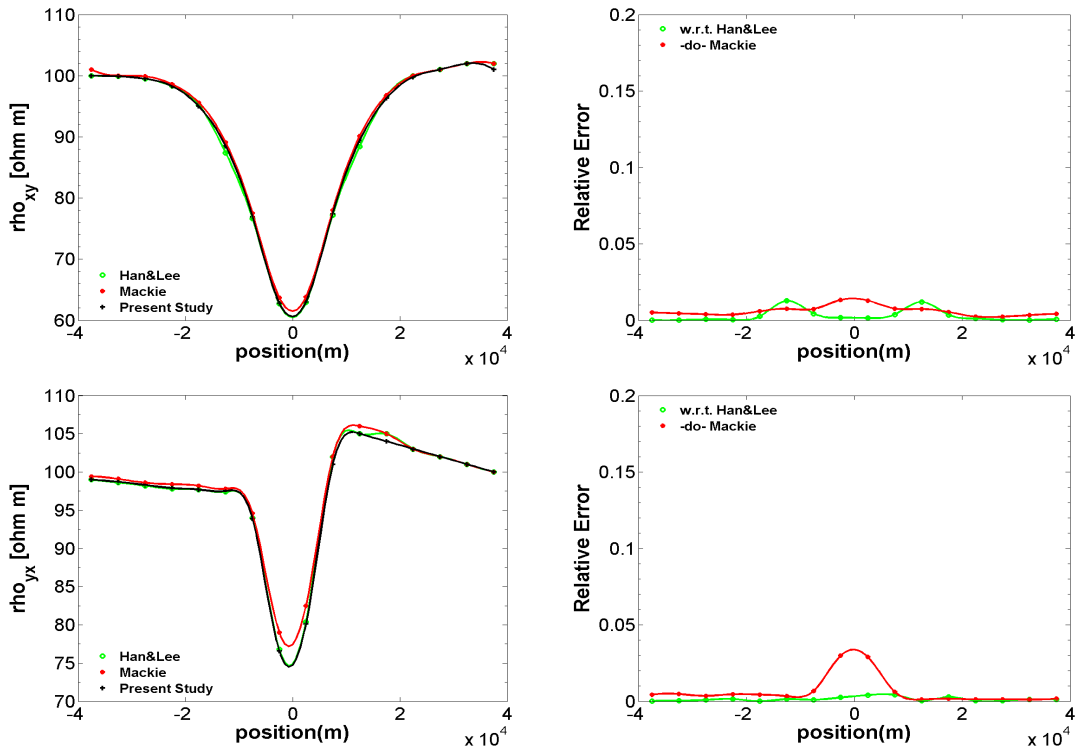


Figure 6.15: Comparison of Apparent resistivities in  $Z_{xy}$  and  $Z_{yx}$  modes for time period 1 sec along profile B.

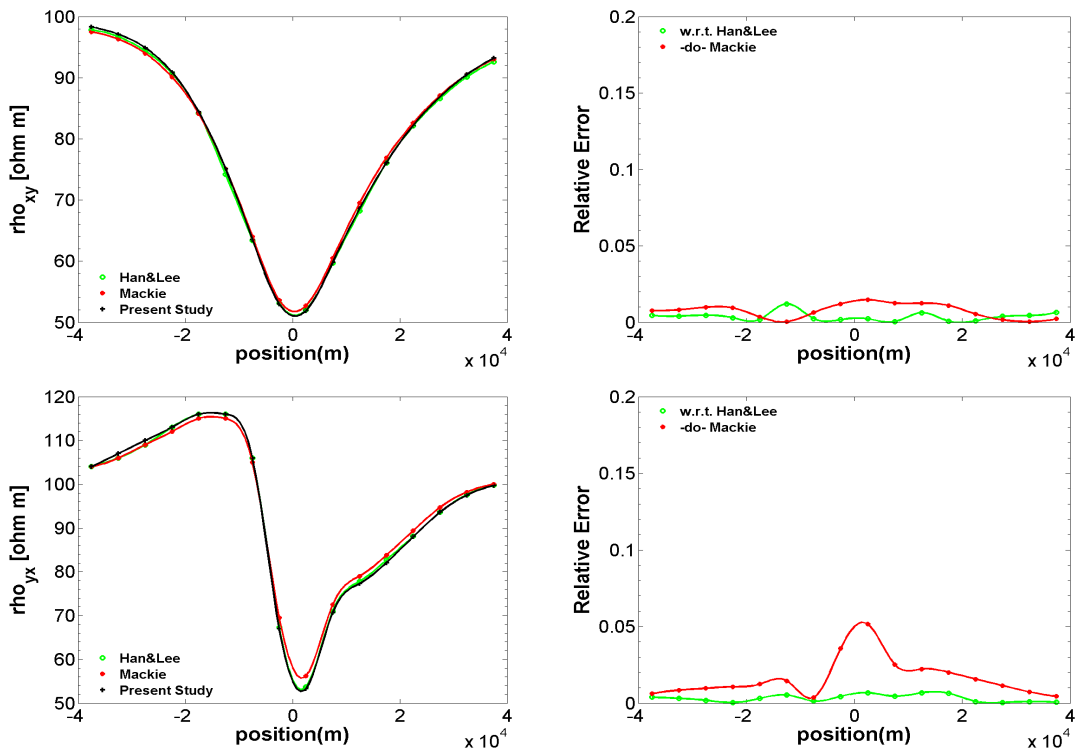


Figure 6.16: Comparison of Apparent resistivities in  $Z_{xy}$  and  $Z_{yx}$  modes for time period 10 sec along profile B.

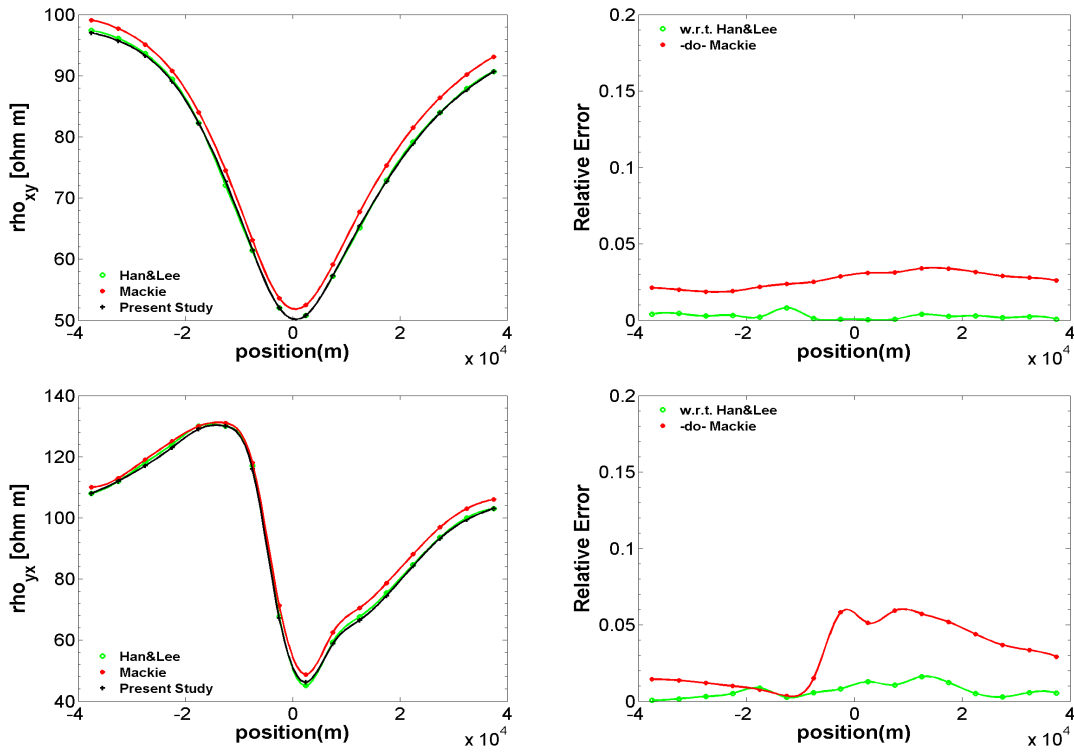


Figure 6.17: Comparison of Apparent resistivities in  $Z_{xy}$  and  $Z_{yx}$  modes for time period 100 sec along profile B.

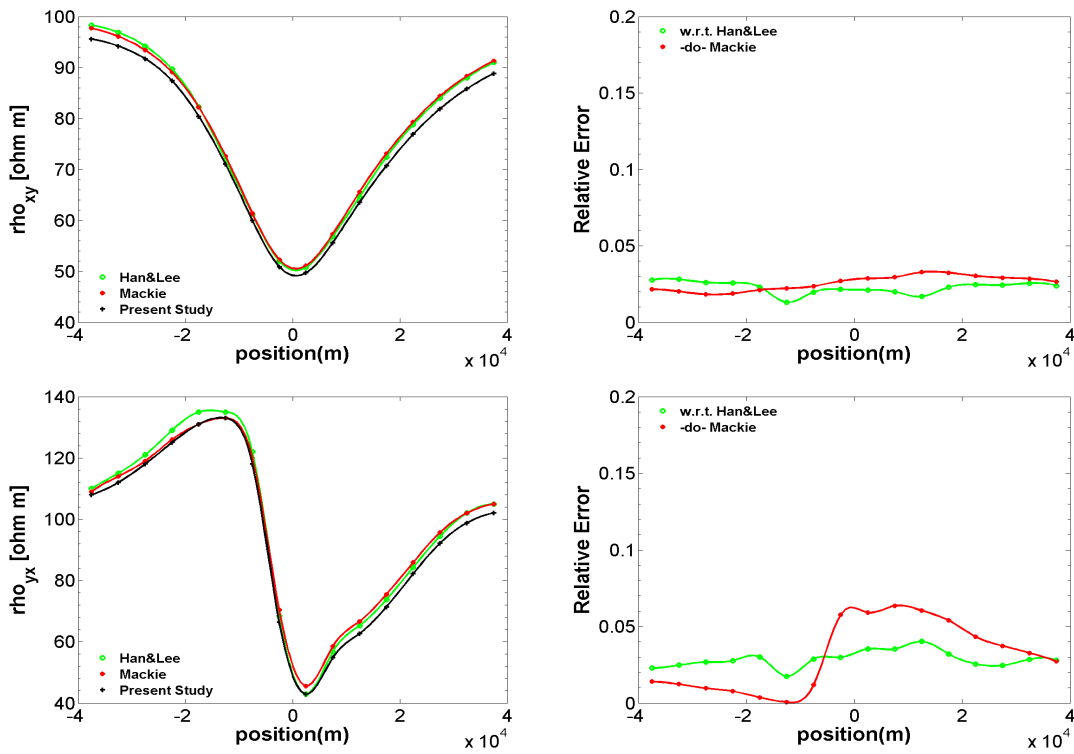


Figure 6.18: Comparison of Apparent resistivities in  $Z_{xy}$  and  $Z_{yx}$  modes for time period 1000 sec along profile B.

## 6.3 Algorithm Optimization

After the accuracy of the forward modeling algorithm is established by comparing its response with the published results, the next task was to improve the efficiency of the algorithm. As the **3DINV\_FD** algorithm is based on quasi-linearization approach, hence, during the inversion process hundreds of forward problems are solved making it computationally expensive and solution of forward problems constitutes the major part of the total computational time of the inversion algorithm.

So, the efficiency of the inverse algorithm depends on two major factors, the first being the efficient implementation of computations involving sensitivity matrix and other, is how efficiently the forward problem is solved. The first objective is achieved by bypassing the explicit sensitivity matrix computation as explained in Chapter 5 and the efficiency of the forward modeling algorithm is improved by implementing the following

- Choosing the optimal computational parameters for applying static divergence correction.
- Parallel computation of forward problems for multi-frequency case.

### 6.3.1 Optimal Computational Parameters for Divergence Correction

The main feature of forward modeling that controls its convergence at low frequencies is the divergence correction. And the efficiency of the forward modeling algorithm can be adversely effected if it is not applied properly. The efficient implementation of divergence correction is dependent on two parameters, namely,

1. Upto what accuracy divergence problem is to be solved for obtaining the scalar  $\Phi$  .
2. After how many BICGSTAB iterations, the iterative solution needs be corrected by applying static divergence correction.

The optimal value of these parameters is fixed after rigorous testing on different models.

The experiment designed for this specific purpose and the observation of the experiment is discussed next.

#### **6.3.1.1 Experiment Design**

The experiment for finding the optimal values of computational parameters pertaining to the divergence correction is divided into four cases as:

- A. The iterative solution is corrected using divergence correction after every 20 BICGSTAB iterations and the divergence problem is solved seeking accuracy of the order of  $10^{-2}$ ,  $10^{-3}$ ,  $10^{-4}$  and  $10^{-5}$  in different runs. The computation time for each run is then compared to find the combination, which results in minimum computation time.
- B. The iterative solution is corrected using divergence correction after every 30 iterations and rest of the details are same as explained in case A.
- C. The iterative solution is corrected using divergence correction after every 40 iterations and rest of the details are same as explained in case A.
- D. The iterative solution is corrected using divergence correction after every 50 iterations and rest of the details are same as explained in case A.



After finding the minimum computation time for each case, the optimal computational parameters are fixed by choosing the combination which results in minimum computation time among themselves. This experiment is carried out for different models and the results for two models are presented here.

### 1. Conducting Block Model

This model consists of a single conducting body of resistivity  $1 \Omega\text{-m}$  buried in a homogeneous half space of resistivity  $100 \Omega\text{-m}$ . The lateral dimension of the body is  $-12 \text{ km}$  to  $12 \text{ km}$  in  $X$  and  $Y$  directions and the its thickness is  $5 \text{ km}$ . The body is buried at a depth of  $0.1 \text{ km}$  below the earth surface. The diagram of the model is given in Figure 6.19. Now, the response is computed for two time periods ( $100 \text{ sec}$ ,  $1000 \text{ sec}$ ) and the computation time for all 4 cases is shown in Figure 6.20a - 6.20d and the comparison among minimum computation time of each case is shown in Figure 6.20e. From Figure 6.20e it is clear that the optimal computation time is taken in solving the forward problem when the divergence correction is applied after 40 BICGSTAB iterations and divergence problem is solved seeking an accuracy of  $10^{-3}$ .

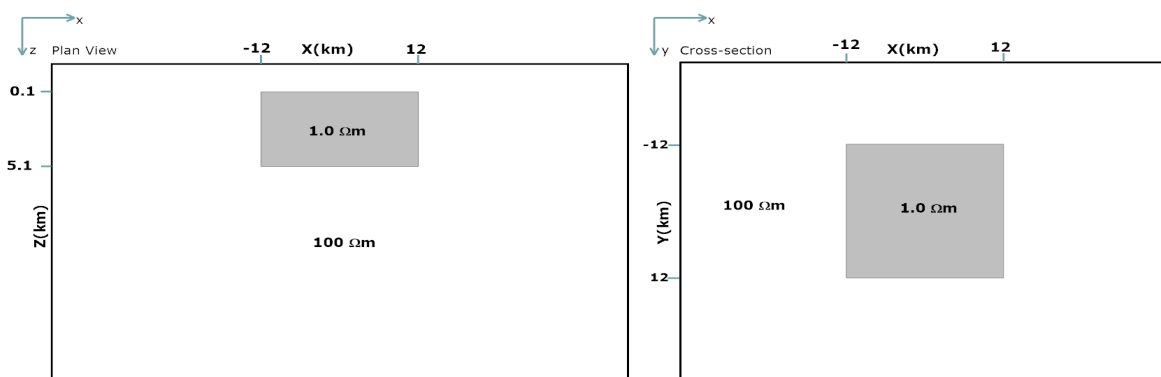
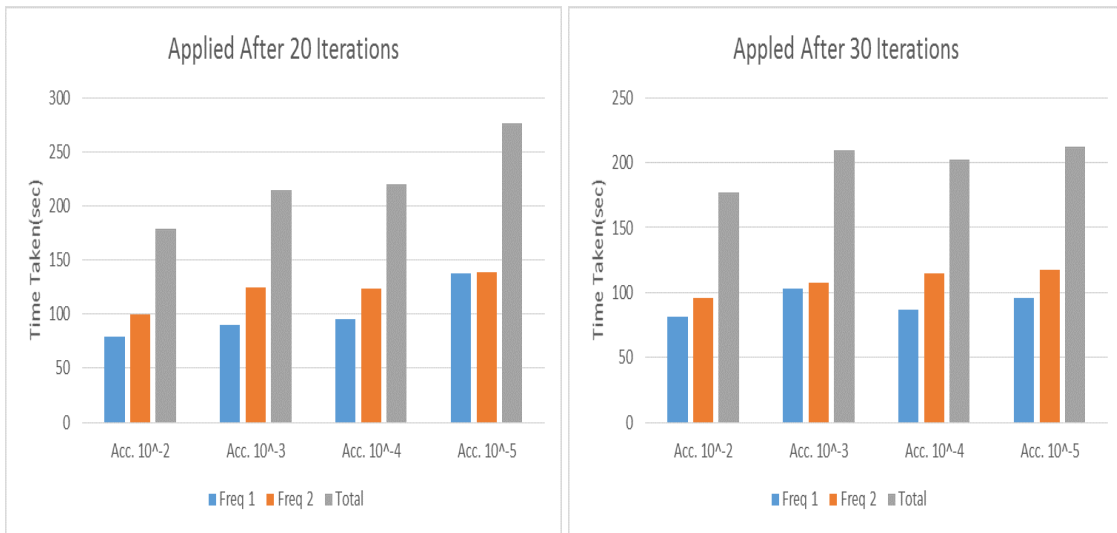
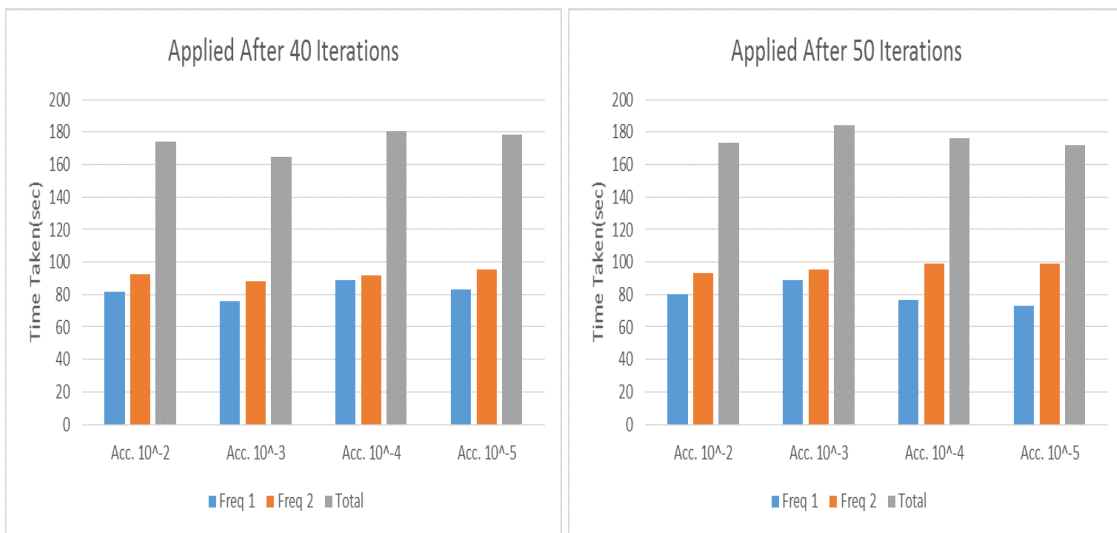


Figure 6.19: Plan and cross-section view of the model.



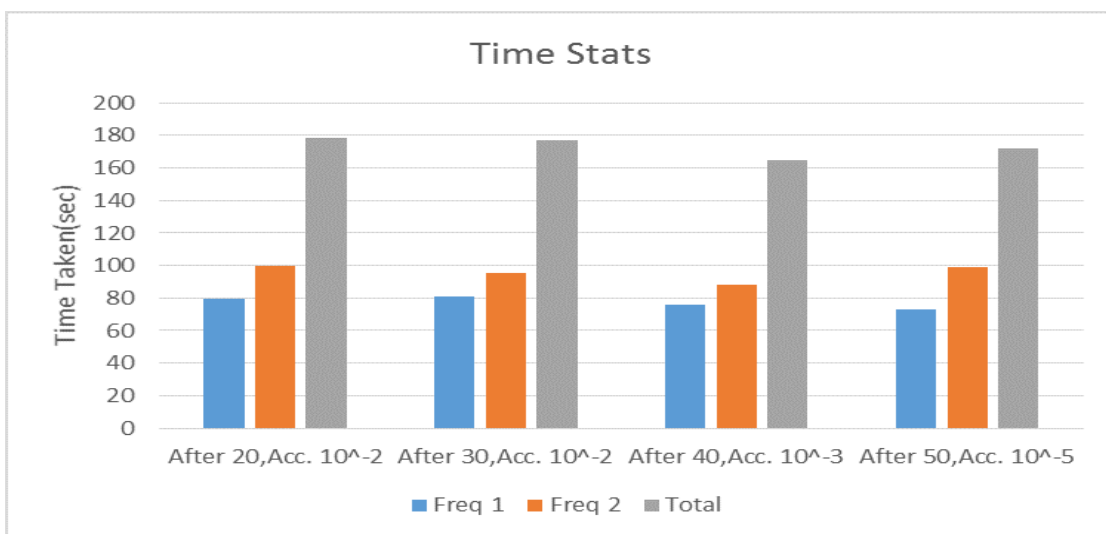
(a)

(b)



(c)

(d)



(e)

Figure 6.20: Computation time comparison

## 2. Dublin Test Model 1

The same experiment is carried out for DTM1 (Figure 6.10), solving the forward problem for two time periods (100 sec and 1000 sec). The comparison of computation time for each case is shown in Figure 6.21a - 6.21e.

From the analysis of these tests conducted on different models, it is concluded that for optimal computation time for forward problem the divergence problem should be solved upto an accuracy  $10^{-3}$  and be applied after every 40 BiCGSTAB iterations.

### 6.3.2 Parallel Programming

To improve the efficiency of the **3DINV\_FD** algorithm, OpenMP application programming interface (API) is used for parallelizing the algorithm. There are two reasons for this choice, first is the availability of shared memory computer and second is its simplicity to implement on such hardware. Now a days personal computers/laptops have multi-core processor with shared memory architecture, so one can take full advantage of all the available cores while running this code even on these system. The parallel computing can be very efficiently implemented if a task can be divided into many small tasks and each one can be done independently. As, in the developed algorithm, the most computationally costly part is the solution of forward problem for computing predicted response for multiple frequencies and solution of pseudo forward problem in CG iterations during the product of the Jacobian matrix (or its transpose) with an arbitrary vector for multiple frequencies. So, the loop which runs over number of time periods is parallelized while solving these forward and pseudo-forward problems. To demonstrate the gain, in regards to computation time, that we are getting by



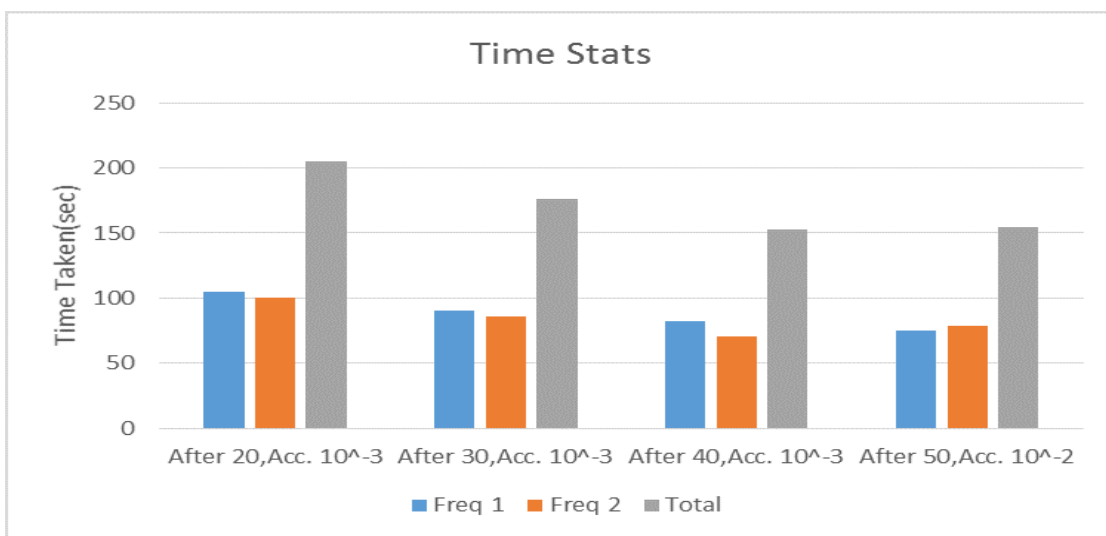
(a)

(b)



(c)

(d)



(e)

Figure 6.21: Computation time comparison

parallelizing the algorithm, Table 6.3 lists the time taken while computing the forward response for COMMEMI model 3D-2 for 8 time periods (case 1: all 8 time periods are taken 100 sec, case 2: .1 sec, .5 sec, 1 sec, 5 sec, 10 sec, 50 sec, 100 sec and 500 sec). It may be noted here that the gain in case 2 is less compared to case 1

Table 6.3: Comparison between computation time of serial and parallel code

	Time Period (sec)	Serial Time (sec)	Parallel Time (sec)
Case 1	100	953.5	213.8
Case 2	.1,.5,1,5,10,50,100,500	621.7	180.4

is expected, as the processors doing computation for low time period/high frequency will be sitting ideal waiting for the processors doing high time period computation to finish their task.

# 3D MT INVERSION RESULTS

## 7.1 Introduction

The accuracy and efficiency of forward modeling code having been established, we employ it as an engine for the inversion in 3D inversion algorithm **3DINV\_FD**. In this chapter we establish how our 3D inversion algorithm using Gauss-Newton with conjugate gradient method, performs in practice on synthetic but realistic numerical examples. Furthermore, in Subsection 7.2.3 we demonstrate the robustness of the algorithm by successfully inverting the synthetic data generated by ModEM algorithm (Kelbert et al. [61]). After testing the algorithm on different synthetic data sets, synthetic experiments conducted to study the effect of number of sites and their distribution on the inversion result are also discussed in this chapter.

## 7.2 Inversion Results

To test the developed inversion program, inversion of different synthetic models is performed. All computations are carried out on an Intel Core i7 3.6 GHz machine with 4 Gbyte of RAM, as a result any modern day common PC can reproduce these

computations. The inversion of different data sets is discussed next.

### 7.2.1 Synthetic Data Set 1

First we consider the model (Figure 7.1), consisting of a single conductive body of  $1 \Omega\text{m}$  embedded in  $100 \Omega\text{m}$  half space. The block is buried at a depth of 250 m below the earth surface and its dimensions are 24 km, 34 km and 5 km along X,Y and Z axis respectively. The response is calculated at 81 sites (Figure 7.2) located on 9 profiles parallel to Y axis separated by 4km (from  $y = -16 \text{ km}$  to  $Y = 16 \text{ km}$  ). Each profile has 9 sites separated by 4 km (from  $X = -16 \text{ km}$  to  $X = 16 \text{ km}$ ), by solving the forward problem on  $60 \times 60 \times 30$  (+7 air layers) grid . The full complex impedance tensor ( $\mathbf{Z}_{xx}, \mathbf{Z}_{xy}, \mathbf{Z}_{yx}$  and  $\mathbf{Z}_{yy}$ ) for five periods (0.1,1,10,100 and 1000s) is inverted after adding 2% random Gaussian noise in the data.  $39 \times 39 \times 21$  (+7 air layers) grid is used during inversion, which is different from the one used for data generation. The data covariance is taken to be 2% of  $|\mathbf{Z}_{xy}\mathbf{Z}_{yx}|^{1/2}$ . The initial guess model used for inversion is a  $50 \Omega\text{m}$  halfspace, which is also used as the base model,  $\mathbf{m}_0$  for inversion.

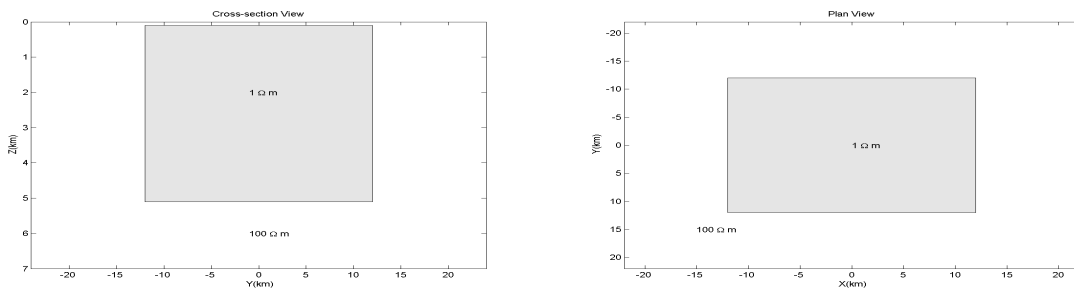


Figure 7.1: Cross-section and plan view of the simple synthetic model used for testing inversion algorithm.

During the inversion, the selection of regularization parameter,  $\lambda$ , and its cooling during the iterative process was done in a manner similar to the idea of Newman

and Alumbaugh [91]. The inversion process converged to the desired misfit in eight iterations. Each iteration took about 25 min, for a total of 3.2 hours for eight iterations. The model recovered after inversion is shown in Figure 7.3. Figure 7.3a shows the cross-section view through the conductive body at  $X = 0$  m while the plan views at 100 m depth, 1 km depth and 5 km depth are shown in Figures 7.3b - 7.3d. From Figure 7.3 it is evident that the the conductivity, shape and position of the anomalous body is recovered by the inversion algorithm. It is clear that the shape is not perfect near the edges, which is mainly due to the limited number of sites. Moreover, the bottom of the conductive block is well resolved which is the intrinsic difficulty of MT inversion, and is not a limitation of our algorithm, e.g., see Siripunvaraporn and Egbert [126], Newman and Alumbaugh [92] or Siripunvaraporn et al. [130], among others.

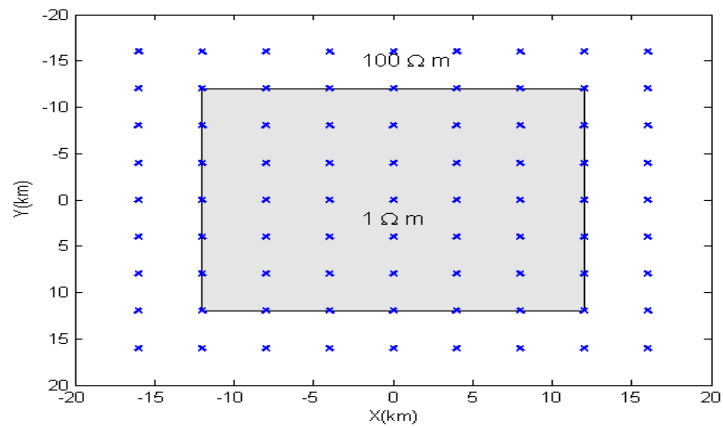
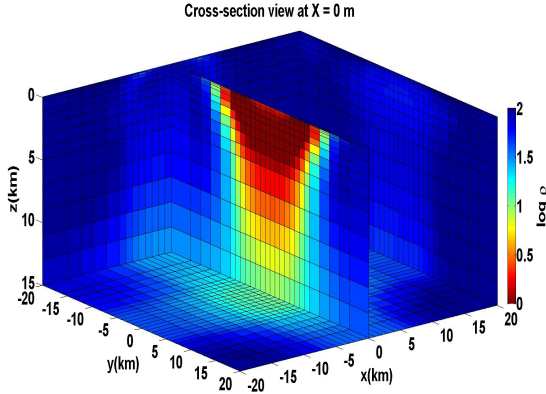
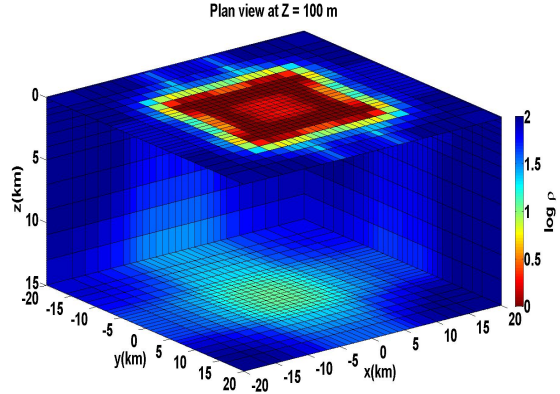


Figure 7.2: Distribution of sites for data generation.

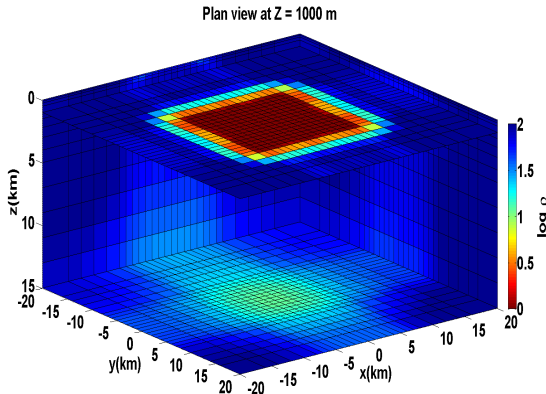




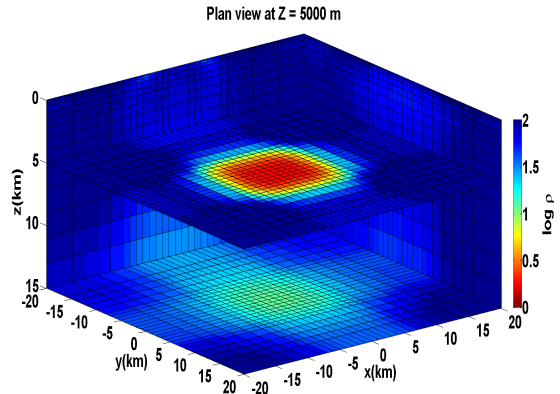
(a) YZ plan at  $X = 0$  m.



(b) XY plan at  $Z = 100$  m.



(c) XY plan at  $Z = 1000$  m.



(d) XY plan at  $Z = 5000$  m.

Figure 7.3: Inversion result of fitting the synthetic data generated from single block model (Figure 7.1).

## 7.2.2 Synthetic Data Set 2

We also tested the inversion algorithm on a more complex model called COMMEMI 3D-2 model (Figure 6.3a), used in different modeling and inversion papers (Wannamaker [152], Mackie et al. [74], Avdeev et al. [6], Siripunvaraporn et al. [130], Avdeev and Avdeeva [5], among others). This model consists of two adjacent anomalous bodies in the top layer of three-layered earth. The response is calculated at 40 sites (Figure 7.4) located on 8 profiles parallel to Y axis at  $y = -28, -21, -13, -4, 4, 13, 21$  and  $28$

km . Each profile has 5 sites separated by 14 km (from  $X = -28$  km to  $X = 28$  km). A  $48 \times 68 \times 21$  (+7 air layers) grid was used for solving the forward problem. The full complex impedance tensor ( $\mathbf{Z}_{xx}, \mathbf{Z}_{xy}, \mathbf{Z}_{yx}$  and  $\mathbf{Z}_{yy}$ ) for five periods (0.1, 1, 10, 100 and 1000s) is inverted after adding 2% random Gaussian noise in the data.  $39 \times 39 \times 21$  (+7 air layers) grid is used during inversion, which is different from the one used for data generation. The initial guess model and the base model,  $\mathbf{m}_0$  used for inversion is a  $50 \Omega\text{m}$  halfspace. The inversion process converged to the desired misfit in six iterations. Each iteration took about 15 min, for a total of 1.5 hours for six iterations. The model recovered after inversion is shown in Figure 7.5. Figure 7.5a shows the cross-section view through the conductive body at  $X = 0$  m while the plan views at the surface, 1 km depth and 6 km depth are shown in Figures 7.5c - 7.5d. From Figure 7.5 it is evident that the the conductivity, position of both the resistive and conductive body is recovered by the inversion algorithm but similar to case I the shape is not perfect near the edges.

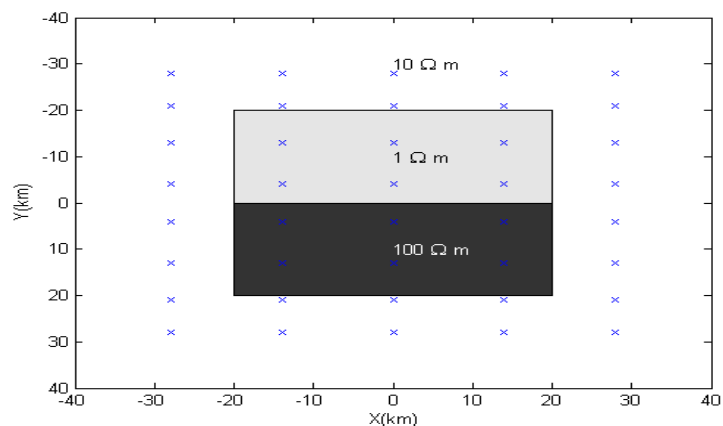


Figure 7.4: Distribution of sites for data generation.

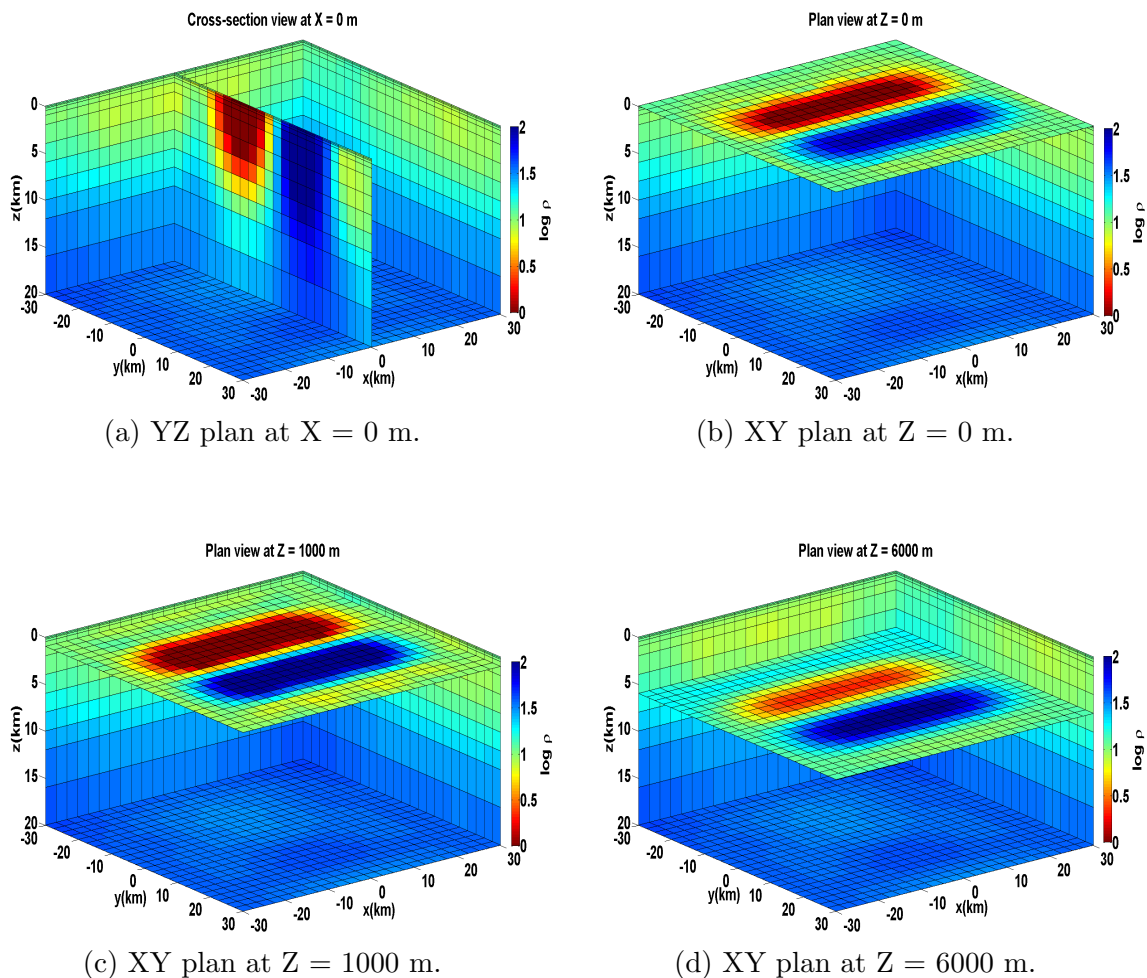


Figure 7.5: Inversion result of fitting the synthetic data generated from two block model.

### 7.2.3 Synthetic Data set 3

Colton and Kress [26] coined the term "inverse crime" to denote the act of using the same algorithm for generating the synthetic data and in inversion and observed that it should be avoided as this leads to trivial inversion. So, to ensure the robustness and versatility of the developed algorithm, the inversion is performed for data generated from ModEM algorithm (Kelbert et al. [61]). For 5 periods (0.1,1,10,100 and 1000s) data is generated for the single conducting block model used in case I. Full impedance tensor is inverted after adding 2% random Gaussian noise to the data. The inversion

recovers the conductive body from the background. For comparison the YZ plans at  $X=0$  m of the models recovered by inverting the data generated from our algorithm and from ModEM are shown in Figures 7.6a and 7.6b respectively.

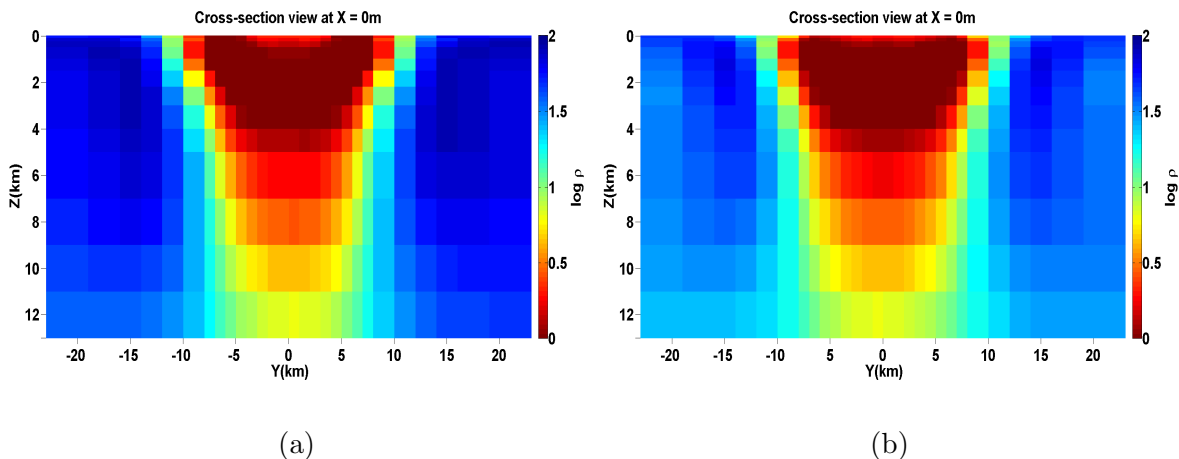


Figure 7.6: Cross-section view across the conductive block at  $X = 0$  m of inversion results of fitting synthetic data generated from (a): algorithm developed in present work, (b): ModEM algorithm (Kelbert et al. [61]).

### 7.3 Synthetic Experiment

After the robustness and efficiency of the 3D inversion algorithm has been tested by running the program on different synthetic data sets, 2 synthetic experiments are designed to gain insight on the effect of number of sites and their distribution on the final result of inversion. These experiments are conducted on a simple conductive block model (Figure 7.1) used for testing the algorithm. For 5 time periods (0.1,1,10,100 and 1000 sec), the complex impedance tensor ( $\mathbf{Z}_{xx}$ ,  $\mathbf{Z}_{xy}$ ,  $\mathbf{Z}_{yx}$  and  $\mathbf{Z}_{yy}$ ) after adding 2% random Gaussian noise is inverted. The inversion is started from a half space of  $50 \Omega\text{m}$  resistivity.

### 7.3.1 Experiment 1: Effect of number of sites

The experiment for analyzing the effect of number of sites on inversion is divided into four cases as:

- A. The data is generated on 81 sites (Figure 7.2) located on 9 profiles parallel to Y axis separated by 4km (from  $y = -16$  km to  $Y = 16$  km ). Each profile has 9 sites separated by 4 km (from  $X = -16$  km to  $X = 16$  km). The inversion result of this data set (Figure 7.3) is termed as "full data set inversion (FDI) result".
- B. In this case, the data is generated on 45 sites (Figure 7.7) located on 5 profiles parallel to Y axis separated by 4km (from  $y = -8$  km to  $Y = 8$  km ) and each profile has 9 sites separated by 4 km (from  $X = -16$  km to  $X = 16$  km). The plan view at different depths of the inverted model along with the corresponding relative misfit in the model parameters with respect to the FDI result is shown in Figure 7.8.
- C. Next, the data is generated on 27 sites (Figure 7.9) located on 3 profiles parallel to Y axis separated by 4km (from  $y = -4$  km to  $Y = 4$  km ). Each profile has 9 sites separated by 4 km (from  $X = -16$  km to  $X = 16$  km). The plan view of the inverted model and the corresponding relative misfit in the model parameters with respect to the FDI result is shown in Figure 7.10.
- D. Finally, the data is generated on 9 sites (Figure 7.11) separated by 4 km (from  $X = -16$  km to  $X = 16$  km), located on 1 profile parallel to Y axis at  $Y = 0$  km. The plan view of the inverted model along with the corresponding relative misfit in the model parameters with respect to the FDI result is shown in Figure 7.12.

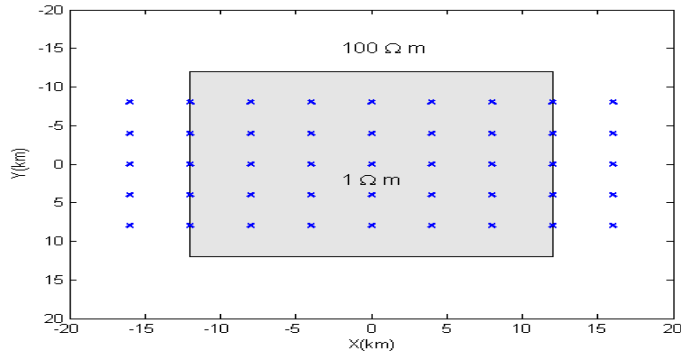


Figure 7.7: Location of observation sites where data is recorded.

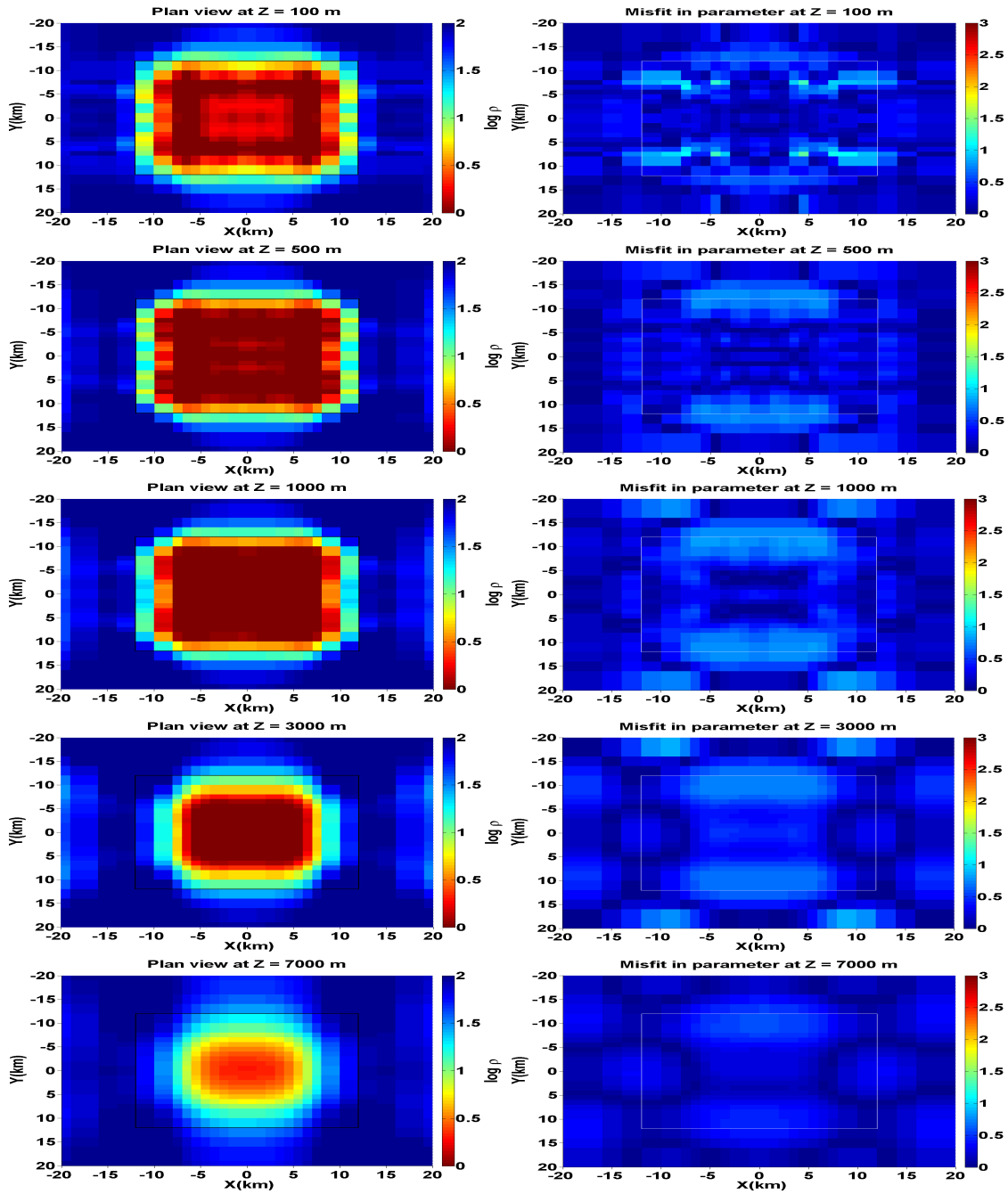


Figure 7.8: Left column: Plan view at different depths of the inverted model for 5 profile case. Right column: Relative misfit in resolved parameters with respect to the FDI results.

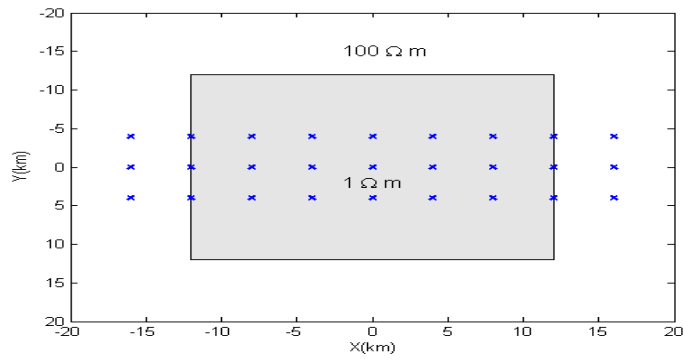


Figure 7.9: Location of observation sites where data is recorded.

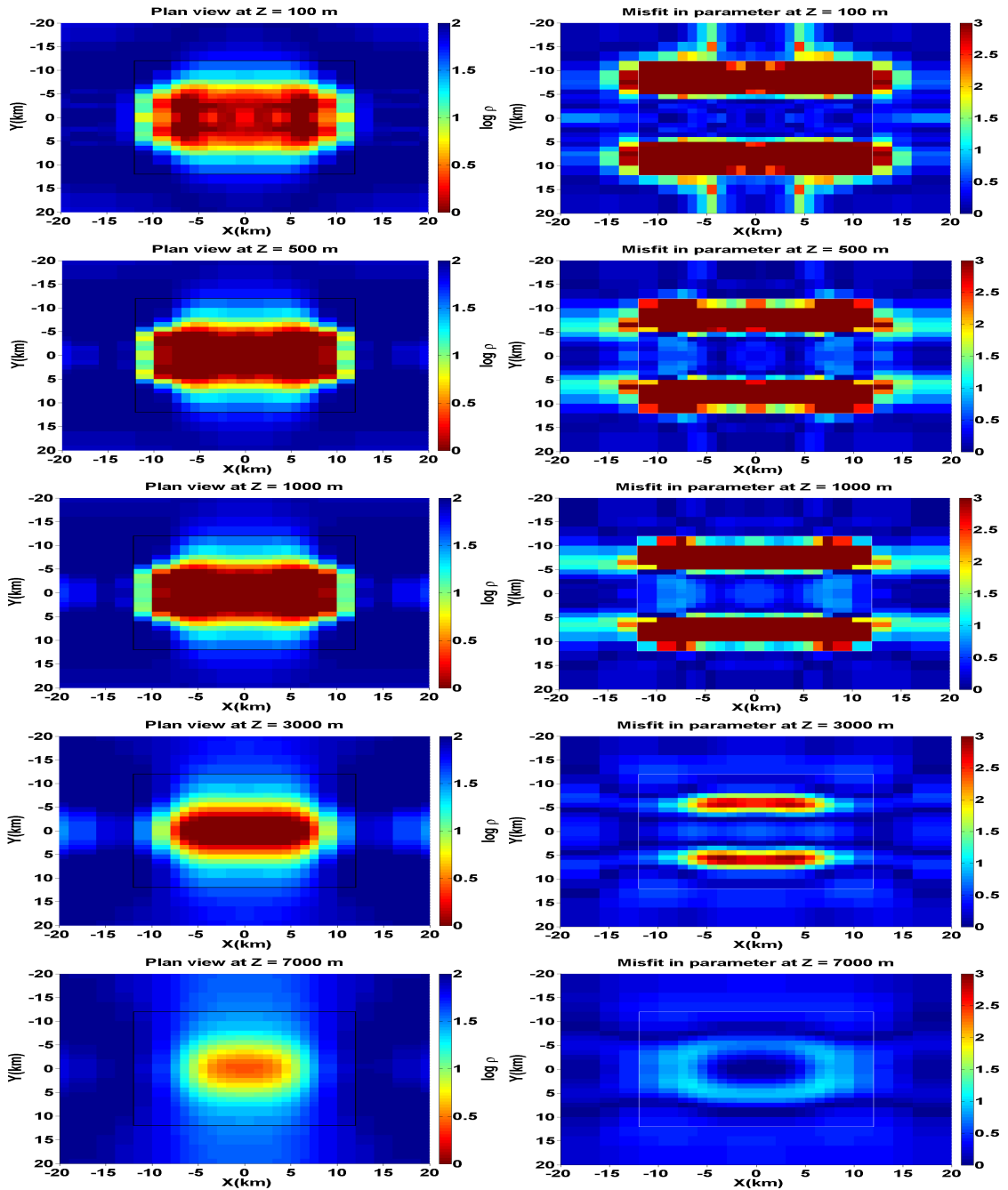


Figure 7.10: Left column: Plan view at different depths of the inverted model for 3 profile case. Right column: Relative misfit in resolved parameters with respect to the FDI results.

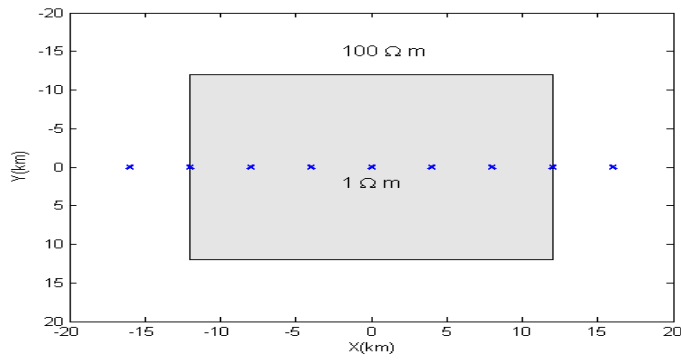


Figure 7.11: Location of observation sites where data is recorded.

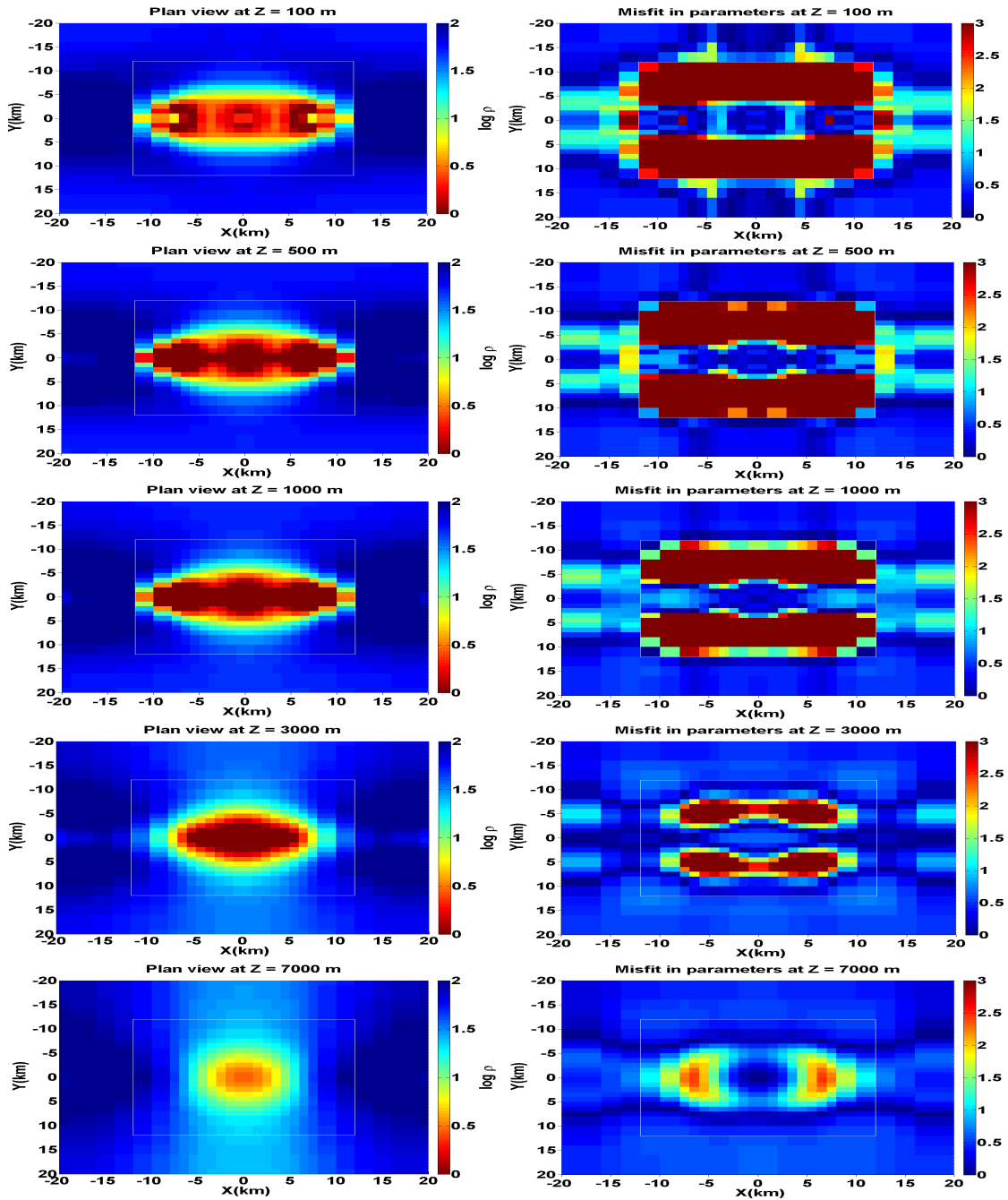


Figure 7.12: Left column: Plan view at different depths of the inverted model for single profile case. Right column: Relative misfit in resolved parameters with respect to the FDI results.



### 7.3.2 Experiment 2: Effect of distribution of sites

In real world, acquiring MT data along a profile may not be possible always because of many reasons such as rough terrain, presence of water body or inaccessibility by road. So, to overcome these limitations the MT data is acquired at sites which are located within a corridor about the profile line. Now, in order to analyze the effect of site locations on inversion, the positions of all 81 sites (Figure 7.2) are perturbed using normalized Gaussian distribution limiting to  $\pm 2$  km in both X and Y direction about the profile line and the experiment designed for this purpose is categorized into four cases as:

- A. The data is generated on 81 sites whose position is perturbed about the respective 9 profile lines parallel to Y axis separated by 4km (from  $y = -16$  km to  $Y = 16$  km ) as shown in Figure 7.13. The inversion result of this data set is termed as "perturbed full data set inversion (PFDI) result". The plan view at different depths of the inverted model along with the corresponding relative misfit in the model parameters with respect to the FDI result is shown in Figure 7.14.
- B. In this case, the data is recorded on 45 sites which are perturbed about the respective 5 profile lines parallel to Y axis separated by 4km (from  $y = -8$  km to  $Y = 8$  km ) as shown in Figure 7.15. The plan view at different depths of the inverted model along with the corresponding relative misfit in the model parameters with respect to the PFDI result and FDI result is shown in Figure 7.16.
- C. Next, the data is recorded on 27 sites which are perturbed about the respective 3 profile lines parallel to Y axis separated by 4km (from  $y = -4$  km to  $Y = 4$

km )as shown in Figure 7.17. The plan view at different depths of the inverted model along with the corresponding relative misfit in the model parameters with respect to the PFDI result and FDI result is shown in Figure 7.18.

D. Finally, the data is recorded on 9 sites which are perturbed about the profile line parallel to Y axis at  $Y = 0$  km as shown in Figure 7.19. The plan view at different depths of the inverted model along with the corresponding relative misfit in the model parameters with respect to the PFDI result and FDI result is shown in Figure 7.20.

The outcome of these experiments are on expected line. From Figures 7.8 - 7.12, it is evident that the lateral extent of anomalous body is resolved from the background within the data coverage area and decreasing the number of profile do not effect the depth resolution as it is dependent on the time period used for data generation. The relative misfit in parameters shown in Figures 7.14 - 7.20, shows that the conductivity of the anomalous body is recovered well where data site density is better, resulting in the distortion of the shape of the anomalous body. These experiments suggest that for good quality inversion the data should be recorded in straight profiles if allowed by the geology of the area. The prior information about the geology of the area from other studies, will help in optimal sites selection.

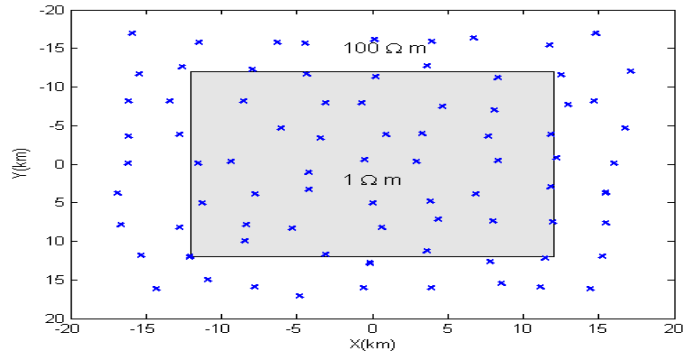


Figure 7.13: Location of observation sites where data is recorded.

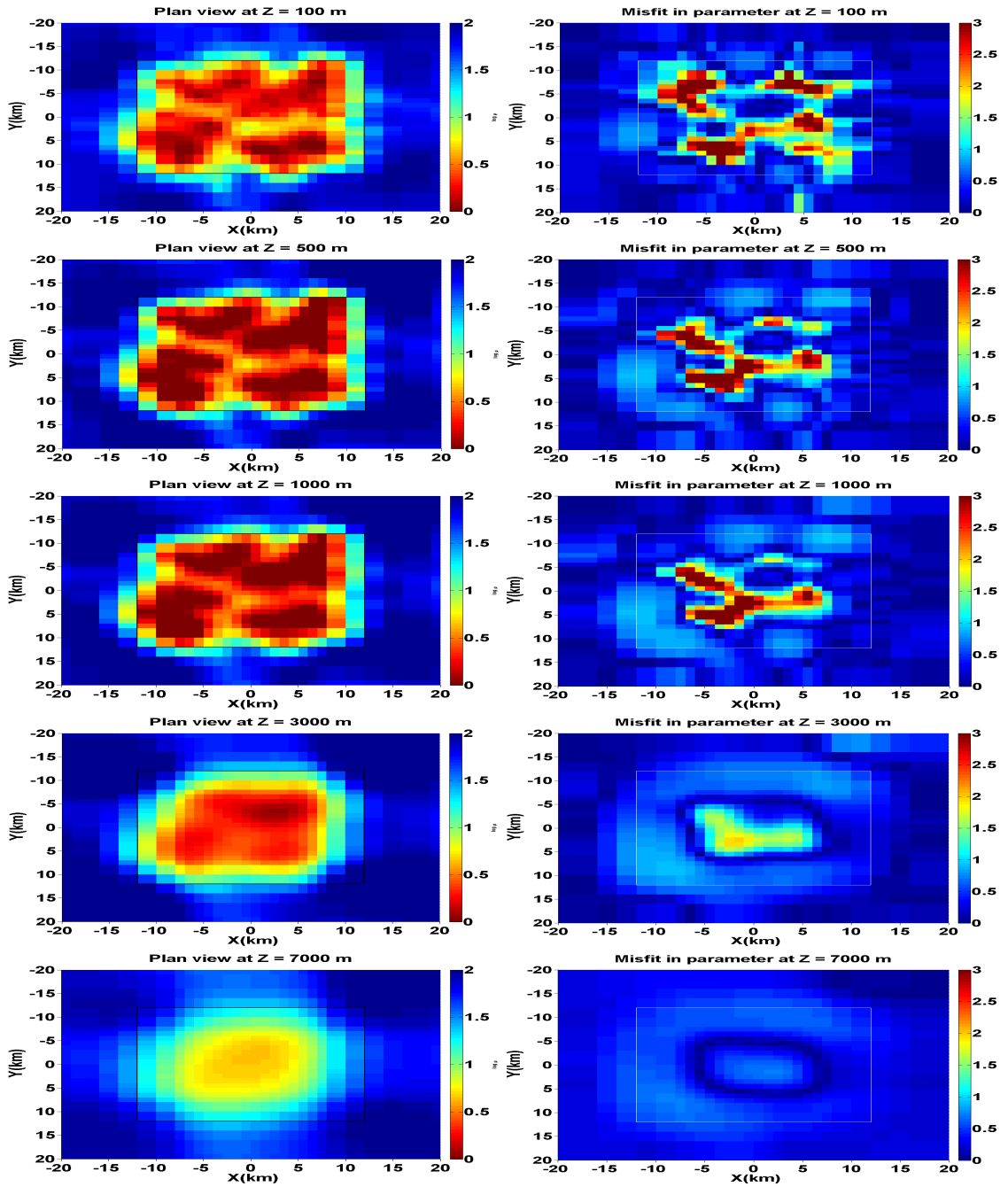


Figure 7.14: Left column: Plan view at different depths of the inverted model for 9 perturbed profile case. Right column: Relative misfit in resolved parameters with respect to the FDI results.

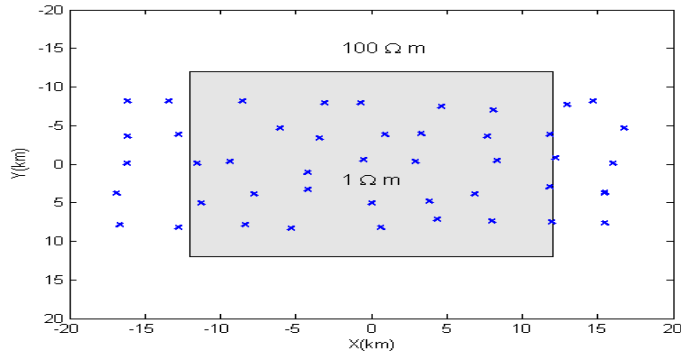


Figure 7.15: Location of observation sites where data is recorded.

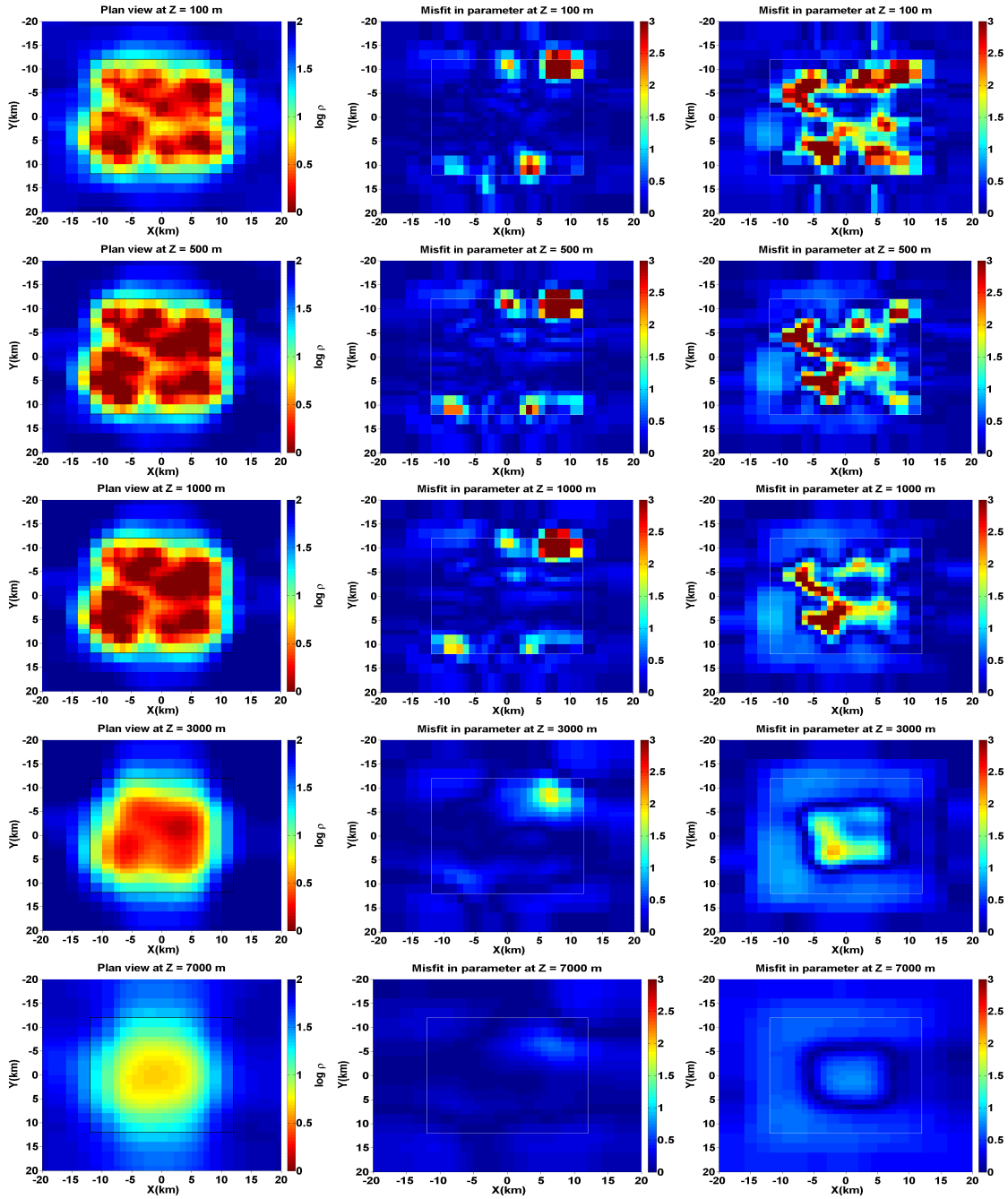


Figure 7.16: Left column: Plan view at different depths of the inverted model for 5 perturbed profile case. Relative misfit in resolved parameters with respect to the PFDI results (middle column) and FDI results (right column).

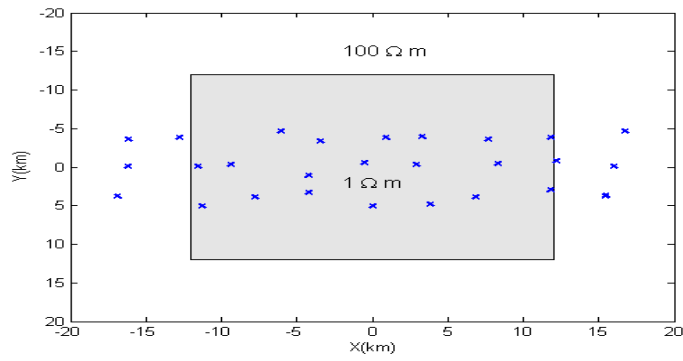


Figure 7.17: Location of observation sites where data is recorded.

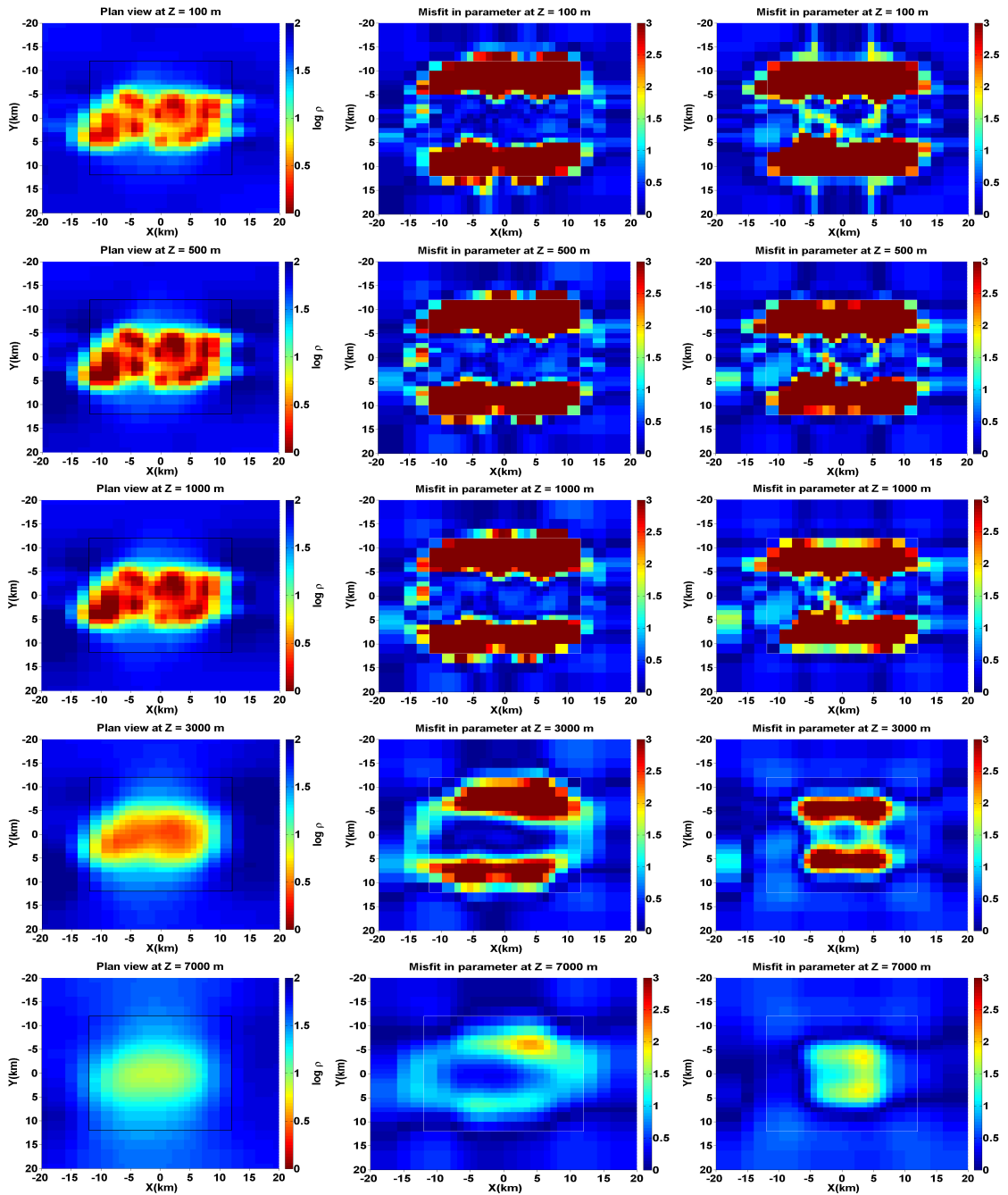


Figure 7.18: Left column: Plan view at different depths of the inverted model for 3 perturbed profile case. Relative misfit in resolved parameters with respect to the PFDI results (middle column) and FDI results (right column).

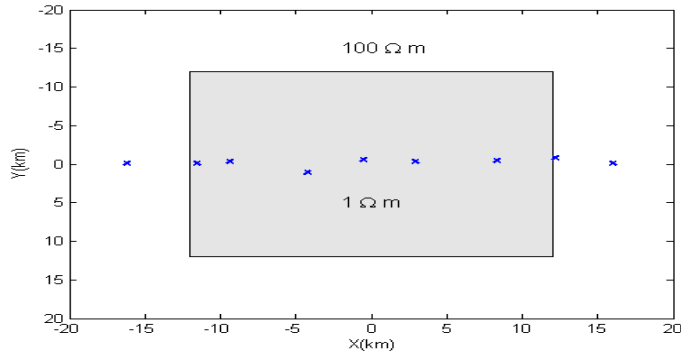


Figure 7.19: Location of observation sites where data is recorded.

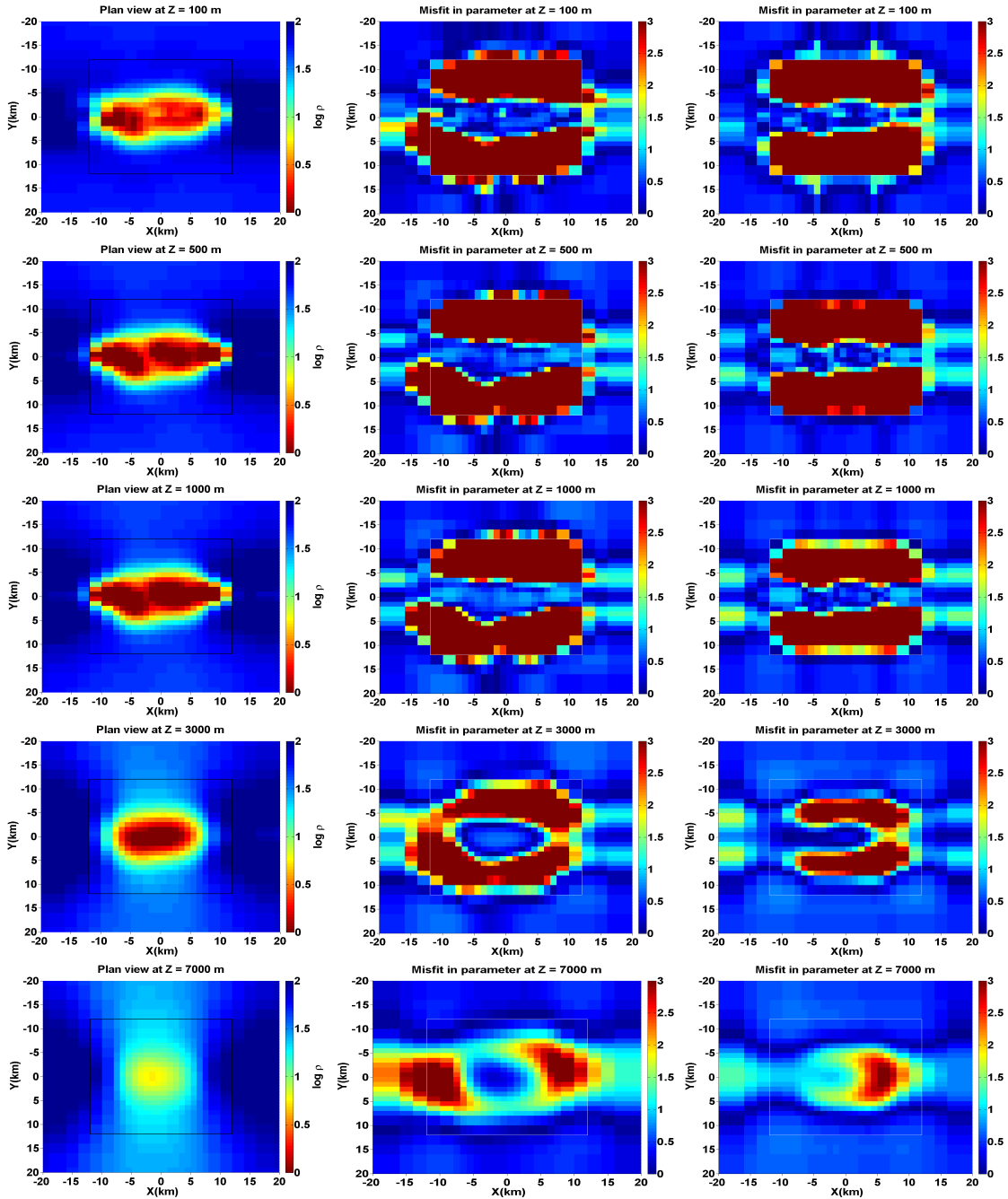


Figure 7.20: Left column: Plan view at different depths of the inverted model for one perturbed profile case. Relative misfit in resolved parameters with respect to the PFDI results (middle column) and FDI results (right column).



### CONCLUSION AND FUTURE SCOPE

3D MT inversion is a very large scale and computationally extensive task. Therefore, there are only few 3D MT inversion programs/codes available and most of these are not free. To the best of my knowledge, WSINV3DMT code of Siripunvaraporn et al. [130] and ModEM code of Kelbert et al. [61] are available for academic use. WSINV3DMT code is based on data space Occam's inversion and the NLCG method is employed in ModEM code. As advised in Avdeev [4] and Siripunvaraporn [125], to improve the 3D MT inversion, new codes must be developed using different approaches and made available to others to test and use. To this end, the work on this thesis started with an objective of developing an efficient algorithm of 3D magnetotelluric data inversion. It is well known that an efficient modeling algorithm is a prerequisite for developing a competent inversion algorithm for data interpretation. The work presented herein is description and discussion related with the development of an efficient 3D modeling algorithm based on finite difference method and employing same to develop the 3D inversion algorithm using Gauss-Newton with conjugate gradient method.



## 8.1 Conclusion

The algorithms, **3DFWD\_FD** and **3DINV\_FD**, developed in this thesis, are efficient and reliable softwares respectively for forward modeling and inversion of 3D magnetotelluric data. The forward problem is solved using staggered grid finite difference method, where BICGSTAB is used as a matrix solver and to improve the convergence at lower frequency the divergence correction is applied. The inversion algorithm is developed using Gauss-Newton with conjugate gradient method.

The efficiency of the forward modelling algorithm and hence the inversion algorithm is improved by using the optimal parameters for divergence correction. The experiments conducted for choosing these parameters conclude that

- the divergence problem to be solved upto an accuracy of  $10^{-3}$  and
- the divergence correction to be applied after every 40 iterations of BICGSTAB to correct the iterative solution,

for optimum computation time. To reduce the computation time furthermore, OpenMP is used for computing response of different frequencies in parallel.

After testing the inversion algorithm on different synthetic data set, to ensure the versatility and robustness of the algorithm the inversion of synthetic data generated from ModEM code is performed and these results shows that inversion algorithm recovers the model effectively. The synthetic experiments performed in the present work to determine the effect of number of sites and their distribution on inversion conclude that

1. inversion with reduced number of profiles recovers the anomalous structure's shape and conductivity within the data range and

2. inversion with perturbed site locations along and across profiles recovers the anomalous structure's conductivity but its shape is distorted.

## 8.2 Scope for Further Research

The present thesis has turned out to be an exploratory effort during which two computer program **3DFWD\_FD** and **3DINV\_FD** have been developed with an aim to enable quantitative interpretation of 3D MT data. However, for better understanding of the complex nature of the EM inverse problem, there exists significant scope for further development, which may possibly be carried out on the following lines :

- Implementation of auto grid generator which employs the skin depth criterion in the forward modeling algorithm.
- At the bottom of the modeling domain, perfectly conducting boundary condition is employed in the algorithm. This constraint forces one to take bottom at sufficient distance so that the tangential electric field will be zero at the domain boundary, resulting in a large modeling domain. Implementation of integral boundary condition at the bottom boundary of the domain .
- The algorithm can be modified for the computation of responses in case of controlled source EM methods simply by replacing the present primary field response computation subprogram with one corresponding to the given EM source.
- Present algorithm works for isotropic medium and it can be modified in subsequent versions for anisotropic medium.

- Due to the constraints of computing resources, OpenMP is used for parallel computations. For more efficient computations, adaptation of the code for parallel programming on distributed memory environment using MPI is recommended.

## Appendix A

---

### Basic steps of BICGSTAB method to solve matrix equation $\mathbf{Ax} = \mathbf{b}$

```
 $\mathbf{x}_0$  is an initial guess,  $\mathbf{r}_0 = \mathbf{b} - \mathbf{Ax}_0$   
Choose  $\tilde{\mathbf{r}}$ :  $\tilde{\mathbf{r}} = \mathbf{r}_0$   
for  $i = 1, 2, \dots$   
     $\rho_{i-1} = \tilde{\mathbf{r}}^T \mathbf{r}_{i-1}$   
    if  $\rho_{i-1} = 0$ , method fails  
    if  $i = 1$   
         $\mathbf{p}_i = \mathbf{r}_{i-1}$   
    else  
         $\beta_{i-1} = (\rho_{i-1} / \rho_{i-2})(\alpha_{i-1} / \omega_{i-1})$   
         $\mathbf{p}_i = \mathbf{r}_{i-1} + \beta_{i-1}(\mathbf{p}_{i-1} - \omega_{i-1}\mathbf{v}_{i-1})$   
    endif  
    Solve  $\hat{\mathbf{p}}$  from  $\mathbf{K}\hat{\mathbf{p}} = \mathbf{p}_i$   
     $\mathbf{v}_i = \mathbf{A}\hat{\mathbf{p}}$   
     $\alpha_i = \rho_{i-1} / \tilde{\mathbf{r}}^T \mathbf{v}_i$   
     $\mathbf{s} = \mathbf{r}_{i-1} - \alpha_i \mathbf{v}_i$   
    if  $\|\mathbf{s}\|$  small enough then  
         $\mathbf{x}_i = \mathbf{x}_{i-1} + \alpha_i \hat{\mathbf{p}}$ , quit  
    Solve  $\hat{\mathbf{s}}$  from  $\mathbf{K}\hat{\mathbf{s}} = \mathbf{s}$   
     $\mathbf{t} = \mathbf{A}\hat{\mathbf{s}}$   
     $\omega_i = \mathbf{t}^T \mathbf{s} / \mathbf{t}^T \mathbf{t}$   
     $\mathbf{x}_i = \mathbf{x}_{i-1} + \alpha_i \hat{\mathbf{p}} + \omega_i \hat{\mathbf{s}}$   
    if  $\mathbf{x}_i$  is accurate enough then quit  
     $\mathbf{r}_i = \mathbf{s} - \omega_i \mathbf{t}$   
    for continuation it is necessary that  $\omega_i \neq 0$   
end
```

**Basic steps of CG method  
to solve matrix equation  $\mathbf{Ax} = \mathbf{b}$**

```
x0 is an initial guess, r0 = b-Ax0  
for i = 1,2,...  
     $\rho_{i-1} = \mathbf{r}_{i-1}^T \mathbf{r}_{i-1}$   
    if i = 1  
        pi = ri-1  
    else  
         $\beta_{i-1} = (\rho_{i-1} / \rho_{i-2})$   
        pi = ri-1 +  $\beta_{i-1}$ pi-1  
    endif  
    vi = Api  
     $\alpha_i = \rho_{i-1} / \mathbf{p}_i^T \mathbf{v}_i$   
    xi = xi-1 +  $\alpha_i$ pi  
    ri = ri-1 -  $\alpha_i$ vi  
    if xi is accurate enough then quit  
end
```

## DILU Preconditioner

Splitting the coefficient matrix into its diagonal, lower triangular and upper triangular parts as

$$\mathbf{A} = \mathbf{L}_A + \mathbf{D}_A + \mathbf{U}_A,$$

the preconditioner can be written as

$$\mathbf{K} = (\mathbf{D} + \mathbf{L}_A)\mathbf{D}^{-1}(\mathbf{D} + \mathbf{U}_A),$$

where  $\mathbf{D}$  is the diagonal matrix containing the pivots generated as described below..

```
Let  $S$  be the nonzero set  $\{(i, j) : a_{ij} \neq 0\}$ 
for  $i = 1, 2, \dots$ 
    set  $d_{ii} = a_{ii}$ 
    for  $i = 1, 2, \dots$ 
        set  $d_{ii} = 1/d_{ii}$ 
        for  $j = i + 1, i + 2, \dots$ 
            if  $(i, j) \in S$  and  $(j, i) \in S$  then
                set  $d_{jj} = d_{jj} - a_{ji}d_{ii}a_{ij}$ 
            endif
        end
    end
end
```



## Appendix B

---

### Documentation on input requirements of the algorithm 3DINV\_FD

**nt** : *number of time periods for response computation*

**nx** : *number of cells in X direction*

**ny** : *number of cells in Y direction*

**nz** : *number of cells in Z direction*

**nl** : *number of layers in host layered earth*

**np** : *number of anomalous bodies*

**ixa, ixb** : *anomalous body edge position in X direction*

**iya, iyb** : *anomalous body edge position in Y direction*

**iza, izb** : *anomalous body edge position in Z direction*

**itmax** : *number of BICGSTAB iterations after which divergence*

*correction is applied*

**xlc, xrc** : *inversion domain boundary in X direction*

**ylc, yrc** : *inversion domain boundary in Y direction*

**zucc, zdc** : *inversion domain boundary in Z direction*

**eps** : *desired tolerance value*



FRWRD\_INP.dat

```
5          !nt : total number of time-period
0.1       !time-period values
1.0
10.
100.
1000.
1000      !scale

*** Synthetic model grid details:
55        !nx : no of cells in x direction
-544000
-288000
-160000
-96000
-64000
-48000
-36000
-32000
-28000
-24000
-20000
-18000
-16750
-15500
-14250
-13000
-12000
-10500
-9250
-8625
-8000
-7375
-6750
-5500
-4250
-3000
-1750
-500
500
1750
3000
4250
5500
6750
7375
8000
8625
9250
10500
12000
13000
14250
15500
16750
18000
20000
24000
28000
32000
36000
48000
```

64000  
96000  
160000  
288000  
544000  
55  
-544000  
-288000  
-160000  
-96000  
-64000  
-48000  
-36000  
-32000  
-28000  
-24000  
-20000  
-18000  
-16750  
-15500  
-14250  
-13000  
-12000  
-10500  
-9250  
-8625  
-8000  
-7375  
-6750  
-5500  
-4250  
-3000  
-1750  
-500  
500  
1750  
3000  
4250  
5500  
6750  
7375  
8000  
8625  
9250  
10500  
12000  
13000  
14250  
15500  
16750  
18000  
20000  
24000  
28000  
32000  
36000  
48000  
64000  
96000  
160000  
288000  
544000

!ny : no of cells in y direction

```

36                                !nz : no of cells in z direction
-1000000
-100000
-10000
-2400
-1000
-200
-50
0
50
100
318
552
856
1000
1766
2434
3303
4433
5100
5901
7810
10292
13518
17712
23165
30253
39467
51446
67019
87263
113580
147793
192270
250089
325255
422970
550000

```

\*\*\* Synthetic model resistivity structure details:

```

1.0E+12                        !rho_air
1                               !nl
100.0                          !rho0
550000.0                       !depth1
1                               !np
1.0                             !rho1
-12000. 12000. -12000. 12000. 100. 5100. !ixa, ixb, iya, iyb, iza, izb

```

\*\*\* Convergence estimation parameters

```

1600                          !bicg_itmax
40                             !itmax
1.0E-06                       !bicg_tol
1.0E-16                       !bicg_stol

```

\*\*\* Counter for data generation:

```

1      !response_counter (1: full impedance 2: off diagonal elements)

```

\*\*\* Counter for problem

```

0      !problem_counter (-1:only forward modeling 0:both 1:only version)

```

```

                    INV_INP.dat
5                    !nt : total number of time-period
0.1                  !time-period values
1.0
10.
100.
1000.

```

\*\*\* Guess model grid details:

```

38                    !nx : no of cells in x direction
-520000
-263000
-135000
-71000
-39000
-23000
-19000
-16000
-14000
-12000
-10000
-8000
-7000
-6000
-5000
-4000
-3000
-2000
-1000
0
1000
2000
3000
4000
5000
6000
7000
8000
10000
12000
14000
16000
19000
23000
39000
71000
135000
263000
520000

```

```

38                    !ny : no of cells in y direction
-520000
-263000
-135000
-71000
-39000
-23000
-19000
-16000
-14000
-12000
-10000
-8000
-7000

```

-6000  
-5000  
-4000  
-3000  
-2000  
-1000  
0  
1000  
2000  
3000  
4000  
5000  
6000  
7000  
8000  
10000  
12000  
14000  
16000  
19000  
23000  
39000  
71000  
135000  
263000  
520000

27  
-1000000  
-100000  
-10000  
-2400  
-400  
-100  
0  
100  
250  
500  
1000  
1500  
2200  
3000  
4000  
5000  
7000  
9000  
11000  
13000  
15000  
19000  
27000  
43000  
75000  
139000  
267000  
520000

!nz : no of cells in z direction

\*\*\* Inversion domain

-43000           !xlc  
  43000           !xrc  
-43000           !ylc  
  43000           !yrc  
          0        !zuc  
  43000           !zdc

```
*** Guess model resistivity structure details:
1.0E+12      !rho_air
1            !nl
100.0        !rho0
520000.0     !depth1
1            !np
50.          !rho1
-43000. 43000. -43000. 43000. 0. 43000.      !ixa,ixb,iya,iyb,iza,izb

*** Run time parameters
20           !inv_iter
1.5          !eps
20           !cg_itmax
1.0E-02      !cg_tol
0.1 200.0    !rhomin,rhobox
```

81  
 -16  
 -12  
 -8  
 -4  
 0  
 4  
 8  
 12  
 16  
 -16  
 -12  
 -12  
 -8  
 -4  
 0  
 4  
 8  
 12  
 16  
 -16  
 -12  
 -8  
 -4  
 0  
 4  
 8  
 12  
 16  
 -16  
 -12  
 -8  
 -4  
 0  
 4  
 8  
 12  
 16  
 -16  
 -12  
 -8  
 -4  
 0  
 4  
 8  
 12  
 16  
 -16  
 -12  
 -8  
 -4  
 0  
 4  
 8  
 12  
 16  
 -16  
 -12  
 -8  
 -4  
 0  
 4  
 8  
 12  
 16  
 -16  
 -12  
 -8  
 -4  
 0  
 4  
 8  
 12  
 16

! No of sites where data is recorded  
 ! Site position in km

Synthetic Model Response

Zxx:

x_obs	y_obs	Re(Zxx)	Im(Zxx)	RHO xx	PH xx
-1.60000E+04	-1.60000E+04	5.61829E-05	7.77224E-05	1.16485E-04	5.41381E+01
-1.20000E+04	-1.60000E+04	-4.62524E-05	2.64350E-04	9.12147E-04	-8.00756E+01
-8.00000E+03	-1.60000E+04	3.12110E-06	-2.53391E-05	8.25532E-06	-8.29781E+01
-4.00000E+03	-1.60000E+04	2.53532E-05	3.15666E-05	2.07612E-05	5.12298E+01
0.00000E+00	-1.60000E+04	9.89314E-06	-2.58168E-06	1.32400E-06	-1.46256E+01
4.00000E+03	-1.60000E+04	-3.22268E-05	-9.13269E-06	1.42099E-05	1.58221E+01
8.00000E+03	-1.60000E+04	2.77678E-07	-4.95807E-06	3.12317E-07	-8.67945E+01
1.20000E+04	-1.60000E+04	2.22923E-05	-2.45743E-04	7.71136E-04	-8.48167E+01
1.60000E+04	-1.60000E+04	-5.14269E-05	-1.07673E-04	1.80330E-04	6.44699E+01
-1.60000E+04	-1.20000E+04	-8.84094E-05	4.95189E-04	3.20464E-03	-7.98773E+01
-1.20000E+04	-1.20000E+04	-1.04119E-02	-9.14381E-04	1.38360E+00	5.01886E+00
-8.00000E+03	-1.20000E+04	7.20705E-06	-5.10168E-06	9.87486E-07	-3.52937E+01
-4.00000E+03	-1.20000E+04	-2.64596E-06	-9.98909E-06	1.35242E-06	7.51640E+01
0.00000E+00	-1.20000E+04	-6.64823E-08	-2.87876E-07	1.10557E-09	7.69961E+01
4.00000E+03	-1.20000E+04	2.00044E-06	1.03569E-05	1.40921E-06	7.90679E+01
8.00000E+03	-1.20000E+04	-2.15334E-06	3.14830E-06	1.84261E-07	-5.56290E+01
1.20000E+04	-1.20000E+04	1.04032E-02	9.04738E-04	1.38108E+00	4.97034E+00
1.60000E+04	-1.20000E+04	6.77552E-05	-5.01002E-04	3.23713E-03	-8.22981E+01
-1.60000E+04	-8.00000E+03	1.00883E-04	8.88775E-05	2.28942E-04	4.13800E+01
-1.20000E+04	-8.00000E+03	-1.82458E-04	3.38264E-04	1.87081E-03	-6.16579E+01
-8.00000E+03	-8.00000E+03	8.69730E-07	9.69891E-07	2.14943E-08	4.81165E+01
-4.00000E+03	-8.00000E+03	-1.30822E-06	-2.18401E-06	8.20871E-08	5.90784E+01
0.00000E+00	-8.00000E+03	3.42247E-06	5.00693E-07	1.51526E-07	8.32308E+00
4.00000E+03	-8.00000E+03	1.09946E-06	2.77612E-06	1.12918E-07	6.83943E+01
8.00000E+03	-8.00000E+03	-9.59014E-07	-1.20894E-06	3.01588E-08	5.15761E+01
1.20000E+04	-8.00000E+03	1.77189E-04	-3.18428E-04	1.68183E-03	-6.09063E+01
1.60000E+04	-8.00000E+03	-4.19059E-05	-1.02514E-04	1.55341E-04	6.77661E+01
-1.60000E+04	-4.00000E+03	1.21918E-05	2.87534E-05	1.23536E-05	6.70225E+01
-1.20000E+04	-4.00000E+03	-3.44875E-06	2.78376E-05	9.96527E-06	-8.29377E+01
-8.00000E+03	-4.00000E+03	1.46856E-06	-2.05624E-06	8.08643E-08	-5.44657E+01
-4.00000E+03	-4.00000E+03	3.07608E-06	-9.29489E-07	1.30783E-07	-1.68130E+01
0.00000E+00	-4.00000E+03	-6.65649E-06	1.84478E-06	6.04281E-07	-1.54901E+01
4.00000E+03	-4.00000E+03	2.66074E-06	2.57946E-06	1.73932E-07	4.41114E+01
8.00000E+03	-4.00000E+03	-2.41192E-06	1.36053E-06	9.71218E-08	-2.94267E+01
1.20000E+04	-4.00000E+03	2.05378E-06	-2.64208E-05	8.89443E-06	-8.55551E+01
1.60000E+04	-4.00000E+03	1.77360E-05	-1.42296E-05	6.54846E-06	-3.87401E+01
-1.60000E+04	0.00000E+00	-2.47165E-05	-2.06422E-05	1.31339E-05	3.98673E+01
-1.20000E+04	0.00000E+00	3.28391E-06	1.90633E-06	1.82608E-07	3.01355E+01
-8.00000E+03	0.00000E+00	-4.90161E-08	2.46752E-06	7.71442E-08	-8.88620E+01
-4.00000E+03	0.00000E+00	-2.58004E-06	-2.85993E-06	1.87897E-07	4.79454E+01
0.00000E+00	0.00000E+00	5.69721E-06	2.27070E-06	4.76391E-07	2.17305E+01
4.00000E+03	0.00000E+00	-4.08229E-06	-2.92170E-06	3.19180E-07	3.55913E+01
8.00000E+03	0.00000E+00	5.33711E-07	2.82183E-06	1.04456E-07	7.92898E+01
1.20000E+04	0.00000E+00	4.88878E-06	-3.16519E-07	3.03968E-07	-3.70439E+00
1.60000E+04	0.00000E+00	-3.15509E-05	-1.42107E-05	1.51653E-05	2.42471E+01
-1.60000E+04	4.00000E+03	2.44933E-05	-1.82983E-06	7.64050E-06	-4.27249E+00
-1.20000E+04	4.00000E+03	-1.56371E-06	-3.04347E-05	1.17623E-05	8.70588E+01
-8.00000E+03	4.00000E+03	-2.35753E-06	5.67233E-07	7.44673E-08	-1.35285E+01
-4.00000E+03	4.00000E+03	2.33810E-06	3.16855E-06	1.96391E-07	5.35760E+01
0.00000E+00	4.00000E+03	-8.65198E-06	1.78336E-06	9.88351E-07	-1.16468E+01
4.00000E+03	4.00000E+03	4.49941E-06	-6.65798E-07	2.62016E-07	-8.41724E+00
8.00000E+03	4.00000E+03	4.92797E-07	-2.98021E-06	1.15563E-07	-8.06107E+01
1.20000E+04	4.00000E+03	-8.28784E-06	2.64561E-05	9.73460E-06	-7.26059E+01
1.60000E+04	4.00000E+03	2.47167E-05	2.66328E-05	1.67208E-05	4.71370E+01
-1.60000E+04	8.00000E+03	-6.10689E-05	-9.19859E-05	1.54399E-04	5.64201E+01
-1.20000E+04	8.00000E+03	1.80030E-04	-3.20031E-04	1.70765E-03	-6.06406E+01
-8.00000E+03	8.00000E+03	1.92635E-06	-2.02634E-06	9.90017E-08	-4.64491E+01
-4.00000E+03	8.00000E+03	8.56886E-09	2.42579E-06	7.45283E-08	8.97976E+01
0.00000E+00	8.00000E+03	6.03947E-06	-4.28429E-07	4.64289E-07	-4.05765E+00
4.00000E+03	8.00000E+03	-5.68463E-07	-2.52907E-06	8.51013E-08	7.73321E+01
8.00000E+03	8.00000E+03	2.70954E-06	7.74443E-07	1.00578E-07	1.59511E+01
1.20000E+04	8.00000E+03	-1.72230E-04	3.35035E-04	1.79733E-03	-6.27938E+01
1.60000E+04	8.00000E+03	7.70766E-05	9.44997E-05	1.88343E-04	5.07984E+01





## BIBLIOGRAPHY

---

- [1] Abubakar, A., Habashy, T. M., Druskin, V. L., Knizhnerman, L., and Alumbaugh, D. (2008). 2.5d forward and inverse modeling for interpreting low-frequency electromagnetic measurements. *Geophysics*, 73:165–177.
- [2] Abubakar, A., Habashy, T. M., Li, M., and Liu, J. (2009). Inversion algorithms for large-scale geophysical electromagnetic measurements. *Inverse Problem*, 25:1–30.
- [3] Arora, B., Unsworth, M. J., and Rawat, G. (2007). Deep resistivity structure of the northwest indian himalaya and its tectonic implications. *Geophysical Research Letters*, 34(4).
- [4] Avdeev, D. (2005). Three-dimensional electromagnetic modeling and inversion from theory to application. *Geothermics*, 26:767–799.
- [5] Avdeev, D. and Avdeeva, A. (2009). 3d magnetotelluric inversion using a limited-memory quasi-newton optimization. *Geophysics*, 74:F45–F57.
- [6] Avdeev, D. B., Kuvshinov, A. V., Pankratov, O. V., and Newman, G. A. (1997). High-performance three-dimensional electromagnetic modelling using modified neumann series. wide-band numerical solution and examples. *Journal of geomagnetism and geoelectricity*, 49:1519–1539.
- [7] Avdeev, D. B., Kuvshinov, A. V., Pankratov, O. V., and Newman, G. A. (2002). Three-dimensional induction logging problems, part i: An integral equation solution and model comparisons. *Geophysics*, 67(2):413–426.
- [8] Backus, G. and Gilbert, F. (1970). Uniqueness in the inversion of inaccurate

- gross earth data. *Philosophical Transactions of the Royal Society of London A: Mathematical, Physical and Engineering Sciences*, 266(1173):123–192.
- [9] Backus, G. E. and Gilbert, J. F. (1967). Numerical applications of a formalism for geophysical inverse problems. *Geophysical Journal International*, 13(1-3):247–276.
- [10] Badea, E., Everett, M., Newman, G., and Biro, O. (2001). Finite-element analysis of controlled-source electromagnetic induction using coulomb-gauged potentials. *Geophysics*, 66(3):786–799.
- [11] Barrett, R., Berry, M. W., Chan, T. F., Demmel, J., Donato, J., Dongarra, J., Eijkhout, V., Pozo, R., Romine, C., and Van der Vorst, H. (1994). *Templates for the solution of linear systems: building blocks for iterative methods*, volume 43. Siam.
- [12] Becken, M., Ritter, O., and Burkhardt, H. (2008a). Mode separation of magnetotelluric responses in three-dimensional environments. *Geophysical Journal International*, 172:67–86.
- [13] Berdichevskii, M. N., Zhdanov, M. S., and Keller, G. V. (1984). *Advanced theory of deep geomagnetic sounding*. Elsevier.
- [14] Berdichevsky, M., Golubtsova, N., Varentsov, I. M., Pushkarev, P. Y., Rybin, A., and Sokolova, E. Y. (2010). Geoelectric section of the central tien shan: Sequential inversion of the magnetovariational and magnetotelluric data along the naryn line. *Izvestiya, Physics of the Solid Earth*, 46(8):698–706.
- [15] Bhattacharya, B. B. and Shalivahan (2002). The electric moho underneath eastern indian craton. *Geophysical Research Letters*, 29(10):14–1.

- [16] Börner, R.-U. (2010). Numerical modeling in geo-electromagnetics: advances and challenges. *Surveys in Geophysics*, 31:225–245.
- [17] Brasse, H., Schäfer, A., Díaz, D., Alvarado, G. E., Muñoz, A., and Mütschard, L. (2015). Deep-crustal magma reservoirs beneath the nicaraguan volcanic arc, revealed by 2-d and semi 3-d inversion of magnetotelluric data. *Physics of the Earth and Planetary Interiors*, 248:55–62.
- [18] Brasse, H. and Soyer, W. (2001). A magnetotelluric study in the southern chilean andes. *Geophysical Research Letters*, 28(19):3757–3760.
- [19] Brewitt-Taylor, C. and Weaver, J. (1976). On the finite difference solution of two-dimensional induction problems. *Geophysical Journal International*, 47(2):375–396.
- [20] Broyden, C. (1967). Quasi-newton methods and their application to function minimization. *Mathematics of Computation*, 21:368.
- [21] Bubnov, V., Yakovlev, A., Aleksanova, E., Yakovlev, D., Berdichevsky, M., and Pushkarev, P. (2007a). Magnetotelluric studies of the east-european craton and adjacent regions. *Acta Geophysica*, 55(2):154–168.
- [22] Bubnov, V., Yakovlev, A., Aleksanova, E., Yakovlev, D., Berdichevsky, M., and Pushkarev, P. Y. (2007b). Regional magnetotelluric explorations in russia. *Electromagnetic sounding of the Earth s interior. Amsterdam et al*, pages 351–369.
- [23] Cagniard, L. (1953). Basic theory of the magnetotelluric method of geophysical prospecting. *Geophysics*, 18.

- [24] Cantwell, T. (1960). *Detection and Analysis of Low Frequency Magnetotelluric Signals*. PhD thesis, Massachusetts Institute of Technology.
- [25] Coggon, J. (1971). Electromagnetic and electrical modeling by the finite element method. *Geophysics*, 36(1):132–155.
- [26] Colton, D. and Kress, R. (1998). *Inverse acoustic and electromagnetic scattering theory*, volume 93. Springer Berlin Heidelberg.
- [27] Commer, M. and Newman, G. (2004). New advances in three-dimensional controlled-source electromagnetic inversion. *Geophysical Journal International*, 172:513–535.
- [28] Commer, M. and Newman, G. (2009). Three-dimensional controlled-source electromagnetic and magnetotelluric joint inversion. *Geophysical Journal International*, pages doi:10.1111/j.1365–246X.2009.04216.x.
- [29] Constable, C., Parker, R., and Constable, C. (1987). Occam’s inversion: a practical algorithm for generating smooth models from electromagnetic sounding data. *Geophysics*, 52:289–300.
- [30] Cumming, W. and Mackie, R. (2010). Resistivity imaging of geothermal resources using 1d, 2d and 3d mt inversion and tdem static shift correction illustrated by a glass mountain case history. In *Proceedings world geothermal congress*, Bali, Indonesia.
- [31] Degroot-Hedlin, C. and Constable, S. (1990). Occam’s inversion to generate smooth, two-dimensional models from magnetotelluric data. *Geophysics*, 55(12):1613–1624.

- [32] Eaton, P. A. (1989). 3d electromagnetic inversion using integral equations. *Geophysical prospecting*, 37(4):407–426.
- [33] Ellis, R. G. et al. (2002). Electromagnetic inversion using the qmr-fft fast integral equation method. In *2002 SEG Annual Meeting*. Society of Exploration Geophysicists.
- [34] Farquharson, C. and Craven, J. (2008). Three-dimensional inversion of magnetotelluric data for mineral exploration: an example from the mcarthur river uranium deposit, saskatchewan, canada. *Journal of Applied Geophysics*, 68:450–458.
- [35] Farquharson, C. and Miensopust, M. (2011). Three-dimensional finite-element modelling of magnetotelluric data with a divergence correction. *Journal of Applied Geophysics*, 75(4):699–710.
- [36] Farquharson, C. G. and Oldenburg, D. W. (1998). Non-linear inversion using general measures of data misfit and model structure. *Geophysical Journal International*, 134(1):213–227.
- [37] Fomenko, E. and Mogi, T. (2002). A new computation method for a staggered grid of 3d em field conservative modeling. *Earth Planets Space*, 54:499–509.
- [38] Forsythe, G. E. and Wasow, W. R. (1960). *Finite-difference methods for partial differential equations*. Applied mathematics series.
- [39] Freund, R. W. and Nachtigal, N. M. (1991). Qmr: a quasi-minimal residual method for non-hermitian linear systems. *Numerische mathematik*, 60(1):315–339.
- [40] Grant, F. S. and West, G. F. (1965). *Interpretation theory in applied geophysics*. International series in the earth sciences. McGraw-Hill Book Company.

- [41] Gribenko, A., Green, M., Cuma, M., and Zhdanov, M. (2010). Efficient 3d inversion of mt data using integral equations method and the receiver footprint approach: application to the large-scale inversion of the earthscope mt data. In *Expanded Abstracts of the SEG meeting*, page 644–649, Denver, Colorado.
- [42] Gribenko, A. and Zhdanov, M. (2007). Rigorous 3d inversion of marine csem data based on the integral equation method. *Geophysics*, 72:WA73–WA84.
- [43] Gunther, T., Rucker, C., and Spitzer, K. (2006). Three-dimensional modeling and inversion of dc resistivity data incorporating topography–ii: Inversion. *Geophysical Journal International*, 166:506–517.
- [44] Gurk, M., Smirnov, M., Savvaidis, A., Pedersen, L., and Ritter, O. A 3d magnetotelluric study of the basement structure in the mygdonian basin (northern greece).
- [45] Haber, E. (2005). Quasi-newton methods for large scale electromagnetic inverse problem. *Inverse Problem*, 21:305–317.
- [46] Haber, E., Asher, U., and Oldenburg, D. (2000). On optimization techniques for solving nonlinear inverse problems. *Inverse Problem*, 16:1263–1280.
- [47] Habibian, B. D., Brasse, H., Oskooi, B., Ernst, T., Sokolova, E., Varentsov, I., Group, E. W., et al. (2010). The conductivity structure across the trans-european suture zone from magnetotelluric and magnetovariational data modeling. *Physics of the Earth and Planetary Interiors*, 183(3):377–386.
- [48] Hadamard, J. (1932). Le problème de Cauchy et les équations aux dérivées partielles linéaires hyperboliques. Paris: Hermann & Cie, 542 pp.

- [49] Han, N., Nam, M., Kim, H., Song, Y., and Suh, J. (2009). A comparison of accuracy and computation time of three-dimensional magnetotelluric modeling algorithms. *Journal of Geophysics and Engineering*, 6:136 doi:10.1088/1742-2132/6/2/005.
- [50] Heise, W., , Caldwell, T., Bibby, H., and Bennie, S. (2010). Three-dimensional electrical resistivity image of magma beneath an active continental rift, taupo volcanic zone, new zealand. *Geophysical Research Letters*, 37 (10):art. no. L10301.
- [51] Heise, W., Caldwell, T., Bibby, H., and Bannister, S. (2008). Three-dimensional modelling of magnetotelluric data from the rotokawa geothermal field, taupo volcanic zone, new zealand. *Geophysical Research Letters*, 173:740-750.
- [52] Hildebrand, F. B. (1987). *Introduction to numerical analysis*. Courier Corporation.
- [53] Hill, G., Caldwell, T., Heise, W., Chertkoff, D., Bibby, H., Burgess, M., Cull, J., and Cas, R. (2009). Distribution of melt beneath mount st helens and mount adams inferred from magnetotelluric data. *Nature Geoscience*, 2:785-789doi:10.1038/NGE0661.
- [54] Hohmann, G. (1975). Three dimensional induced polarization and em modeling. *Geophysics*, 40:309-324.
- [55] Jackson, D. D. (1972). Interpretation of inaccurate, insufficient and inconsistent data. *Geophysical Journal International*, 28(2):97-109.
- [56] Jackson, D. D. (1979). The use of a priori data to resolve non-uniqueness in linear inversion. *Geophysical Journal International*, 57(1):137-157.



- [57] Jones, K., Ingham, M., and Bibby, H. (2008). The hydrothermal vent system of mount ruapehu, new zealand– a high frequency mt survey of the summit plateau. *Journal of Volcanology and Geothermal Research*, 176:591–600.
- [58] Kaufman, A. and Keller, G. V. (1981). *The Magnetotelluric Sounding Method*. Elsevier.
- [59] Kaufman, A. A. and Eaton, P. A. (2001). *The theory of inductive prospecting*, volume 33. Elsevier Science.
- [60] Kelbert, A., Egbert, G., and Schultz, A. (2008). Non-linear conjugate gradient inversion for global em induction: resolution studies. *Geophysical Journal International*, 173:365–381.
- [61] Kelbert, A., Meqbel, N., Egbert, G. D., and Tandon, K. (2014). Modem: A modular system for inversion of electromagnetic geophysical data. *Computers and Geosciences*, 66:40 – 53.
- [62] Keller, G. V. and Frischknecht, F. C. (1966). *Electrical methods in geophysical prospecting*. Pergamon Press.
- [63] Kumar, G. P. and Manglik, A. (2011). Effect of himalayan topography on two-dimensional interpretation of magnetotelluric data. *Current Science*, 100(3).
- [64] Kumar, K. (2009). *3D Simulation of Magnetotelluric Data Using Finite Difference Eigenmode Method*. PhD thesis, Indian Institute of Technology Roorkee, India.
- [65] Lahti, I., Korja, T., Smirnov, M., Vaittinen, K., Sandgren, E., Niiranen, T., and Nykänen, V. (2012). 3-d imaging of the central lapland greenstone belt using

magnetotelluric and seismic data. In *Geophysical Research Abstract*, volume 14, page 2652.

- [66] Ledo, J. (2006). 2-d versus 3-d magnetotelluric data interpretation. *Surveys in Geophysics*, 27:111–148.
- [67] Lee, K., Pridmore, D., and Morrison, H. (1981). A hybrid three-dimensional electromagnetic modeling scheme. *Geophysics*, 46(5):796–805.
- [68] Lezaeta, P., Muñoz, M., and Brasse, H. (2000). Magnetotelluric image of the crust and upper mantle in the backarc of the northwestern argentinean andes. *Geophysical Journal International*, 142(3):841–854.
- [69] Li, M., Abubakar, A., and Habashy, T. (2009). Regularized gauss–newton method using compressed jacobian matrix for controlled source electromagnetic data inversion. In *Expanded abstracts of the SEG meeting*, page 704–708, Houston, Texas.
- [70] Lin, C., Tan, H., and Tong, T. (2008). Three-dimensional conjugate gradient inversion of magnetotelluric sounding data. *Applied Geophysics*, 5:314–321.
- [71] Livelybrooks, D. (1993). Program 3dfeem: a multidimensional electromagnetic finite element model. *Geophysical Journal International*, 114(3):443–458.
- [72] Mackie, R. and Madden, T. (1993). Three-dimensional magnetotelluric inversion using conjugate gradients. *Geophysical Journal International*, 115:215–229.
- [73] Mackie, R., Madden, T., and Wannamaker, P. (1993). Three-dimensional magnetotelluric imodeling using difference equations: Theory and comparison to integral equation solutions. *Geophysics*, 58:215–226.

- [74] Mackie, R., Smith, J., and Madden, T. (1994). Three-dimensional electromagnetic modeling using finite difference equations: The magnetotelluric example. *Radio Science*, 29:923–935.
- [75] Mackie, R. and Watts, M. (2007). Joint 3d inversion of marine csem and mt data. In *Expanded abstract of SEG meeting*, page 574–578, San Antonio.
- [76] Manglik, A., Verma, S., Sain, K., Harinarayana, T., and Rao, V. V. (2011). Joint inversion of seismic and mt data—an example from southern granulite terrain, india. In *The Earth’s Magnetic Interior*, pages 83–90.
- [77] Manglik, A. and Verma, S. K. (1998). Delineation of sediments below flood basalts by joint inversion of seismic and magnetotelluric data. *Geophysical Research Letters*, 25(21):4015–4018.
- [78] Marquardt, D. (1963). An algorithm for least-squares estimation of nonlinear parameters. *Journal of the Society for Industrial and Applied Mathematics*, 11:431–441.
- [79] McGillivray, P. and Oldenburg, D. (1990). Methods for calculating frechet derivatives and sensitivities for the non-linear inverse problems. *Geophysics*, 60:899–911.
- [80] Meju, M. A. (1994). *Geophysical data analysis: Understanding inverse problem theory and practice*, volume 6. Society of Exploration Geophysicists Tulsa,, OK.
- [81] Menke, W. (2012). *Geophysical data analysis: Discrete inverse theory*, volume 45. Academic press.

- [82] Miensoopust, M. and Jones, A. 3d mt inversion workshop. [https://www.dias.ie/mt3dinv/3D\\_forward\\_model.html](https://www.dias.ie/mt3dinv/3D_forward_model.html).
- [83] Miensoopust, M. P., Queralt, P., Jones, A. G., et al. (2013). Magnetotelluric 3-d inversion—a review of two successful workshops on forward and inversion code testing and comparison. *Geophysical Journal International*, 193(3):1216–1238.
- [84] Miglani, R., Shahrukh, M., Israil, M., Gupta, P. K., Varshney, S., and Sokolova, E. (2014). Geoelectric structure estimated from magnetotelluric data from the uttarakhand himalaya, india. *Journal of Earth System Science*, 123(8):1907–1918.
- [85] Mitchell, A. R. and Griffiths, D. F. (1980). *The Finite-difference methods in partial differential equations*. John Wiley.
- [86] Mitsuhashi, Y. and Uchida, T. (2004). 3d magnetotelluric modeling using the  $t$ - $\omega$  finite-element method. *Geophysics*, 69(1):108–119.
- [87] Mogi, T. (1996). Three-dimensional modeling of magnetotelluric data using finite element method. *Journal of Applied Geophysics*, 35(2):185–189.
- [88] Nabighian, M. N., editor (1988). *Electromagnetic methods in applied geophysics: Theory*, volume 1. SEG Books.
- [89] Nabighian, M. N., editor (1991). *Electromagnetic methods in applied geophysics: Application*, volume 2. SEG Books.
- [90] Nam, M. J., Kim, H. J., Song, Y., Lee, T. J., Son, J.-S., and Suh, J. H. (2007). 3d magnetotelluric modelling including surface topography. *Geophysical Prospecting*, 55(2):277–287.

- [91] Newman, G. and Alumbaugh, D. (1997). Three-dimensional massively parallel electromagnetic inversion—i theory. *Geophysical Journal International*, 128:345–354.
- [92] Newman, G. and Alumbaugh, D. (2000). Three-dimensional magnetotelluric inversion using non-linear conjugate gradients. *Geophysical Journal International*, 140:410–424.
- [93] Newman, G. and Boggs, P. (2004). Solution accelerators for large-scale three-dimensional electromagnetic inverse problems. *Inverse Problem*, 20:S151–S170.
- [94] Newman, G., Gasperikova, E., Hoversten, G., and Wannamaker, P. (2008). Three-dimensional magnetotelluric characterization of the coso geothermal field. *Geothermics*, page doi:10.1016/j.geothermics.2008.02.006.
- [95] Newman, G. and Hoversten, G. (2000). Solution strategies for two- and three-dimensional electromagnetic inverse problems. *Inverse Problem*, 16:1357–1375.
- [96] Newman, G., Recher, S., Tezkan, B., and Neubauer, F. (2003). Case history 3d inversion of a scalar radio magnetotelluric field data set. *Geophysics*, 68:791–802.
- [97] Ogawa, Y. (2002). On two-dimensional modeling of magnetotelluric field data. *Surveys in Geophysics*, 23:251–272.
- [98] Oldenburg, D. W. (1984). An introduction to linear inverse theory. *IEEE Transactions on Geoscience and Remote Sensing*, (6):665–674.
- [99] Oldenburg, D. W. (1994). Practical strategies for the solution of large-scale electromagnetic inverse problems. *Radio Science*, 29(4):1081–1099.
- [100] Parker, R. (1994). *Geophysical inverse theory*. Princeton University Press, Princeton.

- [101] Parker, R. L. (1977). Understanding inverse theory. *Annual Review of Earth and Planetary Sciences*, 5:35–64.
- [102] Parker, R. L. and Whaler, K. A. (1981). Numerical methods for establishing solutions to the inverse problem of electromagnetic induction. *Journal of Geophysical Research: Solid Earth*, 86(B10):9574–9584.
- [103] Patro, B. P. K., Brasse, H., Sarma, S., and Harinarayana, T. (2005). Electrical structure of the crust below the deccan flood basalts (india), inferred from magnetotelluric soundings. *Geophysical Journal International*, 163(3):931–943.
- [104] Patro, P. and Egbert, G. (2008). Regional conductivity structure of cascadia: preliminary results from 3d inversion of usarray transportable array magnetotelluric data. *Geophysical Research Letters*, 35:art. no. L20311.
- [105] Patro, P. K. and Harinarayana, T. (2009). Deep geoelectric structure of the sikkim himalayas (ne india) using magnetotelluric studies. *Physics of the Earth and Planetary Interiors*, 173(1):171–176.
- [106] Press, W., Teukolsky, S., Vetterling, W., and Flannery, B. (1992). *Numerical Recipes in FORTRAN: the art of scientific computing*. Cambridge University Press, Cambridge, 2nd edition.
- [107] Raiche, A. P. (1988). Inversion of controlled-source electromagnetic data. *Electromagnetic Methods in Applied Geophysics: Applications Part A and*, 2:469–505.
- [108] Rao, C. R. and Mitra, S. K. (1971). *Generalized inverse of matrices and its applications*, volume 7. Wiley New York.

- [109] Rawat, G., Arora, B., and Gupta, P. (2014). Electrical resistivity cross-section across the garhwal himalaya: Proxy to fluid-seismicity linkage. *Tectonophysics*, 637:68–79.
- [110] Reddy, I., Phillips, R., and Rankin, D. (1977). Three-dimensional modelling in magnetotelluric and magnetic variational sounding. *Geophysical Journal*, 51:313–325.
- [111] Rodi, W. (1976). A technique for improving the accuracy of finite element solutions for magnetotelluric data. *Geophysical Journal International*, 44:483–506.
- [112] Rodi, W. and Mackie, R. (2001). Nonlinear conjugate gradients algorithm for 2-d magnetotelluric inversion. *Geophysics*, 66:174–187.
- [113] Rung-Arunwan, T. and Siripunvaraporn, W. (2010). An efficient modified hierarchical domain decomposition for two-dimensional magnetotelluric forward modeling. *Geophysical Journal International*, 183:634–644.
- [114] Saad, Y. (2003). *Iterative methods for sparse linear systems*. Siam.
- [115] Saad, Y. and Schultz, M. H. (1986). Gmres: A generalized minimal residual algorithm for solving nonsymmetric linear systems. *SIAM Journal on scientific and statistical computing*, 7(3):856–869.
- [116] Sabatier, P. (1974). Remarks on approximate methods in geophysical inverse problems. *Proceedings of the Royal Society of London. Series A*, 337:49–71.
- [117] Sarkar, T., Weiner, D., and Jain, V. (1981). Some mathematical considerations in dealing with the inverse problem. *IEEE Transactions on Antennas and propagation*, 29(2):373–379.

- [118] Sasaki, Y. (1999). Three-dimensional frequency-domain modeling using the finite-difference method. *Butsuri-Tansa*, 52:421–431.
- [119] Sasaki, Y. (2001). Full 3d inversion of electromagnetic data on pc. *Journal of Applied Geophysics*, 46:45–54.
- [120] Sasaki, Y. (2004). Three-dimensional inversion of static-shifted magnetotelluric data. *Earth Planets Space*, 56:239–248.
- [121] Schmucker, U. (1970). Anomalies of geomagnetic variations in the southwestern united states. *Bulletin of the Scripps Institute of Oceanography*, 15.
- [122] Shalivahan and Bhattacharya, B. B. (2002). Implications of novel results about moho from magnetotelluric studies. *Current Science*, 83(10):1259–1264.
- [123] Simpson, F. and Bahr, K. (2005). *Practical magnetotellurics*. Cambridge University Press.
- [124] Sinharay, Rajib, K., Shalivahan, and Bhattacharya, B. B. (2001). An analysis of magnetotelluric (mt) data over geothermal region of bakreshwar, west bengal. *Journal of geophysics*, 22(1):31–39.
- [125] Siripunvaraporn, W. (2012). Three-dimensional magnetotelluric inversion: An introductory guide for developers and users. *Surveys in Geophysics*, 33:5–27.
- [126] Siripunvaraporn, W. and Egbert, G. (2000). An efficient data-subspace inversion method for 2d magnetotelluric data. *Geophysics*, 65(3):791–803.
- [127] Siripunvaraporn, W. and Egbert, G. (2007). Data space conjugate gradient inversion for 2-d magnetotelluric data. *Geophysical Journal International*, 170:986–994.



- [128] Siripunvaraporn, W. and Egbert, G. (2009). Wsinv3dmt: vertical magnetic field transfer function inversion and parallel implementation. *Physics of the Earth and Planetary Interiors*, 173:317–329.
- [129] Siripunvaraporn, W., Egbert, G., and Lenbury, Y. (2002). Numerical accuracy of magnetotelluric modeling: a comparison of finite difference approximations. *Earth Planets Space*, 54(6):721–725.
- [130] Siripunvaraporn, W., Egbert, G., Lenbury, Y., and Uyeshima, M. (2005a). Three-dimensional magnetotelluric inversion: data-space method. *Physics of the Earth and Planetary Interiors*, 150:3–14.
- [131] Siripunvaraporn, W., Egbert, G., and Uyeshima, M. (2005b). Interpretation of two-dimensional magnetotelluric profile data with three-dimensional inversion: synthetic examples. *Geophysical Journal International*, 160:804–814.
- [132] Siripunvaraporn, W., Uyeshima, M., and Egbert, G. (2004). Three-dimensional inversion for network-magnetotelluric data. *Earth Planets Space*, 56:893–902.
- [133] Smith, J. (1996a). Conservative modeling of 3-d electromagnetic fields, part i: properties and error analysis. *Geophysics*, 61:1308–1318.
- [134] Smith, J. (1996b). Conservative modeling of 3-d electromagnetic fields, part ii: biconjugate gradient solution and an accelerator. *Geophysics*, 61:1319–1324.
- [135] Streich, R. (2009). 3d finite-difference frequency-domain modeling of controlled-source electromagnetic data: Direct solution and optimization for high accuracy. *Geophysics*, 74(5):F95–F105.

- [136] Stuntebeck, C. (2003). *Three-dimensional electromagnetic modelling by free-decay mode superposition*. PhD thesis, TU Braunschweig.
- [137] Taflove, A., Hagness, S. C., et al. (1995). Computational electrodynamics: the finite-difference time-domain method. *MA: Artech House, Norwood, 2nd Edition*.
- [138] Tarantola, A. (2005). *Inverse problem theory and methods for model parameter estimation*. Siam.
- [139] Tezkan, B. (1994). On the detectability of a highly conductive layer in the upper mantle beneath the black forest crystalline using magnetotelluric methods. *Geophysical Journal International*, 118(1):185–200.
- [140] Tezkan, B., Goldman, M., Greinwald, S., Hördt, A., Müller, I., Neubauer, F., and Zacher, G. (1996). A joint application of radiomagnetotellurics and transient electromagnetics to the investigation of a waste deposit in cologne (germany). *Journal of Applied Geophysics*, 34(3):199–212.
- [141] Tezkan, B., Hördt, A., and Gobashy, M. (2000). Two dimensional inversion of radiomagnetotelluric data: selected case histories for waste site exploration. *Journal of Applied Geophysics*, 44:237–256.
- [142] Tikhonov, A. (1950). On determining electric characteristics of the deep layers of the earth's crust. *Dokl Acad Nauk SSSR*, 73:295–297.
- [143] Tikhonov, A. and Arsenin, V. (1977). *Solutions of Ill-posed problems*. W.H.Winston and Sons, Washington, D.C. USA.
- [144] Travis, B. J. and Chave, A. D. (1989). A moving finite element method

- for magnetotelluric modeling. *Physics of the earth and planetary interiors*, 53(3-4):432–443.
- [145] Tuncer, V., Unsworth, M., Siripunvaraporn, W., and Craven, J. (2006). Exploration for unconformity-type uranium deposits with audiomagnetotelluric data: a case study from the mcarthur river mine, saskatchewan, canada. *Geophysics*, 71:B201–B209.
- [146] Türkoğlu, E., Unsworth, M., and Pana, D. (2009). Deep electrical structure of northern alberta (canada): implications for diamond exploration. *Canadian Journal of Earth Sciences*, 46:139–154.
- [147] Twomey, S. (2013). *Introduction to the mathematics of inversion in remote sensing and indirect measurements*, volume 3. Elsevier.
- [148] Vachiratienchai, C., Boonchaisuk, S., and Siripunvaraporn, W. (2010). A hybrid finite difference-finite element method to incorporate topography for 2d direct current (dc) resistivity modeling. *Physics of the Earth and Planetary Interiors*, 183(3–4):426–434.
- [149] Van der Vorst, H. A. (2003). *Iterative Krylov methods for large linear systems*, volume 13. Cambridge University Press.
- [150] Vozoff, K. (1990). Magnetotellurics: Principles and practice. *Proceedings of the Indian Academy of Sciences (Earth and Planetary Sciences)*, 99(4):441–471.
- [151] Wang, T. and Fang, S. (2001). 3-d electromagnetic anisotropy modeling using finite differences. *Geophysics*, 66(5):1386–1398.

- [152] Wannamaker, P. (1991). Advances in three dimensional magnetotelluric modeling using integral equations. *Geophysics*, 56:1716–1728.
- [153] Wannamaker, P. E., Hohmann, G. W., and SanFilipo, W. A. (1984a). Electromagnetic modeling of three-dimensional bodies in layered earths using integral equations. *Geophysics*, 49(1):60–74.
- [154] Wannamaker, P. E., Hohmann, G. W., and Ward, S. H. (1984b). Magnetotelluric responses of three-dimensional bodies in layered earths. *Geophysics*, 49(9):1517–1533.
- [155] Wannamaker, P. E., Stodt, J. A., and Rijo, L. (1987). A stable finite element solution for two-dimensional magnetotelluric modelling. *Geophysical Journal International*, 88(1):277–296.
- [156] Ward, S. H. and Fraser, D. C. (1967). Part b—conduction of electricity in rocks. *Mining Geophysics: Theory*, 2:197–223.
- [157] Weaver, J. T. (1994). *Mathematical methods for geo-electromagnetic induction*. Research Studies Press Ltd. John Wiley & Sons.
- [158] Weidelt, P. (1975). Em induction in three dimensional structures. *Geophysics*, 41:85–109.
- [159] Whittall, K. P. (1986). Inversion of magnetotelluric data using localized conductivity constraints. *Geophysics*, 51(8):1603–1607.
- [160] Xiong, Z. and Tripp, A. C. (1995). Electromagnetic scattering of large structures in layered earths using integral equations. *Radio Science*, 30:921–921.

- [161] Yan, L., Xiang-Yun, H., Wen-Cai, Y., Wen-Bo, W., Hui, F., Bo, H., and Rong-Hua, P. (2013). A study on parallel computation for 3d magneto-telluric modeling using the staggered-grid finite difference method. *Chinese Journal of Geophysics*, 56(3):287–295.
- [162] Yee, K. (1966). Numerical solution of initial boundary value problems involving maxwell’s equations in isotropic media. *IEEE Transactions on Antennas and Propagation*, AP-14:302–307.
- [163] Zhanxiang, H. and Hu, Zand Luo, W. (2010). Mapping reservoirs based on resistivity and induced polarization derived from continuous 3d magnetotelluric profiling: case study from qaidam basin, china. *Geophysics*, 75:B25–B33.
- [164] Zhdanov, M. (2002). *Geophysical inverse theory and regularization problems*. Elsevier, Amsterdam.
- [165] Zhdanov, M. (2009). *Geophysical electromagnetic theory and methods*. Elsevier.
- [166] Zhdanov, M., Fang, S., and Hursan, G. (2000). Electromagnetic inversion using quasi-linear approximation. *Geophysics*, 65:1501–1513.
- [167] Zhdanov, M., Varentsov, I. M., Weaver, J., Golubev, N., and Krylov, V. (1997). Methods for modelling electromagnetic fields results from commemi—the international project on the comparison of modelling methods for electromagnetic induction. *Journal of Applied Geophysics*, 37:133–271.
- [168] Zhdanov, M. S. and Fang, S. (1996). Quasi-linear approximation in 3-d electromagnetic modeling. *Geophysics*, 61(3):646–665.

- [169] Zhdanov, M. S., Lee, S. K., and Yoshioka, K. (2006). Integral equation method for 3d modeling of electromagnetic fields in complex structures with inhomogeneous background conductivity. *Geophysics*, 71(6):G333–G345.